

AD A140224

12

HDL-CR-83-117-1

March 1984

A Proportional Piezoelectric Electropneumatic
Servovalve Design

by Benjamin M. Herrick

Prepared by
The University of New Hampshire
Durham, NH 03824

Under contract
DAAK21-79-C-0117

Reproduced From
Best Available Copy



DTIC FILE COPY

DTIC
ELECTE
APR 19 1984
S B

U.S. Army Electronics Research
and Development Command
Harry Diamond Laboratories
Adelphi, MD 20783

Approved for public release; distribution unlimited.

20000803048

The findings in this report are not to be construed as an official Department of the Army position unless so designated by other authorized documents.

Citation of manufacturers' or trade names does not constitute an official indorsement or approval of the use thereof.

Destroy this report when it is no longer needed. Do not return it to the originator.

UNCLASSIFIED

SECURITY CLASSIFICATION OF THIS PAGE (When Data Entered)

REPORT DOCUMENTATION PAGE		READ INSTRUCTIONS BEFORE COMPLETING FORM
1. REPORT NUMBER HDL-CR-83-117-1	2. GOVT ACCESSION NO. AD-A140 224	3. RECIPIENT'S CATALOG NUMBER
4. TITLE (and Subtitle) A Proportional Piezoelectric Electropneumatic Servovalve Design		5. TYPE OF REPORT & PERIOD COVERED Contractor Report
		6. PERFORMING ORG. REPORT NUMBER
7. AUTHOR(s) Benjamin M. Herrick (HDL contact: James Joyce)		8. CONTRACT OR GRANT NUMBER(s) DAAK21-79-C-0117
9. PERFORMING ORGANIZATION NAME AND ADDRESS The University of New Hampshire Durham, New Hampshire 03824		10. PROGRAM ELEMENT, PROJECT, TASK AREA & WORK UNIT NUMBERS Program Element: 6.11.02.A
11. CONTROLLING OFFICE NAME AND ADDRESS Harry Diamond Laboratories 2800 Powder Mill Road Adelphi, MD 20783		12. REPORT DATE March 1984
		13. NUMBER OF PAGES 103
14. MONITORING AGENCY NAME & ADDRESS (if different from Controlling Office)		15. SECURITY CLASS. (of this report) UNCLASSIFIED
		15a. DECLASSIFICATION/DOWNGRADING SCHEDULE
16. DISTRIBUTION STATEMENT (of this Report) Approved for public release; distribution unlimited.		
17. DISTRIBUTION STATEMENT (of the abstract entered in Block 20, if different from Report)		
18. SUPPLEMENTARY NOTES HDL project no.: A44934		
19. KEY WORDS (Continue on reverse side if necessary and identify by block number) Fluidics Laminar proportional amplifier Fluerics Electropneumatic interface		
20. ABSTRACT (Continue on reverse side if necessary and identify by block number) This report deals with the development of a new proportional electropneumatic servovalve. The first stage of the valve consists of a piezoelectric bender element of bimorph construction centered between two nozzles. The bimorph acts as a flapper and is deformed by an electrical input signal. This deformation causes a pressure difference to be generated downstream of the nozzles. This pressure difference is then amplified to some usable level using laminar proportional amplifiers.		

- Continued -

UNCLASSIFIED

SECURITY CLASSIFICATION OF THIS PAGE (When Data Entered)

20. abstract (Continued)

An equivalent mathematical model for the behavior of the valve system is developed and verified. The model is then used to select a bimorph and a laminar proportional amplifier gain block. After the system parameters have been selected using the model, a working prototype is then constructed and tested. The validity of the design equations is shown by the correlation with experimental results, and an improved design is suggested.

TABLE OF CONTENTS

	<u>Page</u>
1. INTRODUCTION -----	1
2. CONCEPT OF VALVE DESIGN -----	3
3. DEVELOPMENT OF THE ELECTROMECHANICAL MODEL -----	12
3.1 Piezoelectric Background Material -----	12
3.2 Equivalent Mechanical Circuit -----	20
3.3 Equivalent Electrical Circuit -----	22
3.4 Experimental Verification -----	24
4. DEVELOPMENT OF THE FLUID MODEL -----	32
5. DESIGN AND TESTING OF A VALVE SYSTEM -----	55
5.1 Analytical Design -----	55
5.2 Prototype -----	67
5.3 Testing and Verification -----	70
6. FUTURE CONSIDERATIONS -----	75
LITERATURE CITED -----	82
NOMENCLATURE -----	84
DISTRIBUTION -----	97
APPENDICES -----	90
A. SUMMARY OF THE PROPERTIES OF THE WORKING PROTOTYPE -----	90
B. SUMMARY OF THE PROPERTIES OF THE PROPOSED PROTOTYPE -----	93

DTIC
ELECTE
S APR 19 1984 **D**
B



Accession For	
NTIS GRA&I	<input checked="" type="checkbox"/>
DTIC TAB	<input type="checkbox"/>
Unannounced	<input type="checkbox"/>
Justification	
By _____	
Distribution/	
Availability Codes	
Dist	Avail and/or Special
A-1	

FIGURES

	<u>Page</u>
1. Flapper Valve Schematic -----	4
2. Bender Deformation with Electrical Input Signal -----	6
3. Operation of a Laminar Proportional Amplifier -----	7
4. Amplifier Staging Technique -----	10
5. Piezoelectric Convention for Axis System -----	14
6. Cross Section of a Piezoelectric Bimorph -----	19
7. Equivalent Mechanical Circuit -----	21
8. Equivalent Electrical Circuit -----	23
9. Measured System Step Response -----	28
$R_A = 0.0 \text{ M}\Omega, F_x(t) = 0.0$	
10. Simulated and Experimental System Step Responses -----	33
$R_A = 0.074 \text{ M}\Omega, F_x(t) = 0.0$	
11. Simulated and Experimental System Step Responses -----	34
$R_A = 0.142 \text{ M}\Omega, F_x(t) = 0.0$	
12. Simulated and Experimental System Step Responses -----	35
$R_A = 0.260 \text{ M}\Omega, F_x(t) = 0.0$	
13. Simulated and Experimental System Step Responses -----	36
$R_A = 0.480 \text{ M}\Omega, F_x(t) = 0.0$	
14. Control Volume for Fluid Flow Forces -----	38
15. Equivalent Steady State Fluid Circuit -----	41
16. Locus of Root of Equation -----	68
$0.0 < P_{S1} < 2.0 \times 10^5 \text{ N/m}^2$	
$R = 0.0$	
17. Assembly Drawing of Valve -----	70
18. Static Input-Output Relationship of Valve System -----	71
19. Measured and Predicted System Frequency Response -----	72
$R = 0.0 \text{ M}\Omega$	

	<u>Page</u>
20. Measured and Predicted System Frequency Response ----- R = 0.2 M Ω	74
A-1 Schematic Drawing of Working Prototype -----	92
A-2 Schematic Drawing of Proposed Prototype -----	95

TABLES

	<u>Page</u>
1. Piezoelectric Parameters for Selected Materials -----	15
2. Physical and Material Properties of Lead-Zirconate Titanate -----	24
3. Measured and Analytically Predicted Electromechanical System Parameters Used for Model Testing -----	31
4. Physical and Material Properties of Lead-Zirconate Titanate Ceramic Bimorph Used for Working Prototype -----	58
5. Analytically Predicted System Parameters Used for Working Prototype -----	58
6. LPA Preamplifier Geometric Properties; Stages 1,2 and 3 -----	59
7. Physical and Material Properties of Lead-Zirconate Titanate Ceramic Bimorph Used for Proposed Prototype -----	78
8. Analytically Predicted System Parameters Used for Proposed Prototype -----	79

1. INTRODUCTION

The use of microprocessors in advanced control schemes has resulted in an overall improvement in the engineer's ability to monitor and process information. Utilizing the microprocessor requires interfaces between the system to be controlled and the controlling processor. If the plant to be controlled is mechanical, mechanical-electrical transducers are required for feedback information and electromechanical transducers are required for output actuation. This report deals with the introduction of a new electromechanical transducer. The medium of mechanical actuation is air; therefore, the device discussed herein is an electropneumatic converter.

Pneumatic systems offer the advantages of high power, fast response, and economical control hardware. The electropneumatic converters that have been developed so far have tended to be quite slow and expensive. What is needed is a low cost, low electrical power consumption, high speed transducer to take advantage of the benefits of low cost and reliability which could be obtained with an electropneumatic control system.

An electropneumatic system can be a low cost control system. Because of advances in semiconductor technology, electrical signals can now be processed extensively at a low cost. The technology to convert air under pressure to mechanical actuation is a refined art, and the hardware is available and inexpensive. Therefore, a requirement for the electropneumatic transducer is to devise a minimum-cost device to keep the total system cost low.

Another requirement for the converter is reliability. Reliability is an inherent characteristic of pneumatic actuating hardware. Therefore reliability of the converter is required to avoid the possibility of a weak link in the system. This can be achieved through simplicity of design and a minimum of moving parts.

Low electrical power consumption is a desirable feature for a new design. If the power consumption is low enough, the converter could be attached directly

to the output of an inexpensive low-power electrical signal source. This electrical signal source could be the digital to analog output port of a microprocessor. This would eliminate the need for expensive electrical power amplification. An additional benefit of low electrical power consumption is an application where an onboard power supply is required. A device which uses low power could save additional weight and expense through the use of a small power supply.

A final design consideration is speed of response. The microprocessor used to control the system is a very high-speed device. Pneumatic to mechanical hardware is capable of fast response when the volumes are small and air pressure is high. The interface device should also be as fast as possible to maximize the control capabilities of the processor.

The general design plan for a system that fulfills these requirements is now given. A low electrical power consumption electromechanical component is required. The mechanical output of this component will then be converted to a low-level pressure signal. This low-level pressure signal will then be amplified to a usable level.

The device chosen for the electromechanical conversion is a piezoelectric bender element of a bimorph construction¹. The mechanical-pneumatic conversion uses the bimorph as a flapper centered between two nozzles. The device chosen for the pneumatic amplification is the laminar proportional amplifier².

A piezoelectric bimorph provides a displacement for a given applied voltage. This steady-state relationship between the voltage input to the bimorph and its output displacement is nearly proportional. The bimorph has very low electrical power consumption and a fast response. The reliability of the bimorph appears

¹Application Note, Piezoelectric Bender Elements, Piezo Products Division, Gulton Industries, Inc. (1978).

²F.M. Manion and T.M. Drzewiecki, Analytical Design of Laminar Proportional Amplifiers, Proc. HDL State-of-the-Art Symposium, Vol. 1, Adelphi, MD (Oct. 1974).

to be quite good. And lastly, in quantity, bimorphs are relatively inexpensive. This general information is encouraging enough to explore incorporating a piezoelectric bimorph as the major moving-part, electromechanical component in an electropneumatic converter.

While the piezoelectric bimorph can output a steady-state displacement for an applied voltage, its output force capability is limited. Static and dynamic fluid flow forces, due to the air flowing in the nozzles, should be minimized. This minimizes the load forces which would interfere with the displacement due to the applied voltage. As a result, a low supply pressure and small nozzle diameters are necessary to minimize flow forces. This results in small pressures produced downstream of the nozzles. These low-level pressure differences can be amplified to a usable level using laminar proportional amplifiers.

The laminar proportional amplifier (LPA) is a no-moving-part pneumatic amplifier. It is capable of high gain and high bandwidth. The LPA can also operate at very low supply pressures. Because it operates in the laminar region, the LPA has high output fidelity and low noise. The use of a piezoelectric bimorph, functioning as a flapper between two nozzles in conjunction with cascaded LPA amplifiers, to amplify the low level pressure difference available downstream of the nozzles, results in an attractive solution to the electropneumatic conversion problem.

2. CONCEPT OF VALVE DESIGN

Figure 1 is a schematic drawing of the proposed valve concepts^{3,4}. The valve uses a piezoelectric bimorph element centered between two nozzles. This

³C.K. Taft and B.M. Herrick, A Proportional Electro-Fluidic Pneumatic Valve Design, 20th Anniversary of Fluidics Symposium, The American Society of Mechanical Engineers, Chicago, Illinois (1980).

⁴C.K. Taft and B.M. Herrick, A Proportional Piezoelectric Electro-Fluid Pneumatic Servovalve Design, 1981 Joint Automatic Control Conference, The American Society of Mechanical Engineers, Charlottesville, Virginia (1981).

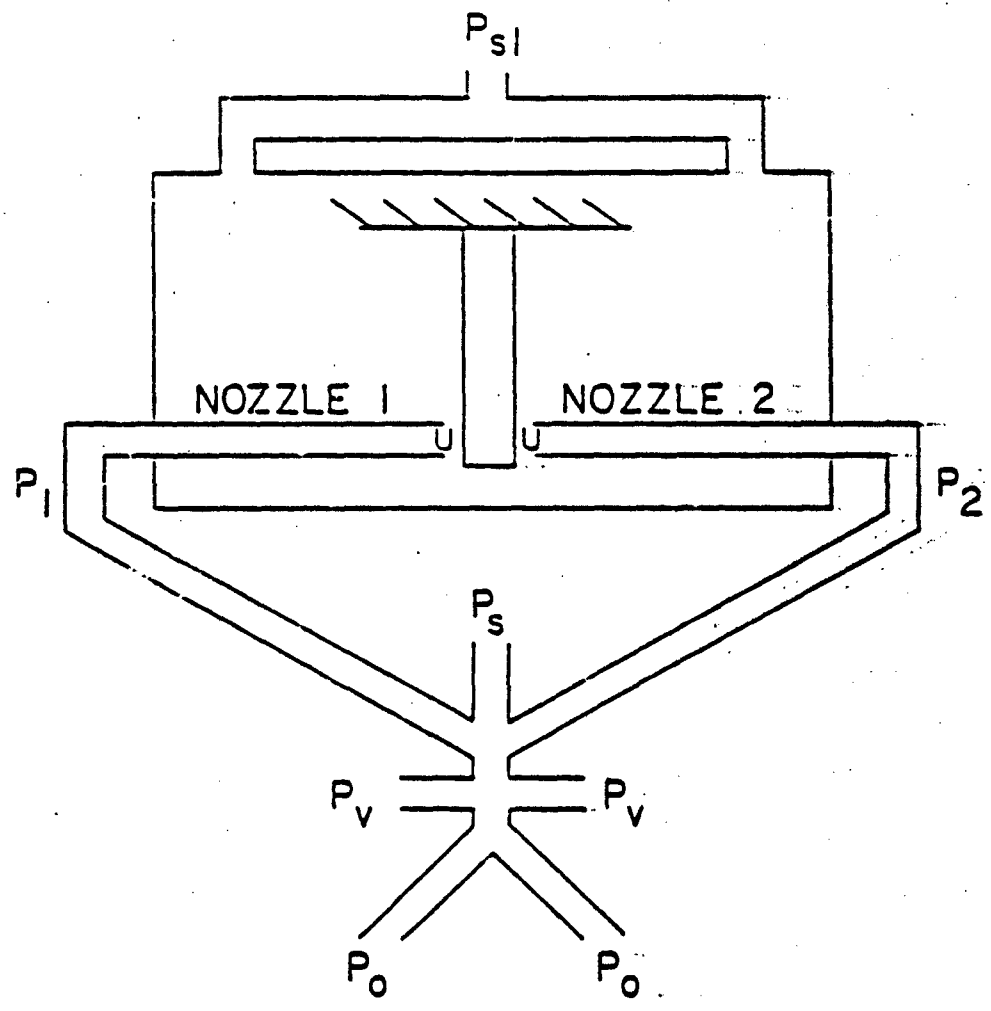


Figure 1. Flapper Valve Schematic

flapper-valve arrangement is pressurized in a chamber by a supply pressure P_{s1} . The pressures, P_1 and P_2 , downstream of the nozzles depend on the location of the bimorph relative to the nozzles.

With a voltage applied to the bimorph as shown in Figure 2, there is a resulting piezoelectric effect which causes the bimorph to deform in such a manner that it will be closer to nozzle 2. The new position of the bimorph results in a difference between the restriction at the entrance to each of the two nozzles. The deflection shown in Figure 2 causes the flow area at the entrance to nozzle 1 to increase and the flow area at the entrance to nozzle 2 to decrease. This will cause the pressure downstream of nozzle 1 to be higher than the pressure downstream of nozzle 2. Therefore, there is a low-level pneumatic signal available at the output of the nozzles. The pneumatic pressure difference is proportional to the electrical input signal for bimorph to nozzle distances less than about one eighth of the nozzle diameter.

This pressure difference is then applied across the input ports of an LPA. While the flapper-nozzle configuration produces a small pressure difference, this difference can be amplified by using several of the LPA amplifiers cascaded together.

Figure 3 illustrates how an LPA operates. A jet of fluid flows from the supply nozzles and traverses a distance where it is separate by a splitting wedge. With zero pressure difference applied to the control ports, the jet is undeflected and assumes the centered position. The same amount of fluid enters each output port which then results in a zero output pressure difference. When a small pressure difference is applied across the jet in the vicinity of the control region, the jet will deflect. The deflection will cause a pressure difference at the output ports. The gain of the amplifier is controlled by its internal geometry. That is, a small jet deflection at the supply nozzle can become substantial at some distance downstream. Typical state-of-the-art amplifier designs result in a pressure gain of ten when the output ports are blocked. These amplifiers can

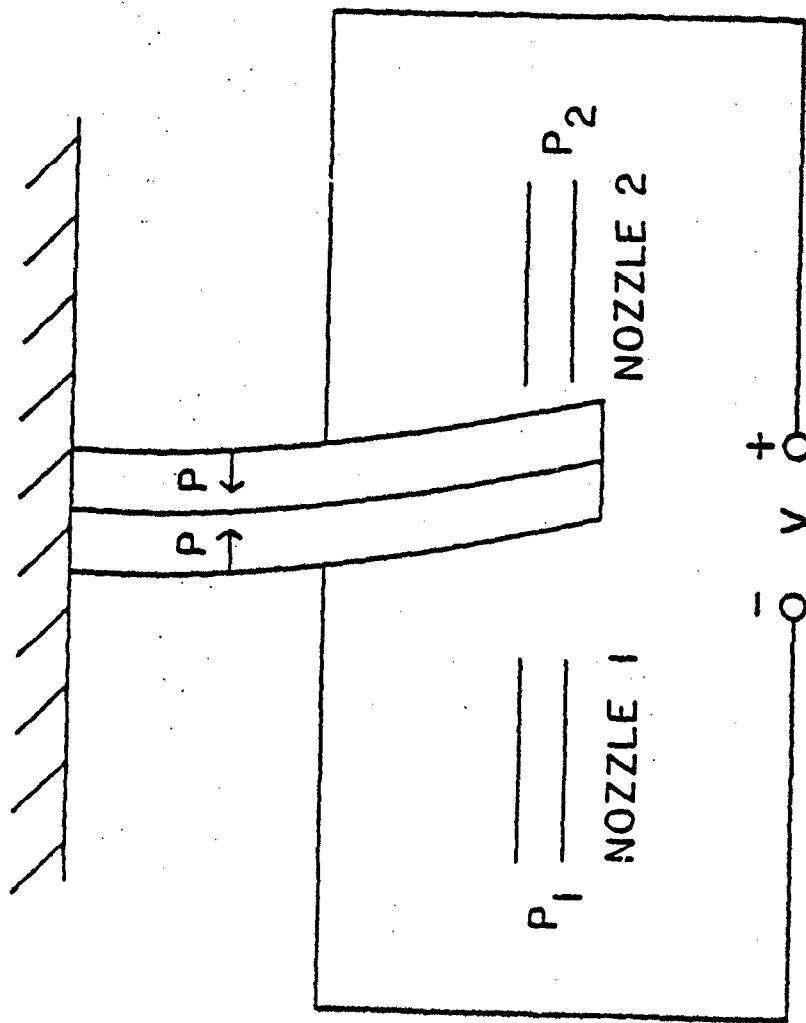


Figure 2. Bender Deformation with Electrical Input Signal

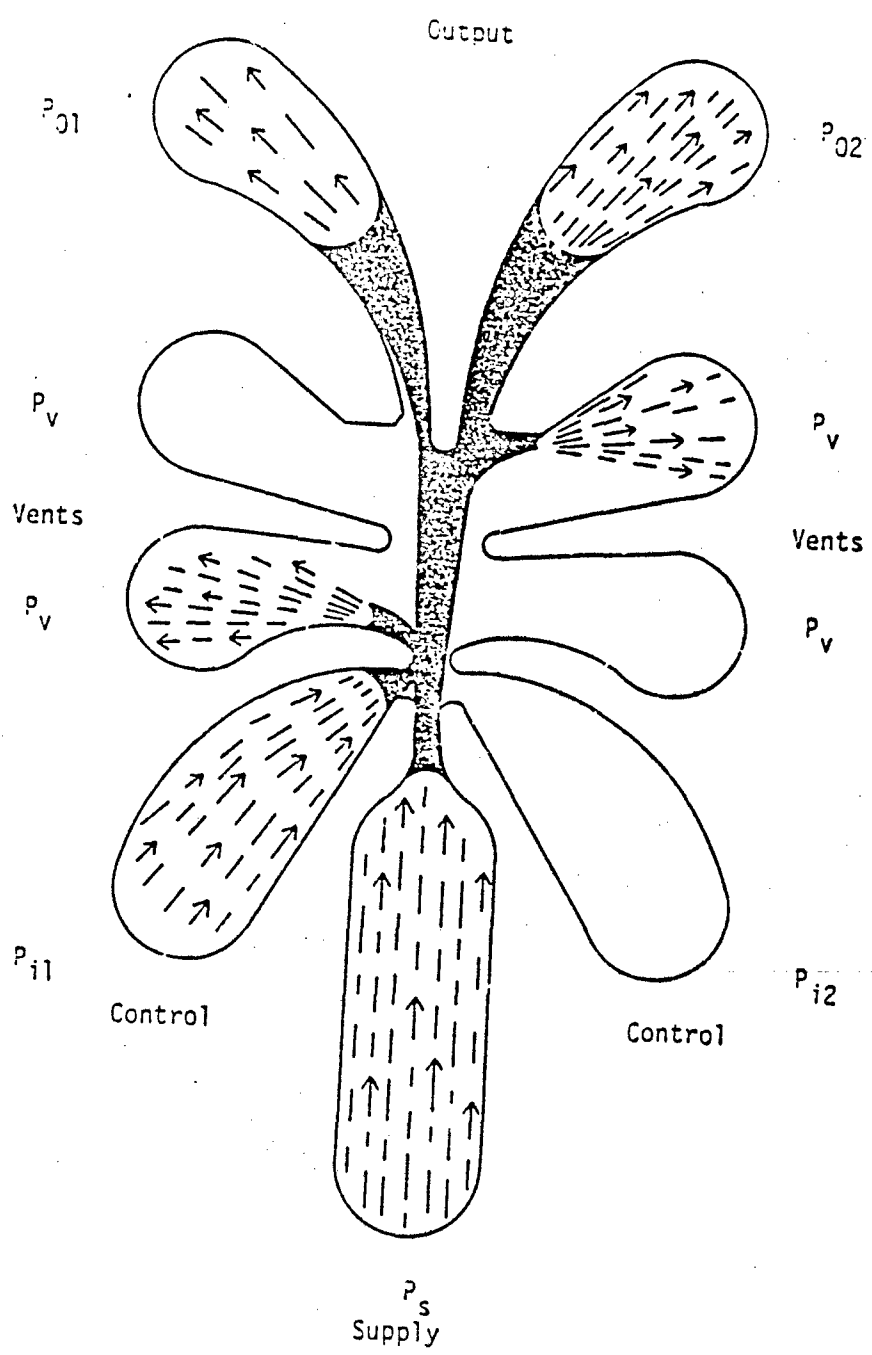


Figure 3. Operation of a Laminar Proportional Amplifier

then be cascaded in series and parallel for impressive system gains in pressure and flow².

The piezoelectric bimorph and the LPA's must now be combined in some way to meet a set of design requirements. For a given application there are several factors that can be varied to change the valve system's output characteristics to suit the application. Examples of output characteristics which can be varied are system sensitivity, bandwidth, pressure, and flow. These factors are all a function of the size and physical characteristics of the piezoelectric bimorph chosen and the size, element thickness, and supply pressure used in LPA assembly.

The LPA is made up of a series of laminations stacked on top of each other. The number of laminations used in each stage of amplification defines an important design parameter, the supply nozzle aspect ratio. The aspect ratio is the supply-nozzle height divided by the supply-nozzle width. Varying the aspect ratio will change the static and dynamic response of the amplifier stage. The aspect ratio is one of the easiest design parameters to vary and which defines the amplifier's characteristics.

Certain qualitative design objectives for an electropneumatic converter can be noted. A given application will require certain output pressure and flow levels. These output characteristics are a function of the LPA design. A matched set of complimentary LPA stages is called an LPA gain block. The gain block may be assembled with each stage arranged in series with the stage before it. It is also possible to arrange a gain block design with some of the stages in parallel with each other.

The series design will maximize the pressure gain that can be obtained. However, the flow level will be relatively low. This will be due to the use of amplifier stages with successively smaller aspect ratios. The use of a smaller

²F.M. Manion and T.M. Drzewiecki, Analytical Design of Laminar Proportional Amplifiers, Proc. HDL State-of-the-Art Symposium, Vol. 1, Adelphi, MD (Oct. 1974).

aspect ratio at each level of amplification is desirable for proper amplifier input-output impedance matching and to maintain laminar flow within the amplifier stages that operate at higher supply pressures.

A series design, with some or all of the amplifier stages within the gain block consisting of identical amplifiers in parallel, will increase the flow through the system. This particular staging technique is shown schematically in Figure 4. The complete set of amplifiers comprising stage 1, stage 2, and stage 3 are all in series with each other. Amplifiers U_2 and X_2 are in parallel with each other, and the amplifiers U_3 , X_3 , Y_3 and Z_3 are also in parallel with each other. The system of Figure 4 will deliver a higher flow at any given output pressure when compared to a similar system which is arranged without the additional parallel amplifiers; but this will occur at the expense of pressure gain. This reduction in pressure gain is due to decreased amplifier input resistance between each series stage.

In addition to designing an overall gain block which is capable of delivering the required output flow and pressure levels, each amplifier in each stage must be designed separately to match the amplifier before and after it. This is accomplished by impedance matching each stage of amplification along with matching jet deflection from one stage to the next. This matching is necessary to assure that in all stages the laminar jet will sweep the same angle for a given input. This will prevent premature saturation of the gain block system.

Also, each stage of amplification must be checked for speed of response. Considering the requirements discussed above, one would usually desire to build a system which is as fast as possible. This is accomplished through proper choice of both the LPA gain block and the piezoelectric bimorph. A smaller bimorph generally results in a faster transduction of electrical energy to motion at the end of the bimorph. As the length of a bimorph is reduced, the motion of its end diminishes, and overall system sensitivity is reduced. This may be compensated for by

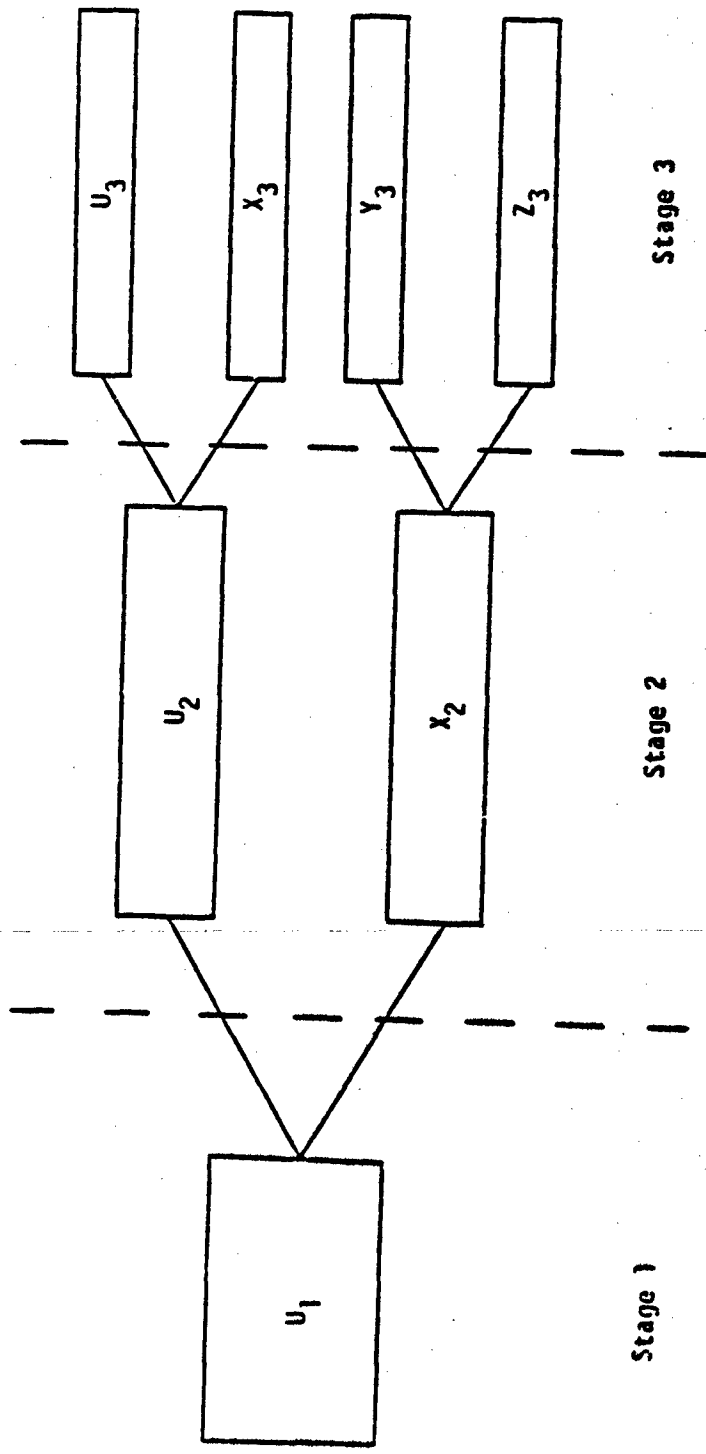


Figure 4. Amplifier Staging Technique

Handwritten notes and scribbles at the bottom of the page, including the number '4' and some illegible markings.

additional stages of amplification, but will result in reduced overall amplifier gain block bandwidth. This reduction in bandwidth is caused by increased signal path length and lower bandwidth found in low supply pressure amplifiers which are required to amplify the reduced output at the nozzles. There is an optimum obtained by trading off bimorph size for the number of amplifier stages.

Finally the static and dynamic fluid forces have to be calculated. Any significant force on the end of the bimorph will degrade its motion. A maximum dynamic flow force coupled with a maximum static pressure area force has to be determined. Thus based on a tolerable maximum flow force, a corresponding maximum supply pressure to the bimorph can be selected. The bimorph supply pressure must then be less than this maximum value.

The above design requirements demonstrate the need for a comprehensive mathematical model describing the behavior of the valve system. With a sufficiently descriptive model, a designer could take a set of specific design requirements and use the model to decide if a given bimorph-LPA system can meet those requirements. This approach to problem solving would both save time and give the designer more insight into how the system works.

The total valve system is broken down into two subsystems. The first subsystem is the electromechanical system consisting of the electrical connection to the bimorph and the piezoelectric bimorph itself. The second subsystem is the mechanical-pneumatic system, which consists of the nozzles and the LPA gain block. The coupling between the two systems is the motion of the end of the bimorph and the fluid forces on it. Section 3 will deal with the development and verification of the electromechanical model. Section 4 will similarly deal with the development of the fluidic model. These two models can then be used with computer simulation to develop a prototype design which will then be built and tested.

3. DEVELOPMENT OF THE ELECTROMECHANICAL MODEL

A dynamic model describing the output motion of the end of the piezoelectric bimorph for a given electrical input is required. This model will enable the designer to select a bimorph and determine if it is suitable for the design requirements that are presented. Before a model can be developed, some general background information on piezoelectric materials and their properties is necessary. This will make the different components of the model easier to understand.

3.1 Piezoelectric Background Material

Certain materials generate an electrical charge when they are deformed. This effect was first discovered by the Curie brothers in 1880. It was also discovered that this is a reversible effect and, therefore, if a charge is applied to one of these materials, deformation will occur. Basic research in this field was performed by Cady⁵, who determined that the electrical polarization of the substance was proportional to its strain and that the effect was sign sensitive. This effect was called the piezoelectric effect, and the materials which exhibited this effect were called piezoelectric materials. It was determined that the piezoelectric effect could only occur in materials that had anisotropic crystal structures.

The piezoelectric effect must not be confused with a similar but fundamentally different effect called electrostriction. The electrostriction effect occurs in all solid dielectric materials. It is a reversible effect, which makes it similar to the piezoelectric effect. The difference occurs because the electrical polarization caused by electrostriction is proportional to the square of the strain. This causes the effect to be sign insensitive. Electrostriction is also smaller in magnitude than piezoelectricity⁶.

⁵W.G. Cady, Piezoelectricity, McGraw Hill Book Co., New York, 1946.

⁶S.Y. Lee, Piezoelectric Actuators for Fluid Control Applications, Eng. Proc., Fluid Control Systems, Pennsylvania State Univ., (July 1965), p. 45.

The two groups of piezoelectric materials which are the most significant and useful are the natural and synthetic crystal group and the polarized ferroelectric ceramic group. The crystal group is comprised of materials such as quartz, lithium sulfate, and rochelle salt. The ferroelectric ceramic group is comprised of materials such as quartz, lithium sulfate, and rochelle salt. The ferroelectric ceramic group is comprised of materials such as barium titanate and lead zirconate titanate. Before any comparisons can be made of any specific examples within these groups, definitions of the general piezoelectric parameters are necessary.

Two main families of constants pertinent to the piezoelectric effect are the g coefficients and the d coefficients. The g coefficient is the ratio of the electrical field strength produced divided by the stress applied. The d coefficient is the ratio of the electrical charge generated divided by the applied force. The nomenclature developed for these coefficients requires a two-digit subscript. The convention used states that the first subscript should indicate the electrical signal field direction and the second subscript the stress direction. Convention also states that the 3-direction is parallel to the direction of piezoelectric polarization of the material. Figure 5 illustrates the coordinate directions and rotations⁷. Since normal and shear stresses can be applied, six directions are specified.

The constant that relates the d coefficient to the g coefficient is called the absolute dielectric constant, ϵ . The absolute dielectric constant is the ratio of the g coefficient divided by the corresponding d coefficient. The magnitude of the dielectric constant gives an indication of the electrical capacitance and dielectric properties of the material.

The product of the g coefficient, the material's elastic modulus, and the d coefficient is the dimensionless parameter, K^2 , which is defined as the square of the coupling coefficient. The coupling coefficient is a measure of the electrical

⁷E.G. Doebelin, Measurement Systems, McGraw Hill Book Co., New York (1975).

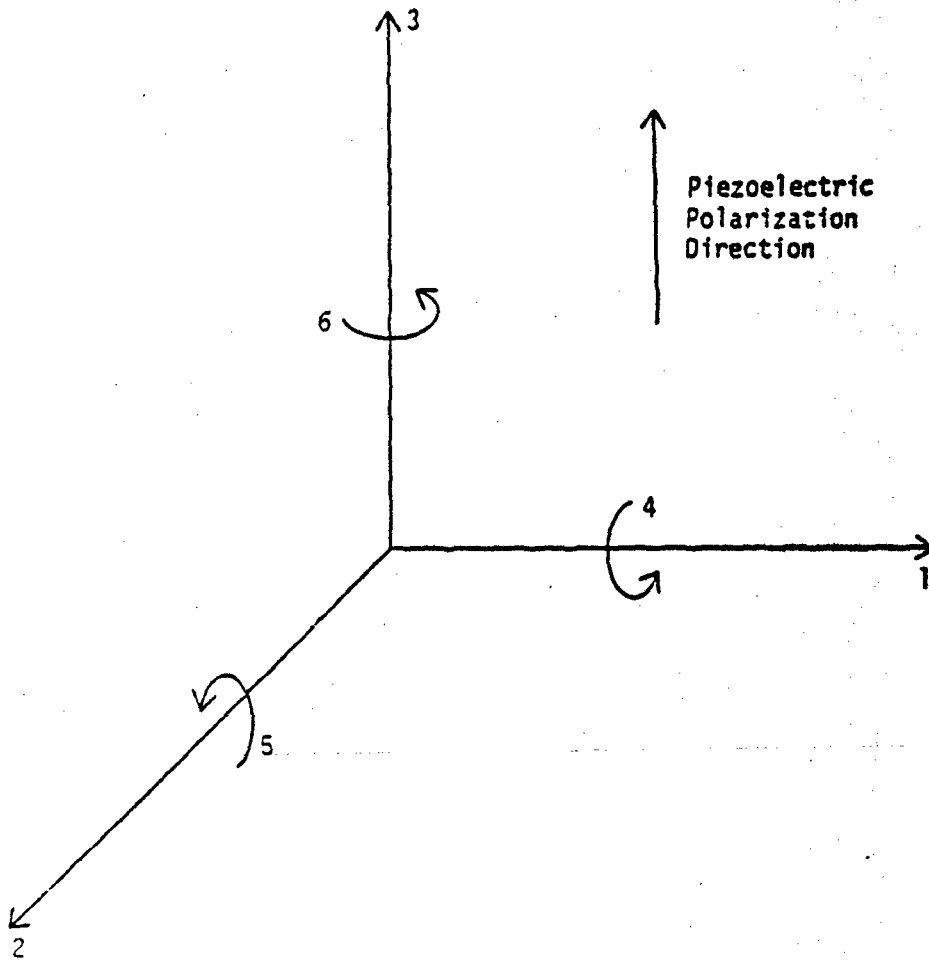


Figure 5. Piezoelectric Convention for Axis System

energy available for a mechanical input. The magnitude of the coupling coefficient is indicative of the relative efficiency of various piezoelectric materials.

The piezoelectric effect is relatively independent of temperature. There is a temperature, though, above which the piezoelectric effect disappears. This temperature is called the Curie point. The Curie point generally occurs at a temperature which results in a crystalline change of phase. This breaks down the anisotropic crystalline structure observed in piezoelectric materials. It is this change of phase which destroys the material's ability to exhibit the piezoelectric effect⁸.

Now that general piezoelectric parameters have been defined, several materials may be examined for their desirability as the material which will comprise the electromechanical component of the converter. Table 1 lists several piezoelectric materials and their properties.

TABLE 1. PIEZOELECTRIC PARAMETERS FOR SELECTED MATERIALS⁸

	d	g	ϵ	E	K	Curie
	Coefficient	Coefficient	Dielectric	Elastic	Coupling	Pt.
	$\times 10^{-12}$	$\times 10^{-3}$	Constant	Modulus	Coefficient	$^{\circ}\text{C}$
	$\frac{\text{meters}}{\text{volt}}$	$\frac{\text{volt-meter}}{\text{newton}}$	$\times 10^{-11}$	$\times 10^{10}$		
			$\frac{\text{farad}}{\text{meter}}$	$\frac{\text{newton}}{\text{meter}}$		
Rochelle Salt	-165	-93	200	1.93	0.53	45
Quartz	-2.3	-5.8	4.5	8.0	0.10	550
Lithium Sulphate	-16	-175	10.3	4.6	0.36	75
Barium Titanate	-148	-16	1150	11.1	0.51	125
Lead Zirconate Titanate	-180	-11	2000	6.0	0.34	330

⁸W.P. Mason, Piezoelectric Crystals and Their Application to Ultrasonics, Van Nostrand, New York, (1950).

Examining the d coefficient provides an opportunity to compare the motion output for an applied voltage. Rochelle salt, barium titanate, and lead zirconate titanate all have relatively high d coefficient values, indicating they would provide a large displacement for a given applied voltage. This property would be advantageous in a flapper design.

The dielectric constant for barium titanate and lead zirconate titanate is relatively high. Since the dielectric constant is a measure of a material's resistance of rupturing with an applied electrical field, both barium titanate and lead zirconate titanate would have relatively high allowable input voltages which would result in larger displacements.

Finally the maximum operating temperatures of the materials are examined. A high maximum operating temperature is desirable for many applications. Normal military specifications, for example, require a maximum operating temperature of 83C. Quartz shows a maximum operating temperature of 550C. This is more than sufficient for most applications. Lead zirconate titanate has a Curie point of 330C, which would make it also acceptable in most applications. Barium titanate has a Curie point of 125C, which would make it a borderline material in military applications. Rochelle salt with a Curie point of 45C makes it unacceptable for military applications.

Considering their sensitivity, dielectric constant and Curie point, barium titanate, lead zirconate titanate, and similar materials are chosen by piezoelectric manufacturers as the materials for production of piezoelectric actuators as the materials for production of piezoelectric motors. Barium titanate and lead zirconate titanate are members of the polarized ferroelectric ceramic group of piezoelectric materials. This group is different than the crystal group in that a processing procedure must be used to give them their piezoelectric properties.

The word ferroelectric is derived from a dielectric analog γ with ferromagnetic. This will become obvious after the processing procedure of the ferroelectric ceramic group is explained. Ferroelectric ceramic substances are polarized by

applying a strong electrical field while heating the substance above its Curie point and then cooling it below the Curie point with the electrical field still applied⁹. The Curie point in this particular case is the temperature at which a polarized ceramic loses its uniform polarization and assumes random polarization. At this temperature there is a breakdown in the piezoelectric properties of the material.

It is not necessary to raise the temperature of a ferroelectric ceramic to its Curie point to polarize it. However, fully polarizing a ferroelectric ceramic requires a much lower electrical field strength if the temperature of the material is raised above its Curie point. The polarization process is more easily understood if the ceramic is considered to be comprised of a set of randomly polarized domains. Therefore an electric field applied to the ceramic will result in an alignment of these domains. A stronger electric field will cause more alignment to occur. There is also a strain and resulting change in dimension that occurs as a result of the applied field. The observed strain of a nonpolarized ferroelectric ceramic is proportional to the square of the applied electric field. Since the strain is also sign insensitive to the applied electric field, the effect observed here is electrostriction and not the piezoelectric effect. Since the ceramic retains some polarization after an electric field has been applied to it, some hysteresis in the steady-state relationship of electrical input versus displacement output should be observed. This is analogous with any type of hysteresis observed in ferromagnetic materials and the reason the material is called ferroelectric⁶.

Once an electrostrictive material is polarized, it develops a sensitivity to bidirectional signals. Also the observed strain is proportional to the applied field in each single domain of the ferroelectric ceramic crystal. This then

⁹E.O. Doebelin, System Dynamics: Modeling and Response, Charles E. Merrill Publishing Co., Columbus, OH (1972).

⁶S.Y. Lee, Piezoelectric Actuators for Fluid Control Applications, Eng. Proc., Fluid Control Systems, Pennsylvania State Univ., (July 1965), p. 45.

indicates that a pure piezoelectric effect is observed in these polarized materials¹⁰. This results in input-output characteristics similar to those found in more traditional piezoelectric materials. Because of this similarity, the same modeling equations that govern the characteristics of piezoelectric materials can be applied to ferroelectric ceramics.

It is now desired to produce a maximum displacement for a given applied voltage. This can be accomplished if the bimorph method of construction is used. Figure 6 is a cross-section of a piezoelectric material with a bimorph construction. Two sheets of material which exhibit piezoelectric properties are each plated on one side with a layer of nickel or silver. The sheets are then bonded to a brass shim to form a bimorph. This same concept may also be extended to multilayered piezoelectric sheets resulting in a multimorph. The multimorph will produce a larger displacement for an applied voltage but consumes more power.

The opposing polarities of the two sheets of piezoelectric material, indicated by Figure 6 demonstrates that this bimorph is to be connected in series with the power supply. If the polarities of the two sheets were aligned, then the bimorph would be connected in parallel to the power supply. A series connection requires twice the voltage to output the same force or displacement as a parallel connection but only half the charge. For this reason a bimorph connected in series to the power supply will have a steady-state input impedance of four times the impedance of the parallel connection.

To further increase the output motion, the bimorph is configured as a bender with the piezoelectric expansion in the length expander mode. The pertinent piezoelectric coefficients in this mode of operation are the g_{31} and the d_{31} coefficients. Therefore, when a voltage is applied to the bender, one piezoelectric component expands while the other contracts. This causes the composite to bend

¹⁰P. L. Anderson, Theory Ferroelectric Behavior of Barium Titanate, Ceramic Age, 57(+), (1951), pp. 29-30, 33, 53-55.

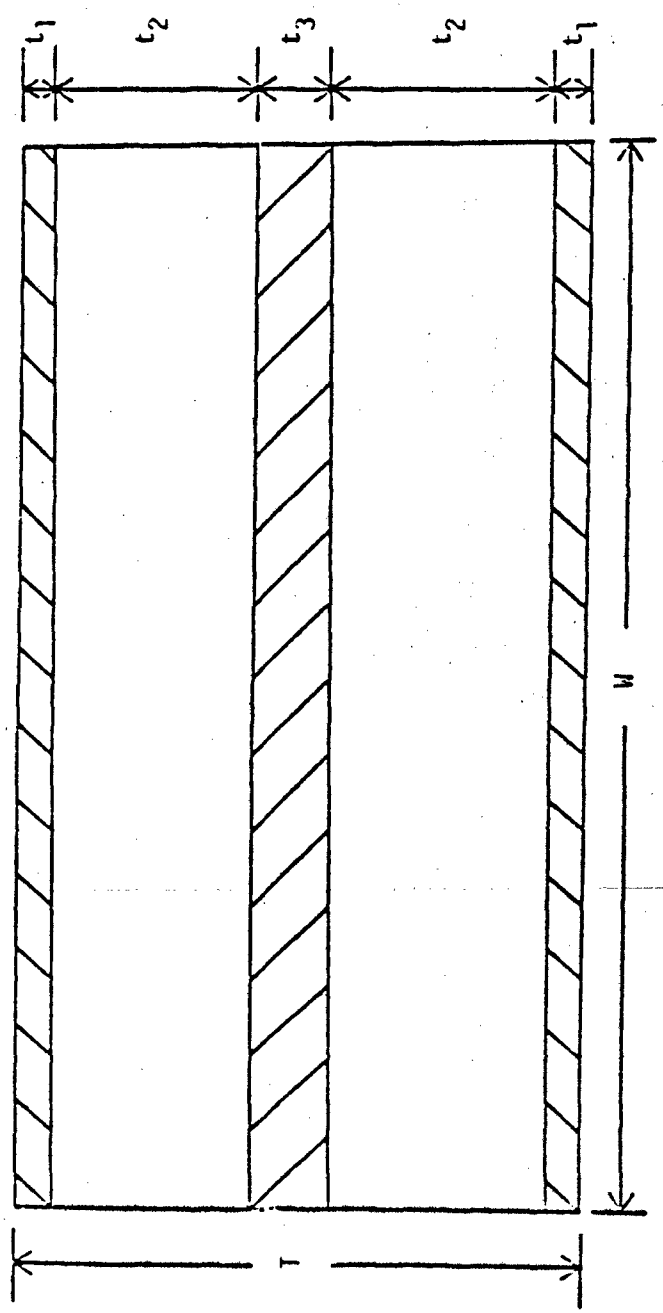


Figure 6. Cross Section of a Piezoelectric Bimorph

like a bimetallic strip. This bender is then used as a flapper in a flapper-nozzle design.

An electromechanical model of the bimorph bender can now be developed and analyzed. The bimorph can be represented by an equivalent mechanical circuit and an equivalent electrical circuit. The two circuits are then combined to provide an overall model relating the motion of the end of the bimorph to the electrical input.

3.2 Equivalent Mechanical Circuit

The first mode transverse motion of the bimorph is modeled as an ideal spring-mass-damper system. Figure 7 shows the bimorph's equivalent mechanical circuit assuming that the motion of the end of the bimorph is nearly in a straight line. This model has been found to be sufficiently accurate for the first mode of vibration of the bimorph.

Summing the forces on the mass element in the X-direction gives

$$M\ddot{X}(t) = -K_s X(t) - B\dot{X}(t) - C_1 V(t) + F_X(t) \quad (1)$$

The mass, M , of the system is an equivalent mass found by matching the frequency of the first mode of vibration for a cantilever mounted beam to that of the simple system shown in Figure 7. The spring constant, K_s , is a parameter which relates the force necessary to produce a given displacement at the end of the bimorph. The damping constant, B , describes a force proportional to the velocity of the end of the bimorph. The product, $C_1 V$, is a coupling force between the mechanical circuit and the electrical circuit. Finally $F_X(t)$ is an external forcing function to represent the fluid flow forces acting on the bimorph in the X-direction.

Taking the Laplace transform of equation (1), setting the initial conditions equal to zero, and solving for $X(S)$ yields

$$X(S) = \frac{F_X(S) - C_1 V(S)}{MS^2 + BS + K_s} \quad (2)$$

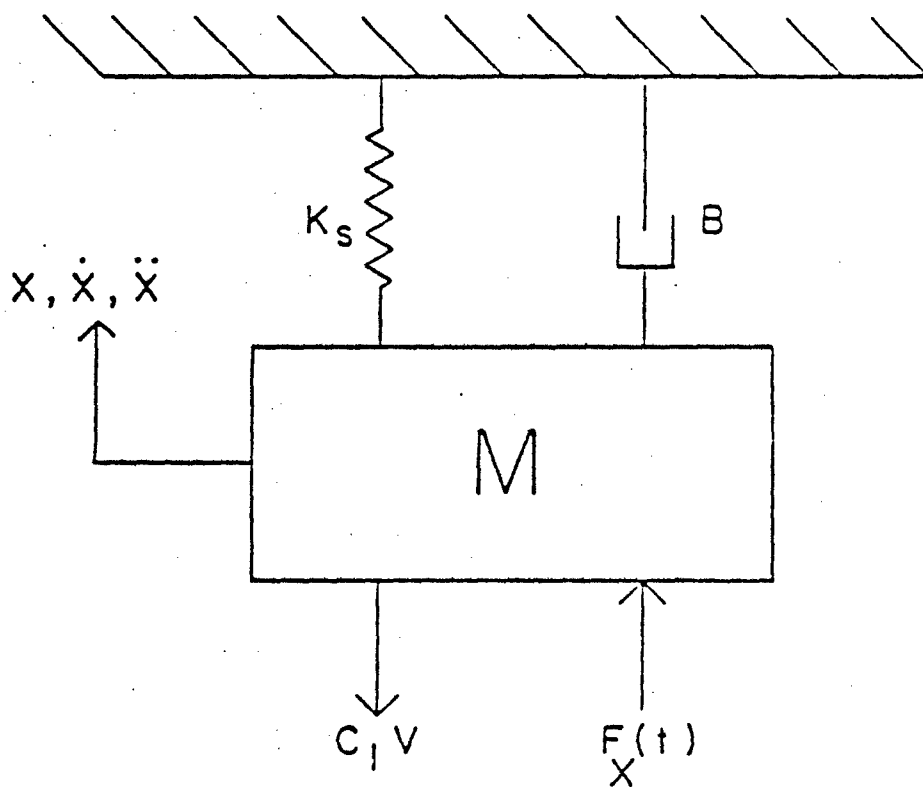


Figure 7. Equivalent Mechanical Circuit

3.3 Equivalent Electrical Circuit

Figure 8 shows an equivalent electrical circuit for the bimorph driven by a voltage source. The bimorph is modeled as a capacitor, C_T , with a leakage resistance, R_T , between the electrical contacts. The current source, K_q , proportional to the velocity of the end of the bimorph, is a result of the charge produced when a piezoelectric device is deformed. The product $K_q \dot{x}$, is the coupling between the electrical system and the mechanical system. It is assumed that the system is driven by an external voltage source, V_A , along with an external series resistor, R_A . The series resistor will be used to modify the frequency response characteristics of the bimorph.

Summing the currents at node V gives

$$K_q \dot{x}(t) - C_T \frac{dV(t)}{dt} - \frac{V(t)}{R_T} - \frac{(V(t) - V_A(t))}{R_A} = 0 \quad (3)$$

Taking the Laplace transform of equation (3) setting the initial conditions equal to zero, and solving for $V(S)$ gives

$$V(S) = \frac{K_q S X(S) + \frac{V_A(S)}{R_A}}{C_T S + \left(\frac{1}{R_T} + \frac{1}{R_A} \right)} \quad (4)$$

Substituting equation (4) into equation (2) and solving for $X(S)$ results in

$$X(S) = \frac{F_X(S) \left[\frac{\bar{C}_T R S + \bar{I}}{K_S} \right] - V_A(S) \left[\frac{R_T C_1}{K_S (R_A + R_T)} \right]}{S^3 \left[\frac{\bar{C}_T M R}{K_S} \right] + S^2 \left[\frac{\bar{C}_T B R + \bar{M}}{K_S} \right] + S \left[\frac{(\bar{C}_T K_S + C_1 K_q) R + \bar{B}}{K_S} \right] + 1} \quad (5)$$

where

$$R = \frac{R_A R_T}{R_A + R_T} \quad (6)$$

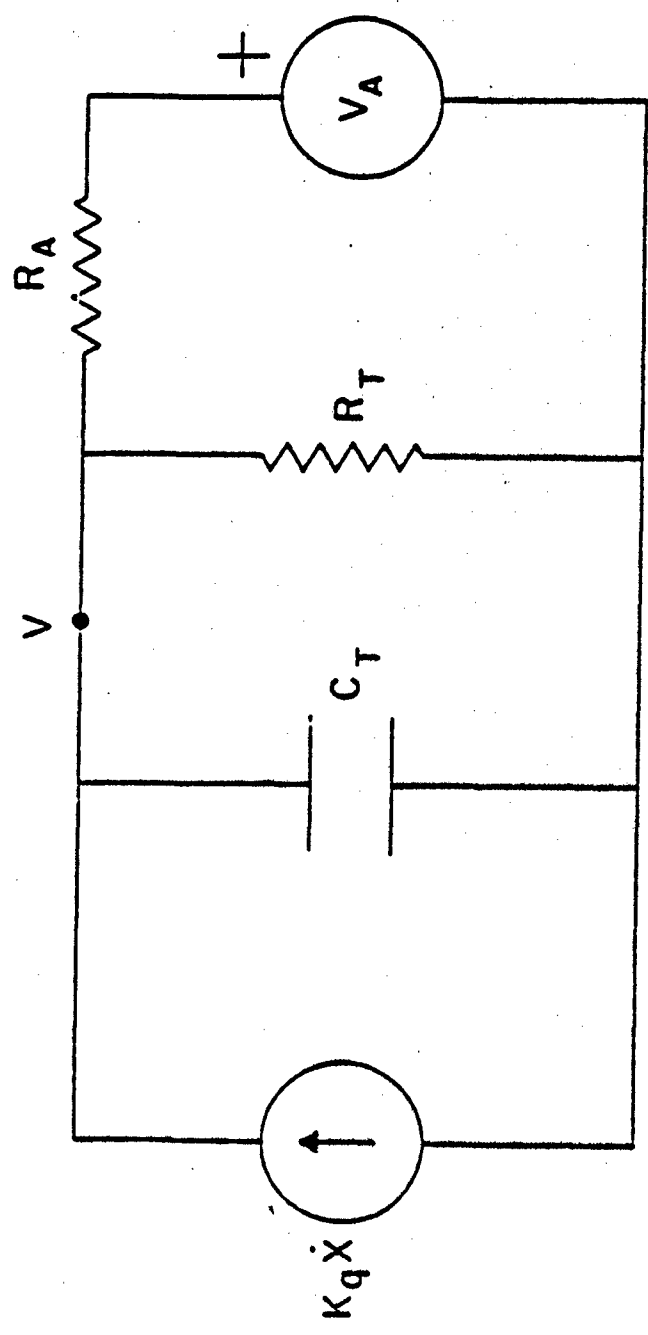


Figure 8. Equivalent Electrical Circuit

3.4 Experimental Verification

Experimental verification of the model was desired to determine its accuracy and resulting suitability for design work. A photo interrupter was used to measure the deflection of the end of the bimorph resulting from an electrical input. The bimorph used to verify the model was of a larger size than the element which was eventually used in the valve. It was necessary to determine the electro-mechanical system parameters, C_T , M , K_S , B , C_1 , K_q , to properly apply the model. The physical and material properties of the test bimorph are given in Table 2. These properties were used to predict the electromechanical system parameters.

TABLE 2. PHYSICAL AND MATERIAL PROPERTIES OF LEAD ZIRCONATE TITANATE CERAMIC BIMORPH USED FOR MODEL TESTING

Property	Measured Value
Length, L	4.3×10^{-2} m
Width, W	1.27×10^{-2} m
Thickness, T	4.9×10^{-4} m
Nickel plate thickness, t_1	1.52×10^{-6} m
Lead zirconate titanate thickness, t_2	1.93×10^{-4} m
Brass shim thickness, t_3	1.03×10^{-4} m
Density, ρ	5.8×10^3 kg/m ³
Piezoelectric charge coefficient, d_{31}	-1.8×10^{-10} m/v
Piezoelectric voltage coefficient, g_{31}	-1.1×10^{-2} v-m/N
Nickel elastic modulus, E_1 (see Appendix A)	1.26×10^{11} N/m ²
Lead zirconate titanate elastic modulus, E_2	1.09×10^{11} N/m ²
Brass elastic modulus, E_3	9.0×10^{10} N/m ²

Lead zirconate titanate was chosen as the ferroelectric ceramic material used to comprise the bimorph. It was chosen because of its high d_{31} coefficient, high dielectric constant, moderately high coupling coefficient, high maximum operating temperature, and commercial availability in bimorph bender form. A series connection was chosen because it allowed a simple electrical connection.

The value of the system spring constant, K_s , can be predicted using beam theory from an expression relating the deflection, Δ , at the free end of a cantilever mounted beam to a force, F' , applied at its end.

$$\Delta = \frac{F'L^3}{3EI} \quad (7)$$

This can be used to obtain an analytical expression for the system spring constant,

$$K_s = \frac{F'}{\Delta} = \frac{3EI}{L^3} \quad (8)$$

Figure 6 illustrates that the material comprising the bimorph is not uniform. Instead, there are laminations of material running lengthwise down the bimorph. An equivalent system spring constant is calculated by creating an equivalent beam with a uniform modulus of elasticity and a resulting equivalent width. Equation (9) can then be applied to obtain the spring constant.

The equivalent width of a lamination varies proportionally with the material's elastic modulus. Therefore,

$$w_{E1} = w \left(\frac{E_1}{E} \right) \quad (9)$$

$$w_{E2} = w \left(\frac{E_2}{E} \right) \quad \text{and} \quad (10)$$

$$w_{E3} = w \left(\frac{E_3}{E} \right) \quad (11)$$

The moment of area of the beam of Figure 6 is given by

$$I = \frac{1}{12} W_{E3} t_3^3 + 2 \left[\frac{1}{3} W_{E2} t_2^3 + W_{E2} t_2 \left(\frac{t_3}{2} \right)^2 \right] + 2 \left[\frac{1}{3} W_{E1} t_1^3 + W_{E1} t_1 \left(\frac{t_3}{2} + t_2 \right)^2 \right]. \quad (12)$$

Substituting the properties of Table 2 into equations (8),(9),(10),(11), and (12) results in an analytically determined system spring constant of $K_s = 310 \text{ N/m}$.

The system spring constant can also be measured to verify this calculation. Recalling equation (1), the spring constant, K_s , can be determined by measuring the displacement due to a steady-state force at the end of the bimorph with the terminals short circuited. The steady-state conditions would require that $\dot{X} = \ddot{X} = 0$, and short circuiting the terminals would make $V = 0$; therefore, equation (1) becomes $K_s X = F_x$. This can be measured experimentally using a photo interrupter to measure displacement and a Celsco force transducer to measure force. This resulted in an experimentally determined system spring constant of, $K_s = 290 \text{ N/m}$.

Another system parameter, the effective mass of the bimorph is obtained by solving the partial differential equation for the first resonant frequency of a cantilever mounted beam modeled by a distributed parameter technique. This first mode natural frequency is set equal to the natural frequency obtained with the single lumped parameter approximation. The bimorph's effective mass can then be found in terms of known system parameters.

The first mode natural frequency of a cantilever mounted beam modeled by a distributed parameter technique is given by Den Hartog¹¹ as

$$\omega_N = 3.52 \sqrt{\frac{EI}{M_A L^3}}. \quad (13)$$

The natural frequency obtained from the single lumped parameter approximation is given by

$$\omega_N = \sqrt{\frac{K_s}{M}}. \quad (14)$$

¹¹J.P. DenHartog, Mechanical Vibrations, McGraw-Hill Book Co., Inc., New York (1956).

Setting equations (13) and (14) equal to each other and using equation (8) results in an expression for the equivalent mass of the bimorph.

$$M = 0.242 M_A \quad (15)$$

where

$$M_A = \rho LWT \quad (16)$$

With the density of the bimorph given in Table 2, the effective mass of the bimorph is calculated to be $M = 3.8 \times 10^{-4}$ kg.

Evaluating the system damping is not as easy. Experience has shown that it is fairly small relative to the other terms. Experimental methods will be used to determine the damping coefficient and the effective bimorph mass, M . If equation (5) is solved for $R_A = 0.0$ and $F_X(S) = 0.0$, the resulting characteristic polynomial is given by

$$\frac{M}{K_S} S^2 + \frac{B}{K_S} S + 1 = 0 \quad (17)$$

This is of the form

$$\frac{1}{\omega_N^2} S^2 + \frac{2\zeta}{\omega_N} S + 1 = 0 \quad (18)$$

where

$$\omega_N = \sqrt{\frac{K_S}{M}} \quad (19)$$

$$\zeta = \frac{B}{2\sqrt{MK_S}} \quad (20)$$

The natural frequency and the damping ratio can be obtained from the experimentally measured step response of the system. Since K_S is known, then both the mass, M , and the damping coefficient, B , can be determined.

Figure 9 is the step response of the system with $R_A = 0.0$ and $F_X(t) = 0.0$. From this figure the damped natural frequency, ω_d , is seen to be $\omega_d = 880 \text{ sec}^{-1}$. Also, using logarithm decrement the damping ratio, ζ , can be shown to be $\zeta = 0.005$. The natural frequency can be determined from the following relationship,

$$\omega_N = \omega_d / \sqrt{1 - \zeta^2} \quad (21)$$

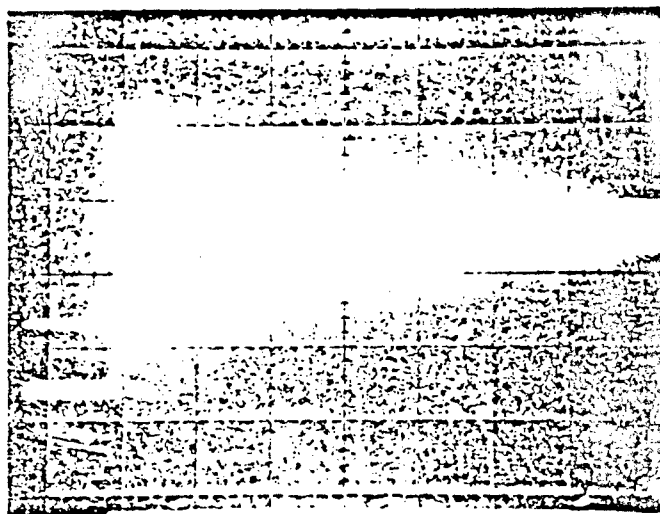


Figure 9. Measured System Step Response

$$R_A = 0.0M.$$

$$F_x(t) = 0.0N$$

Since the damping ratio is so small, the natural frequency is essentially the same as the damped natural frequency and $\omega_N = 880 \text{ s}^{-1}$. The measured effective mass, M , of the system is then calculated to be $M = 3.8 \times 10^{-4} \text{ kg}$. The analytically calculated mass using equation (15) is $M = 3.8 \times 10^{-4} \text{ kg}$, which agrees with the measured value. The system damping is also calculated to be $B = 3.3 \times 10^{-3} \text{ N-sec/m}$.

Equation (2) shows that the piezoelectric force constant, C_1 , can be calculated by dividing the product of the spring constant, K_s , and the steady-state displacement, X , by the applied voltage, V . Also the steady-state displacement, for an applied voltage, at the end of a bimorph with a series electrical connection, is given by¹².

$$X = -2d_{31}V\frac{L^2}{T^2} \quad (22)$$

The piezoelectric force constant, C_1 , is expressed by

$$C_1 = \frac{-K_s X}{V} \quad (23)$$

$$C_1 = 2K_s d_{31} \frac{L^2}{T^2} \quad (24)$$

For the bender of Table 2, C_1 is then calculated to be $C_1 = -8.6 \times 10^{-4} \text{ N/v}$.

The piezoelectric force constant can be verified experimentally. Figure 9 shows that for an applied voltage of 14 V, the steady-state displacement is measured to be $4.0 \times 10^{-5} \text{ m}$. Applying equation (23) results in a measured piezoelectric force constant of $C_1 = -8.3 \times 10^{-4} \text{ N/V}$. This compares favorably with the predicted value of C_1 .

The piezoelectric back current constant can be calculated from a knowledge of the piezoelectric bimorph's properties as a generator. The amount of charge produced is proportional to the applied force. This relationship is given by¹²

$$q = \frac{3}{2} F \frac{L^2}{T^2} d_{31} \quad (25)$$

¹²Piezoceramic Design Note, Gulton Industries, Metuchen, New Jersey, (1978).

Equation (1) shows that, in the steady state with $\dot{X} = \ddot{X} = 0$ and the bimorph open circuited, the applied force is given by

$$F_x = K_s X + C_1 V \quad (26)$$

The voltage potential across the plates of the bimorph can be calculated using Equation (25), (28), (29), (30) and is given by

$$V = \frac{3 FL}{2 WT} g_{31} \quad (27)$$

where the various parameters are defined as

$$q = C_T V \quad (28)$$

$$C_T = \epsilon \frac{LW}{T} \quad (29)$$

$$\epsilon = d_{31}/g_{31} \quad (30)$$

Substituting equations (27) and (26) into equation (25) results in a relationship for the charge produced for a given displacement of the end of the bimorph.

$$\frac{q}{X} = \frac{3}{2} \left[\frac{K_s}{1 - \frac{3}{2} C_1 \frac{L}{WT} g_{31}} \right] \frac{L^2}{T^2} d_{31} \quad (31)$$

Since L, W, and T change very little with the applied force, the piezoelectric back current constant is given by

$$K_q = \frac{\dot{q}}{\dot{X}} = \frac{3}{2} \left[\frac{K_s}{1 - \frac{3}{2} C_1 \frac{L}{WT} g_{31}} \right] \frac{L^2}{T^2} d_{31} \quad (32)$$

Substituting in values for the test bimorph parameters results in a piezoelectric back current constant of $K_q = -7.1 \times 10^{-4} \frac{A-s}{m}$.

The electrical parameters can also be determined analytically. The capacitance of the bimorph, C_T , can be calculated by combining equations (29) and (30),

$$C_T = \frac{d_{31}LW}{g_{31}T} \quad (33)$$

The capacitance of the test bimorph is calculated to be $C_T = 2.7 \times 10^{-8}$ F. For the purpose of the model, the resistance of the bimorph, R_T , is assumed to be infinite. R_T was measured to be greater than 10^{10} ohms, which is very large compared to R_A , so this is a good assumption.

The electrical parameters, C_T , R_T , and R_A , can be verified experimentally. The values for the supply resistor, R_A , and the ferroelectric materials leakage resistance, R_T , can be measured with an ohm meter. The bimorph capacitance, C_T , can be measured as any ordinary capacitor with the motion of the bimorph constrained. The measured value for the bimorph's capacitance is found to be, $C_T = 3.0 \times 10^{-8}$ F. The leakage resistance, R_T , is so large that it is assumed to be open circuited. The supply resistor, R_A , is changed to vary the frequency response characteristics of the bimorph. All of the measured and the analytically predicted system parameters are summarized in Table 3.

TABLE 3. MEASURED AND ANALYTICALLY PREDICTED ELECTRO-MECHANICAL SYSTEM PARAMETERS

Parameter	Measured Value	Analytically Predicted Value
System spring constant, K_s	290 N/m	310 N/m
Effective mass, M	3.8×10^{-4} kg	3.8×10^{-4} kg
System damping, B	3.3×10^{-3} N/m	5×10^{-3} N/m (estimated)
Piezoelectric force constant, C_f	-8.3×10^{-4} N/V	-8.6×10^{-4} N/V
Piezoelectric back current constant, K_q	-	7.1×10^{-4} A-s/m
Bimorph capacitance, C_T	3.0×10^{-8} F	2.6×10^{-8} F

Equation (5) is then simulated on the computer for $F_x(S) = 0.0$ and $V_A(S) = \frac{V_A}{S}$, a step voltage input. The step response of the system is examined analytically predicted system parameters. The analytically determined computer

output is then compared with experimentally determined data. Comparisons between the experimental data and the analytical data, for various values of the supply resistor, are shown in Figures 10, 11, 12, and 13.

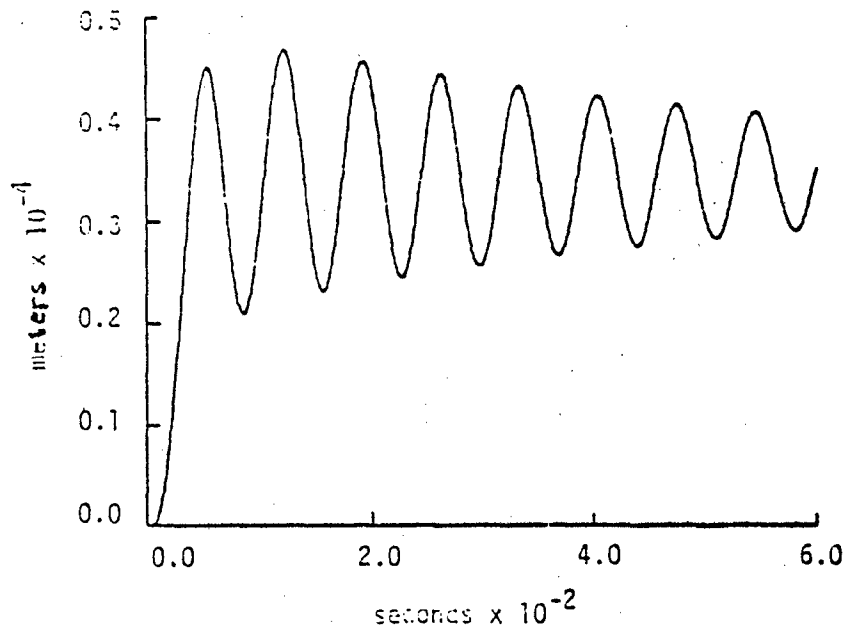
The close match between the analytical data and the experimental data suggests that the model is sufficiently accurate for design work in the frequency range less than the first mode of resonant vibration. This model will be applied in Section 5 in the design of an electropneumatic converter.

4. DEVELOPMENT OF THE FLUID MODEL

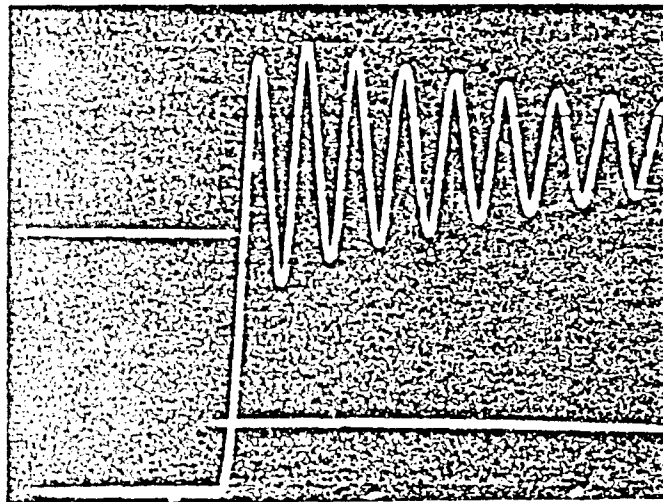
A fluid model describing the output pressure difference of the LPA for a given input motion of the end of the piezoelectric bimorph is needed to match a gain block with a flapper-nozzle system. This is accomplished by combining an equivalent steady-state resistive model for the nozzles with a model for the LPA. A set of static design equations for the LPA is then used to design the LPA gain block. Finally the gain block is checked for speed of response. In this manner an LPA system can be matched to the nozzles.

The effect of static and dynamic fluid flow forces on the dynamic response of the bimorph is also important. Increasing the supply pressure to the bimorph chamber causes flow forces to be exerted on the bimorph. Therefore, the bimorph supply pressure should be reduced to a level that maintains system stability. This problem is approached analytically with a control volume analysis of the flapper-nozzle region.

The goals of the fluid model are twofold. The first goal is to demonstrate that higher supply pressures to the bimorph will result in a potentially unstable dynamic response. This will occur because of the static and dynamic fluid flow forces, which increase with higher bimorph supply pressures. The other goal will be to design an amplifier system capable of a given output pressure and flow with a given system bandwidth.



(a) Simulated

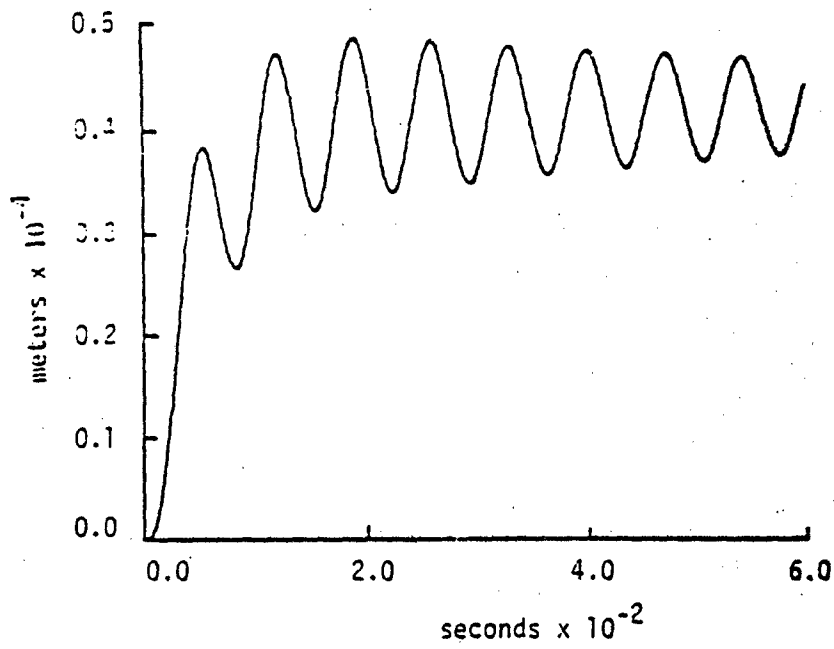


(b) Experimental

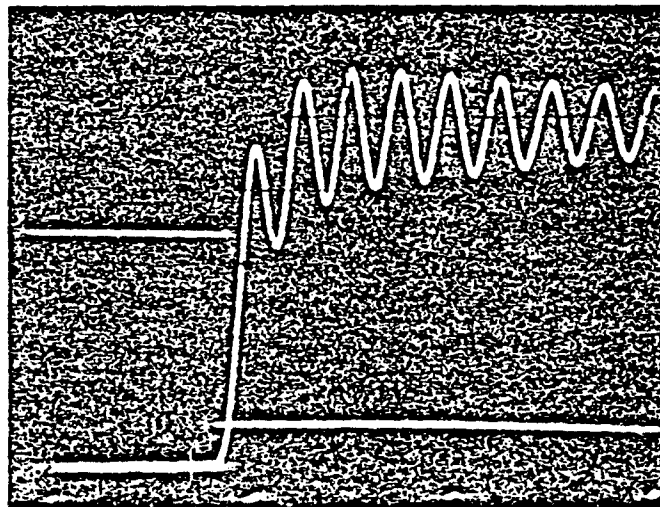
1 Large division horizontal = 1.0×10^{-2} s.

1 Large division vertical = 9.1×10^{-6} m.

Figure 10. System Step Response: (a) Simulated and
(b) Experimental; $R_a = 0.074 M\Omega$, $F_x(t) = 0.0$



(a) Simulated

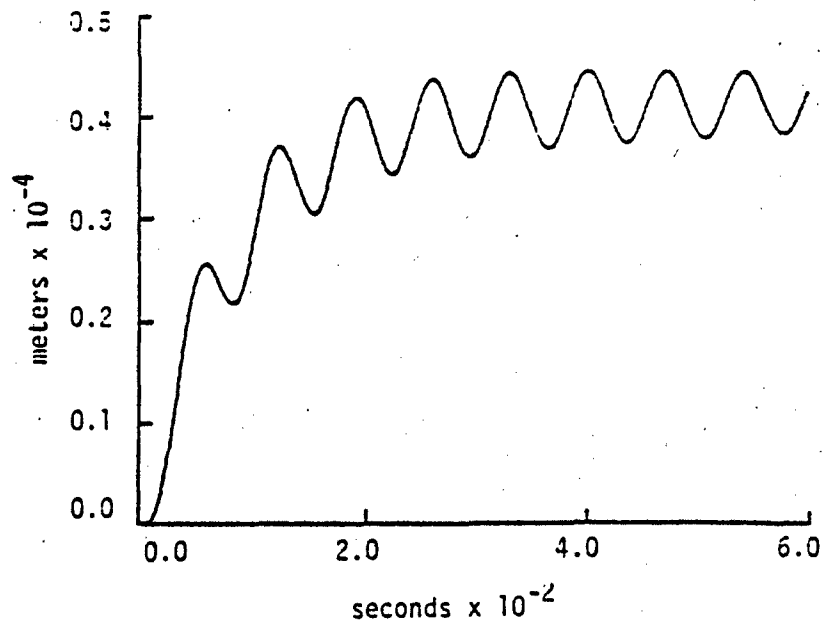


(b) Experimental

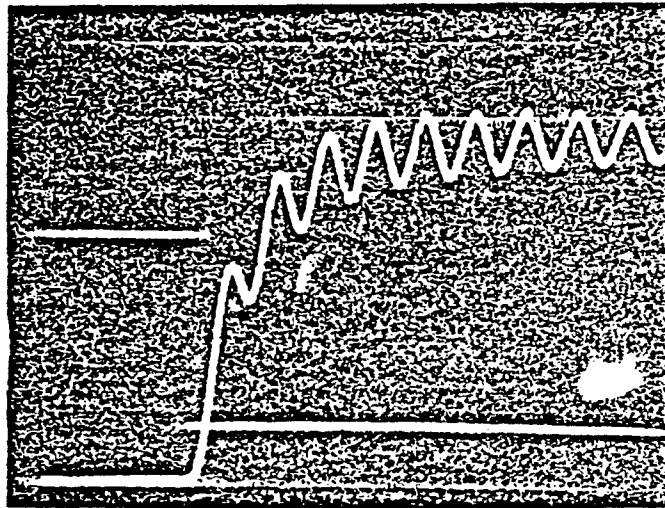
1 Large division horizontal = 1.0×10^{-2} s.

1 Large division vertical = 9.1×10^{-6} m.

Figure 11. System Step Responses: (a) Simulated and (b) Experimental;
 $R_A = 0.142 M\Omega$, $F_x(t) = 0.0$



(a) Simulated



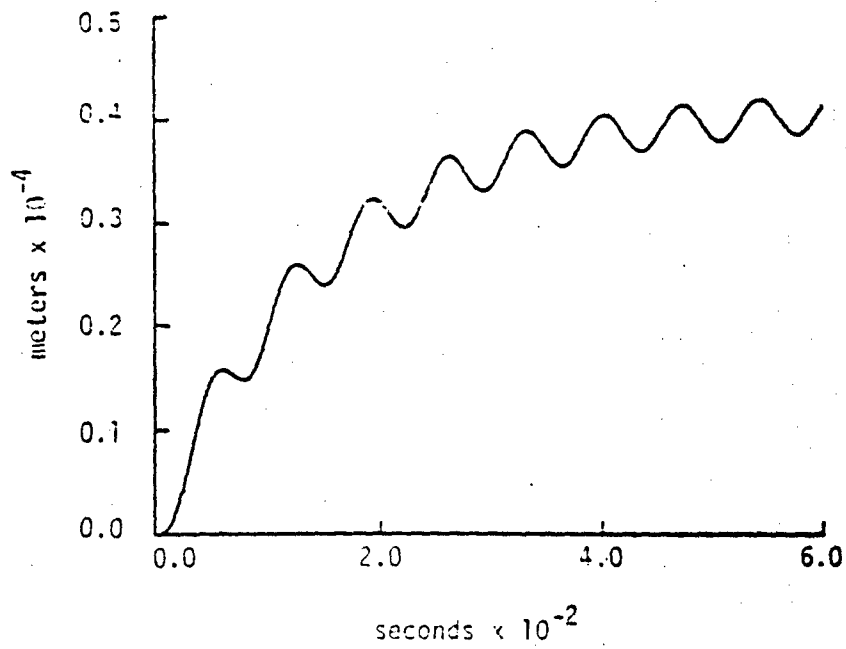
(b) Experimental

1 Large division horizontal = 1.0×10^{-2} s.

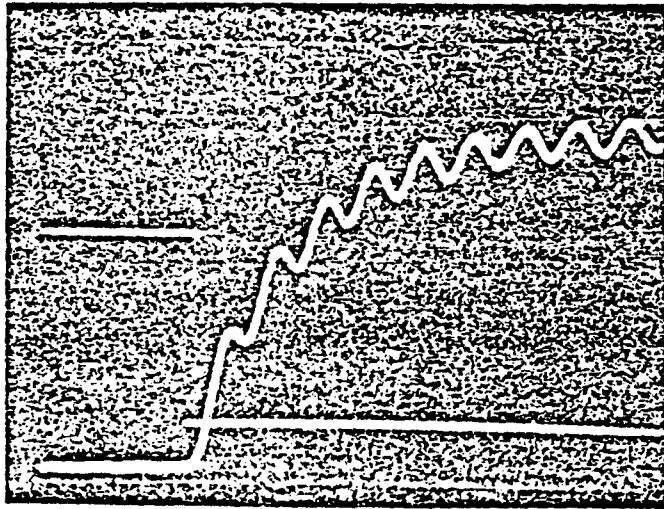
1 Large division vertical = 9.1×10^{-6} m.

Figure 12. System Step Responses: (a) Simulated and (b) Experimental;

$$R_a = 0.260 \text{ M}\Omega, F_x(t) = 0.0$$



(a) Simulated



(b) Experimental

1 Large division horizontal = 1.0×10^{-2} s.

1 Large division vertical = 9.1×10^{-2} m.

Figure 13. System Step Responses: (a) Simulated and (b) Experimental;

$$R_a = 0.480M, F_x(t) = 0.0$$

The flow forces exerted on the bimorph can be calculated using the momentum equation applied to the control volume comprising the air between the bimorph and the nozzle. Figure 14 illustrates this control volume along with the necessary dimensions. Applying the momentum equation for the forces on the control volume, including the force, F , exerted on the control volume by the bender, results in

$$-F - (P_2 - P_1) \pi r^2 = \frac{\partial}{\partial t} \int_{C.V.} \rho \bar{V} dV + \int_{C.S.} \rho \bar{V} (\bar{V} \cdot \hat{n}) dA \quad (34)$$

This vector equation is then rewritten for the force, F_x , exerted by the fluid on the bender in the direction of the motion of the end of the bimorph.

$$F = F_x = (P_1 - P_2) \pi r^2 + \frac{\partial}{\partial t} \left(+ W_1 L_{b1} - W_2 L_{b2} \right) + \left(+ W_1 V_1 - W_2 V_2 \right) \quad (35)$$

Neglecting compressibility, neglecting the rate of change of volume of the control volume due to the motion of the end of the bimorph, and applying the principle of continuity to the control volume of Figure 14 yields

$$W_{1i} = W_{10} = W_1 \quad (36)$$

$$W_{2i} = W_{20} = W_2 \quad (37)$$

Incompressible flow will be assumed because of the low operating supply pressures and low velocities. Using the incompressible flow equations from Anderson¹³ results in

$$W_1 = C_e \pi r(u + x) \sqrt{2(P_{S1} - P_1)/\rho} \quad (38)$$

$$W_2 = C_e \pi r(u - x) \sqrt{2(P_{S1} - P_2)/\rho} \quad (39)$$

$$V_1 = \sqrt{2(P_{S1} - P_1)/\rho} \quad , \quad \text{and} \quad (40)$$

$$V_2 = \sqrt{2(P_{S1} - P_2)/\rho} \quad (41)$$

Substituting in for each component in the momentum equation results in

¹³B.W. Anderson, The Analysis and Design of Pneumatic Systems, John Wiley and Sons, Inc., New York, (1976).

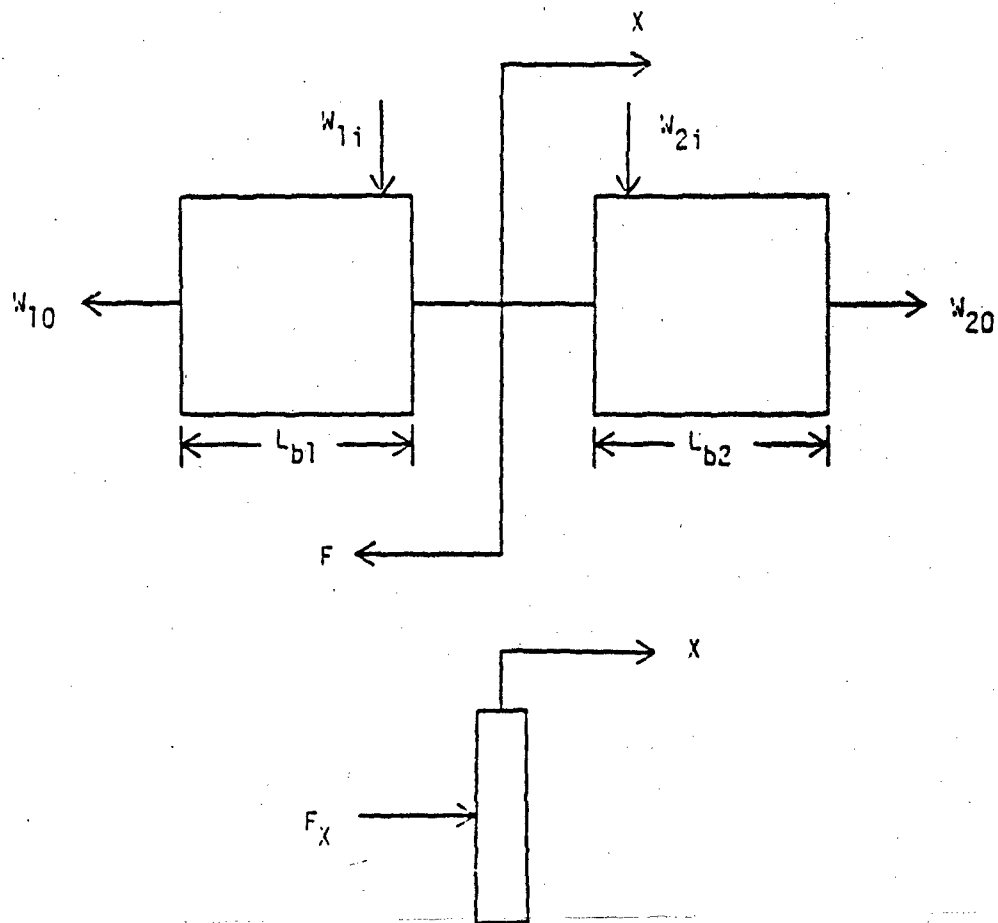


Figure 14. Control Volume for Fluid Flow Forces

$$W_1 V_1 = 2C_e^{-r(u+X)}(P_{S1} - P_1) \quad (42)$$

$$W_2 V_2 = 2C_e^{-r(u-X)}(P_{S1} - P_2) \quad (43)$$

$$W_1 L_{b1} = C_e^{-rL_{b1}} e^{-r(u+X) \sqrt{2(P_{S1} - P_1)/c}} \quad \text{and} \quad (44)$$

$$W_2 L_{b2} = C_e^{-rL_{b2}} e^{-r(u-X) \sqrt{2(P_{S1} - P_2)/c}} \quad (45)$$

where

$$L_{b1} = L_b + u + X \quad (46)$$

$$L_{b2} = L_b + u - X \quad (47)$$

Taking the partial derivative with respect to time of equations (44) and (45) results in

$$\frac{\partial}{\partial t} (W_1 L_{b1}) = (C_e^{-rL_{b1}} e^{-r \sqrt{2(P_{S1} - P_1)/c}}) \dot{X} + \quad (48)$$

$$+ (C_e^{-r(u+X) \sqrt{2(P_{S1} - P_1)/c}}) \dot{X} +$$

$$- (C_e^{-rL_{b1}} e^{-r(u+X) \sqrt{2(P_{S1} - P_1)/c}}) \left(\frac{1}{\sqrt{2(P_{S1} - P_1)}} \right) \dot{P}_1$$

$$\frac{\partial}{\partial t} (W_2 L_{b2}) = - (C_e^{-rL_{b2}} e^{-r \sqrt{2(P_{S1} - P_2)/c}}) \dot{X} + \quad (49)$$

$$- (C_e^{-r(u-X) \sqrt{2(P_{S1} - P_2)/c}}) \dot{X} +$$

$$- (C_e^{-rL_{b2}} e^{-r(u-X) \sqrt{2(P_{S1} - P_2)/c}}) \left(\frac{1}{\sqrt{2(P_{S1} - P_2)}} \right) \dot{P}_2$$

since

$$L_b \gg u + X \Big|_{X=X_{\max}} \quad (50)$$

and

$$L_b \gg u - X \Big|_{X=X_{\min}} \quad (51)$$

Therefore, the second position rate term in equation (48) and (49) is neglected.

McCloy and Martin state that the pressure rate term is small in comparison with the remaining term, so it is also neglected¹⁴.

Making the final substitution into the momentum equation results in

$$F_X = (P_1 - P_2) \pi r^2 + C_e L_b \pi r \left(\sqrt{2(P_{S1} - P_1)/\rho} + \sqrt{2(P_{S1} - P_2)/\rho} \right) \dot{x} + 2 C_e \left[r \dot{x} + (u + x)(P_{S1} - P_1) - (u - x)(P_{S1} - P_2) \right] \quad (52)$$

The pressures P_1 and P_2 must be known before the momentum equation can be solved. A steady-state fluid model is first analyzed to determine these two pressures. Figure 15 is an equivalent resistive circuit for the nozzles and the LPA input.

Using the principle of continuity at the P_{C1} node and the P_{C2} node, respectively, results in

$$W_1 = W_e + W_{A1} \quad (53)$$

$$W_2 = W_e = W_{A2} \quad (54)$$

Using the equations developed by Manion and Drzewiecki² for the LPA input results in an expression for the jet entrainment flow,

$$W_e = \rho Q_e \quad (55)$$

where

$$Q_e = \left[\frac{1.651}{C_d} \left(0.021 C_d C_0 + \frac{C_0 B_C}{N_R} \right)^{1/3} - \frac{1}{2} \right] Q_s \quad (56)$$

and

$$Q_s = C_d h b_s \sqrt{2P_s/\rho} \quad (57)$$

$$N_R = (b_s/\rho) \sqrt{2(P_s - P_v)/\rho} \quad (58)$$

¹⁴D. McCloy and H.R. Martin, The Control of Fluid Power, John Wiley and Sons, Inc. New York (1973).

²F.M. Manion and T.M. Drzewiecki, Analytical Design of Laminar Proportional Amplifiers, Proc. HDL State-of-the-Art Symposium, Vol. 1, Adelphi, MD (Oct. 1974).

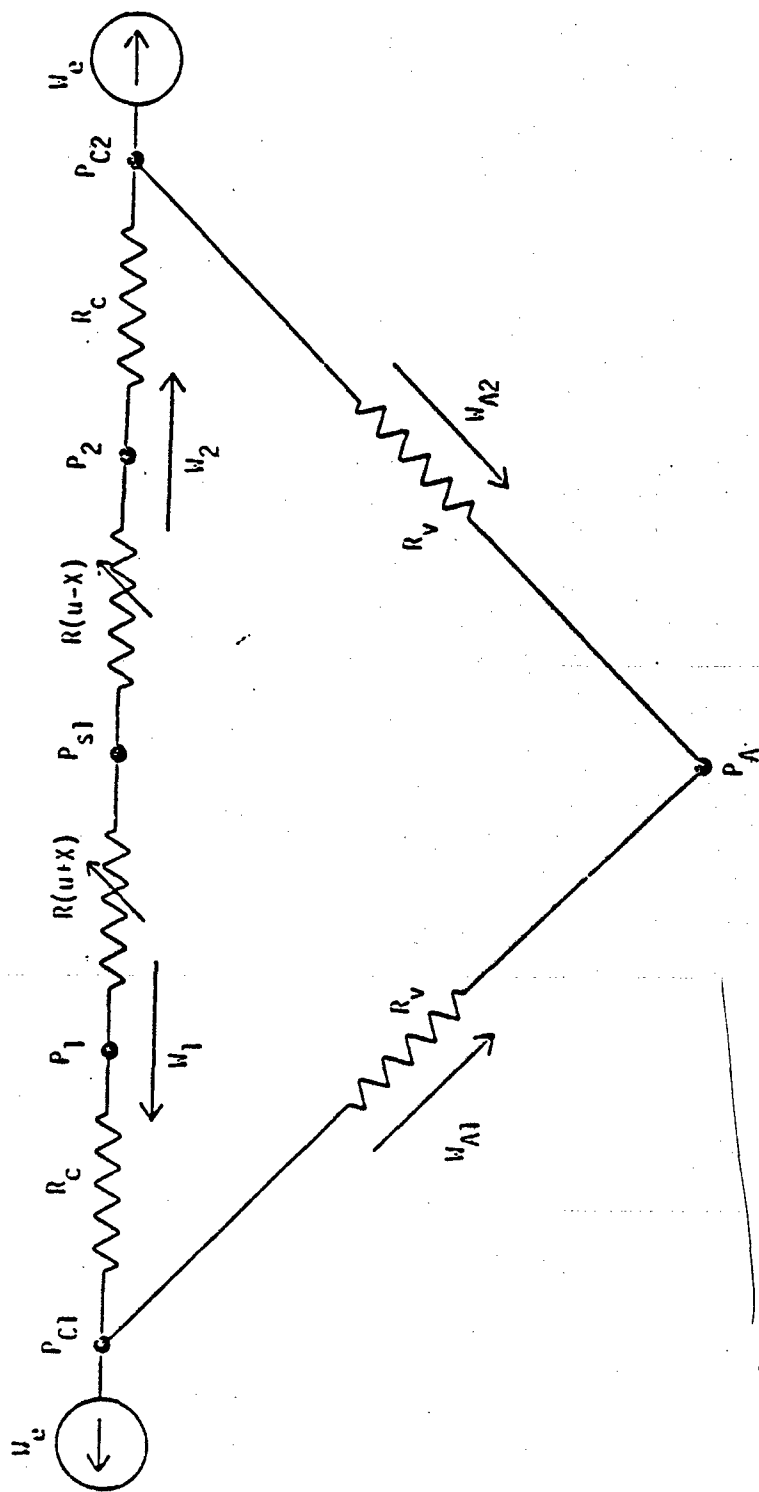


Figure 15. Equivalent Steady-State Circuit

Solving for the LPA input channel resistance² results in

$$R_c = \frac{24 X_c C_d}{\bar{B}_c \sigma N_R} \left[\frac{\sigma}{\bar{B}_c} \left(1 + \left(\frac{\bar{B}_c}{\sigma} \right)^2 \right) + 0.35 \right] R_s, \quad (59)$$

where

$$R_s = \frac{P_s}{Q_s} \quad (60)$$

The LPA vent resistance², R_v , has been found to equal

$$R_v = 3.0 R_s \quad (61)$$

Returning to Figure 15 and solving for the flow escaping from the vents, on side 1, results in

$$W_{A1} = \left(\frac{P_{C1} - P_A}{R_v} \right) \rho \quad (62)$$

where

$$P_{C1} = P_1 - \frac{R_c}{\rho} W_1 \quad (63)$$

Substituting equation (63) into equation (62) and solving for the vent flow using gauge pressures results in

$$W_{A1} = \left(\frac{P_1}{R_v} \right) \rho - \left(\frac{R_c}{R_v} \right) W_1 \quad (64)$$

Similarly,

$$W_{A2} = \left(\frac{P_2}{R_v} \right) \rho - \left(\frac{R_c}{R_v} \right) W_2 \quad (65)$$

Substituting equation (64) and equation (66) into equation (53) and equation (54), respectively, results in

$$W_1 \left[1 + \frac{R_c}{R_v} \right] - \left(\frac{P_1}{R_v} \right) \rho - W_e = 0, \quad (66)$$

$$W_2 \left[1 + \frac{R_c}{R_v} \right] - \left(\frac{P_2}{R_v} \right) \rho - W_e = 0 \quad (67)$$

Equations (52), (66), and (67) describe the fluid flow forces, F_x , exerted on the bender by the nozzles and the pressures, P_1 and P_2 , downstream of the nozzles.

These equations are a set of nonlinear differential equations which can be linearized about an operating point and then applied to the mechanical model. Rewriting equations (52), (66), and (67) by substituting for the control flows and separating the inputs, X , \dot{X} , from the outputs, P_1 , P_2 , F_X , results in

$$W_1'(P_1, X) = A_1(u + X)\sqrt{P_{S1} - P_1} - A_2P_1 - A_3 = 0 \quad (68)$$

$$W_2'(P_2, X) = A_1(u - X)\sqrt{P_{S1} - P_2} - A_2P_2 - A_3 = 0 \quad (69)$$

$$F_X(P_1, P_2, X, \dot{X}) = A_4(P_1 - P_2) + A_5\dot{X}(\sqrt{P_{S1} - P_1} + \sqrt{P_{S1} - P_2}) + A_6((u + X)(P_{S1} - P_1) - (u - X)(P_{S1} - P_2)), \quad (70)$$

where

$$A_1 = C_e \rho \pi r \left(1 + \frac{R_c}{R_v}\right) \sqrt{2/\rho} \quad (71)$$

$$A_2 = \rho/R_v \quad (72)$$

$$A_3 = W_e \quad (73)$$

$$A_4 = \pi r^2 \quad (74)$$

$$A_5 = C_e \rho L_b \pi r \sqrt{2/\rho} \quad (75)$$

$$A_6 = 2C_e \pi r \quad (76)$$

Linearizing equations (68), (69), and (70) about $P_1 - P_2 = 0$, $X = 0$, $\dot{X} = 0$ defines an operating point where the bimorph is stationary and undeflected and the laminar jet is centered. Solving for this point results in

$$A_1 u \sqrt{P_{S1} - P_{10}} - A_2 P_{10} - A_3 = 0 \quad (77)$$

$$A_1 u \sqrt{P_{S1} - P_{20}} - A_2 P_{20} - A_3 = 0 \quad (78)$$

$$F_X = 0 \quad (79)$$

Because of symmetry at the operating point which can be noted in equations (77) and (78), the operating point bias pressures, P_{10} and P_{20} , are equal.

$$P_{10} = P_{20} = P_0 \quad (80)$$

Solving for the input bias pressure from equation (77) or equation (78) results in an equation in quadratic form,

$$\frac{A_2^2}{A_1^2 u^2} P_0^2 + \left(\frac{2A_2 A_3}{A_1^2 u^2} + 1 \right) P_0 + \left(\frac{A_3^2}{A_1^2 u^2} - P_{S1} \right) = 0 \quad (81)$$

Solving equation (81) results in an expression for the amplifier bias pressure for a given bimorph input pressure. Linearizing equations (68), (69), and (70) about the defined operating point, using a Taylor series expansion, and neglecting the higher order terms, results in

$$W_1'(P_0 + \delta P_1, X_0 + \delta X) = W_1'(P_0, X_0) + \left. \frac{\partial W_1'}{\partial P_1} \right|_0 \delta P_1 + \left. \frac{\partial W_1'}{\partial X} \right|_0 \delta X = 0 \quad (82)$$

$$W_2'(P_0 + \delta P_2, X_0 + \delta X) = W_2'(P_0, X_0) + \left. \frac{\partial W_2'}{\partial P_2} \right|_0 \delta P_2 + \left. \frac{\partial W_2'}{\partial X} \right|_0 \delta X = 0 \quad (83)$$

$$F_X(P_0 + \delta P_1, P_0 + \delta P_2, X_0 + \delta X, \hat{X}_0 + \delta \hat{X}) = F_X(P_0, X_0, \hat{X}_0) + \left. \frac{\partial F_X}{\partial P_1} \right|_0 \delta P_1 + \left. \frac{\partial F_X}{\partial P_2} \right|_0 \delta P_2 + \left. \frac{\partial F_X}{\partial X} \right|_0 \delta X + \left. \frac{\partial F_X}{\partial \hat{X}} \right|_0 \delta \hat{X} \quad (84)$$

where

$$\delta P_1 = P_1 - P_0 \quad (85)$$

$$\delta P_2 = P_2 - P_0 \quad (86)$$

$$\delta X = X - X_0 = \hat{X} \quad (87)$$

$$\delta \hat{X} = \hat{X} - \hat{X}_0 = \hat{X} \quad (88)$$

Evaluating equation (82) and solving for the pressure at nozzle 1 results in

$$P_1 = \frac{2A_1 u P^2 - 2A_3 P + A_1 u P_0 + 2A_1 P^2 X}{A_1 u + 2A_2 P} \quad (89)$$

Similarly, evaluating equation (83) and solving for the pressure at nozzle 2 results in

$$P_2 = \frac{2A_1 u P^2 - 2A_3 P + A_1 u P_0 - 2A_1 P^2 X}{A_1 u + 2A_2 P} \quad (90)$$

where

$$P = \sqrt{P_{S1} - P_0} \quad (91)$$

Evaluating equation (84) results in a linearized expression for the system fluid flow-forces.

$$F_X = (A_4 - A_6 u)(P_1 - P_2) + 2A_6 P^2 X + 2A_5 P \dot{X} \quad (92)$$

Substituting equations (89) and (90) into equation (92) results in a final expression for the linearized system fluid flow forces as a function of the position and the velocity of the end of the bimorph.

$$F_X = \left[\frac{4A_1 P^2 (A_4 - A_6 u)}{A_1 u + 2A_2 P} + 2A_6 P^2 \right] X + \left[2A_5 P \right] \dot{X} \quad (93)$$

Taking the Laplace transform of equation (93), setting the initial conditions equal to zero, and solving for $F_X(S)$ gives

$$F_X(S) = X(S)(C_0 + C_2 S) \quad (94)$$

The constant C_0 is the fluid system spring constant and C_2 is the fluid system damping coefficient.

$$C_0 = \frac{4A_1 P^2 (A_4 - A_6 u)}{A_1 u + 2A_2 P} + 2A_6 P^2 \quad (95)$$

$$C_2 = 2A_5 P \quad (96)$$

Substituting equation (94) into equation (5) and solving for $X(S)/V_A(S)$ gives

$$\frac{X(S)}{V_A(S)} = \frac{-C_5 / (1 - C_0 C_4)}{\left[\frac{C_6}{1 - C_0 C_4} \right] S^3 + \left[\frac{C_7 - C_2 C_3}{1 - C_0 C_4} \right] S^2 + \left[\frac{C_8 - C_0 C_3 - C_2 C_4}{1 - C_0 C_4} \right] S + 1} \quad (97)$$

where

$$C_3 = \frac{C_T R}{K_S} , \quad (98)$$

$$C_4 = \frac{1}{K_S} , \quad (99)$$

$$C_5 = \frac{R_T C_1}{K_S (R_A + R_T)} , \quad (100)$$

$$C_6 = \frac{C_T M R}{K_S} , \quad (101)$$

$$C_7 = \frac{C_T B R + M}{K_S} , \quad (102)$$

$$C_8 = \frac{(C_T K_S + C_1 K_q) R + B}{K_S} . \quad (103)$$

It has been experimentally determined that increasing the supply pressure to the bimorph has a destabilizing effect on the system's dynamic response. Equation (97) will be used in Section 5 with specific LPA and bimorph parameters to demonstrate that this is a result of the static and dynamic fluid flow-forces exerted on the bimorph by the nozzle.

Equations (89) and (90) can be used to predict the pressures, P_1 and P_2 , which are output from the flapper-nozzle and are the input to the LPA. Once P_1 and P_2 are known as a function of the flapper-nozzle configuration, a set of LPA design equations can be utilized to amplify this pressure signal to a usable level. The LPA design equations are a set of steady-state design equations. The LPA design method used to devise an LPA gain block is to design it statically and then go back and check if it is fast enough for the intended purpose.

The steady state LPA design equations for pneumatic application are given by¹⁵

Reynolds number, dimensionless

$$N_R = (b_s/v)\sqrt{2(P_s - P_v)/\rho} \quad (104)$$

Modified Reynolds number, dimensionless

$$N'_R = \frac{N_R}{2\left(1 + \frac{1}{\sigma}\right)^2} \quad (105)$$

Supply pressure, mm Hg

$$P_s = 4\left(\frac{N'_R}{120}\right)^2\left(\frac{1}{\sigma}\right)^2\left(\frac{0.5}{B_s}\right)^2 \quad (106)$$

Supply flow, LPM

$$Q_s = 0.3\left(\frac{N'_R}{120}\right)\left(\frac{b_s}{0.5}\right) \quad (107)$$

Supply nozzle fluid resistance, mm Hg/LPM

$$R_s = 13.3\left(\frac{N'_R}{120}\right)\left(\frac{1}{\sigma}\right)^2\left(\frac{0.5}{b_s}\right)^2 \quad (108)$$

Amplifier input resistance, mm Hg/LPM

$$R_i = 0.75 R_s \quad (109)$$

Amplifier output resistance, mm Hg/LPM

$$R_o = 0.50 R_s \quad (110)$$

Aspect ratio, dimensionless

$$\sigma = h_s/b_s \quad (111)$$

Gain, dimensionless

$$G_p = G_{PB} \left[\frac{1}{1 + R_o/R_L} \right] \quad (112)$$

$$G_p = \frac{\Delta P_o}{\Delta P_i}$$

These equations will produce results in the units shown if b_s is given in mm. To maximize the gain of the amplifiers, the modified Reynolds number, N'_R , is chosen as large as possible while keeping the LPA in a laminar region. The maximum modified

¹⁵ Harry Diamond Laboratories Staff, Technical Sheet FC-104, U.S. Army Harry Diamond Laboratories, Adelphi, Md (1977).

Reynolds number, N'_R , for laminar flow in the LPA has been determined by Manion² to be 120. For maximum gain, each stage of amplification will then operate at a supply pressure that will result in a modified Reynolds number of 120.

The dynamic range of an amplifier is defined as the ratio of the largest input to the smallest input to the amplifier that gives uniform gain. For maximum dynamic range, each stage of the LPA gain block should saturate at the same time. This means that for a given pressure difference input, each jet in each stage should sweep the same angle. This will prevent premature saturation of the entire gain block due to saturation of an intermediate stage. This can be accomplished, as shown below, utilizing the LPA design equations¹⁶.

If the gain block is considered to be comprised of N stages of amplification, then the output pressure of the N stage equals the input pressure to that stage multiplied by its gain. Therefore,

$$P_o(N-1) = P_o(N)/G_p \quad (113)$$

Moreover, since the supply pressure is linearly related to the output pressure¹⁶

$$P_s(N-1) = P_s(N)/G_p \quad (114)$$

Equation (106) gives,

$$P_s(N-1) = 4 \left(\frac{N'_R(N-1)}{120} \right)^2 \left(\frac{1}{\sigma(N-1)} \right)^2 \left(\frac{0.5}{b_s(N-1)} \right)^2 \quad (115)$$

and

$$P_s(N) = 4 \left(\frac{N'_R(N)}{120} \right)^2 \left(\frac{1}{\sigma(N)} \right)^2 \left(\frac{0.5}{b_s(N)} \right)^2 = G_p P_s(N-1) \quad (116)$$

If all N stages of amplification are assumed to operate at the same modified Reynolds number and each stage has the same nozzle width, then the optimum aspect ratio for maximum dynamic range is derived by combining equations (115) and (116).

²F.M. Manion and T.M. Drzewiecki, Analytical Design of Laminar Proportional Amplifiers, Proc. HDL State-of-the-Art Symposium, Vol. 1, Adelphi, MD (Oct. 1974).

¹⁶T.M. Drzewiecki, A Fluidic Audio Intercom, 20th Anniversary of Fluidics Symposium, The American Society of Mechanical Engineers, (1981).

This is given by

$$\frac{\sigma(N)}{\sigma(N-1)} = 0.3 \quad , \quad (117)$$

where

$$G_p = 10.$$

These are generally good assumptions because the modified Reynolds number, N_R^1 , is usually fixed as high as possible, while still remaining in the laminar region, to maximize the amplifier's gain. Also the nozzle width would remain constant if identical amplifier laminations were used for each stage. Therefore, the easiest design parameter to vary to satisfy equations (114), (115) and (116) is the aspect ratio since this can be adjusted by adding or taking away amplifier laminations.

When applying equation (117) it is important to note that there are limitations on the size of the aspect ratio. Drzewiecki¹⁶ has determined that amplifiers with an aspect ratio of less than 0.3 have reduced gain due to viscous losses. Therefore, allowing $\sigma(N) = 0.3$ as the smallest allowable aspect ratio for the final stage of amplification, the optimum aspect ratios of a gain block can then be calculated. This results in aspect ratios of $\sigma(N) = 0.3$, $\sigma(N-1) = 1.0$, $\sigma(N-2) = 3.3$, $\sigma(N-3) = 11.1$, etc. Aspect ratios for gain blocks of more than three stages are too large for practical purposes. Therefore, a gain block of three stages is the largest practical size which can be built if the same amplifier laminations are to be used for each stage and the system is to have maximum dynamic range.

If more gain is required of a system than can be achieved from just three stages of amplification, the supply nozzle width can also be varied to design a gain block with maximum dynamic range. Each supply nozzle width would have three stages of amplification associated with it. These three internal stages would have aspect ratios calculated using equation (117). If an aspect ratio becomes

¹⁶T.M. Drzewiecki, A Fluidic Audio Intercom, 20th Anniversary of Fluidics Symposium, The American Society of Mechanical Engineers, (1981).

too large or too small for practical purposes, equation (116) could be used to calculate a new optimum supply nozzle width, and the staging could continue.

An example of this would be if four or more stages of amplification were necessary for a given application. This example would require the designer to pick an initial supply nozzle width, b_s , and use that value for the first three stages of amplification with $\sigma(N) = 0.3$, $\sigma(N-1) = 1.0$, $\sigma(N-2) = 3.3$. To maximize the dynamic range of the next set of three amplifier stages, the aspect ratio of the (N-3) stage is chosen to be $\sigma(N-3) = 0.3$. Applying equation (116) to this results in an expression for the supply nozzle width ratio for this next stage.

$$\frac{b_s(m)}{b_s(m-1)} = 0.03 \quad (118)$$

The number of three-stage amplifier sets under consideration in equation (118) is designed by m . Stages (N-4) and (N-5) can then be designed with $\sigma(N-4) = 1.0$, an $\sigma(N-5) = 3.3$. This process can continue in this manner until enough amplification has been realized. The disadvantage with this approach is that the physical size of the amplifiers becomes large quickly, making a large gain-block prohibitive. Therefore, other techniques for designing a gain block with more than three stages is necessary.

Large gain blocks can be fashioned in a manner which places less of a penalty dynamic range and stresses other factors which may be important to the system design. The two best methods for this type of design are a self-staging technique and a common-sense approach which uses a knowledge of the input signal size and avoids a gain block that saturates for those inputs.

The self-staged amplifier gain block is a set of identical amplifier stages cascaded together. The advantages of self-staging are simplicity of design and the ability for increased gain. There is only one pneumatic supply in a self-staged gain block and, therefore, no need for dropping resistors to supply each

separate stage. The resolution of the LPA is sufficiently high so that an amplifier may be self-staged many times before any significant reduction in output resolution is detectable. The disadvantages of a self-staged amplifier are a lower dynamic range, since the first jet in the gain block will sweep a much smaller angle than the last jet, a smaller usable frequency range, and lower gain per stage due to a poorer input-output impedance match.

The final approach to LPA gain block design is for special purpose amplification. Occasionally, achieving maximum dynamic range is not as important as another design criterion. The designer may desire to operate each stage at as high a supply velocity as possible to minimize transport delay. The designer may also choose to design LPA stages with an improved input-output impedance match. This may be necessary to maintain reasonable gain within a gain block with many parallel stages. In any case, the approach used to devise a special purpose amplifier is to identify the characteristics which are most important in the design. The gain block is then designed analytically and the trade-offs for the special purpose application are examined. If the trade-offs are acceptable, the design is used.

The LPA gain block system is designed using one of the approaches described above. Once an approach has been selected, the next points of interest are static gain and frequency response. The static gain of one stage of amplification is given by equation (112). The total gain of the gain block is the product of the gains of each stage. The output pressure difference of the gain block is then the input pressure difference times the gain.

The input pressure difference, for a given bimorph displacement to the gain block, can be derived by combining equations (89) and (90). This results in an equation describing the input pressure difference to the gain block for a steady-state position of the end of the bimorph.

$$\frac{P_1 - P_2}{X} = \frac{4A_1 P^2}{A_1 u + 2A_2 P} \quad (119)$$

The pressure difference output of the nozzle for an input deflection of the end of the bimorph, expressed by equation (119), can be used to design the first stage of amplification. The linear pressure recovery for an LPA stage is given by Drzewiecki to be ¹⁷

$$P_{01} - P_{02} \Big|_{\max} = 0.70 P_s, \quad (120)$$

where

$$\left(P_{01} - P_{02} \right) = G_p \left(P_{i1} - P_{i2} \right) \quad (121)$$

It is important that the maximum input pressure difference is matched to the amplifier gain block to avoid saturation in any of the stages. The supply pressure, P_s , to an amplifier stage is given by equation (106). Equation (106) also shows that the supply pressure, P_s , is inversely proportional to the square of the aspect ratio, the most easily varied design parameter. Therefore, for a given input pressure difference, the first-stage aspect ratio may be varied to achieve a matched first-stage amplifier, where a maximum sweep of the first stage jet is realized and the amplifier gain block does not saturate.

Each additional stage is designed using an optimum dynamic range staging technique, self-staging technique, or a special purpose technique. The gain of the system is then calculated using equation (112) for each stage.

Equation (112) states that the single-stage gain of an amplifier is a function of the blocked load gain, G_{PB} , the amplifier's output impedance, R_0 , and the impedance of the load, R_L . In a cascaded network the load impedance of the (N-1) stage is equal to the input impedance of the (N) stage. The blocked load gain, G_{PB} , of standard LPA amplifiers varies between 9 and 10 per stage. With this information,

¹⁷T.M. Drzewiecki, A Fluidic Voice Communication System and Data Link, Ph.D. Thesis, Naval Post Graduate School, Monterey, Ca. (March 1980).

one may use equations (108), (109), (110), and (112) to calculate the gain of an LPA gain block.

The final consideration of the amplifier system is its frequency response. The phase response component of the system frequency response is generally dominated by signal transport lag between stages ^{2,16,17,18}. The phase lag is derived by calculating the time for propagation of the signal through the amplifier system.

The magnitude response of the system has been determined by Drzewiecki^{2,16,17,18} and a guide for the upper limit of the usable frequency range for uniform gain of Z-identical, self-staged amplifiers is given by

$$f = 0.03 \frac{C_d U_s}{b_s} Z^{-2/3} \quad (122)$$

Equation (122) demonstrates that self-staging an amplifier, with $Z > 1$, will result in a lower usable frequency range than the single-stage amplifier would. The technique for calculating the usable frequency range for an LPA gain block is to calculate the usable frequency range for each stage of amplification. The dominant stage would be the stage with the lowest usable frequency range; this frequency value can be used as a guide to the usable range of the entire gain block. A more exact representation of the dynamic behavior of the LPA can be made by examining the work of Manion and Drzewiecki² and Drzewiecki^{16,17,18} and applying one of the models presented in those papers to each stage of the gain block. Once the gain as a function of frequency for each LPA stage is determined, the overall LPA gain block frequency response can be calculated. This is the product of the gains of each amplifier stage as a function of frequency.

²F.M. Manion and T.M. Drzewiecki, Analytical Design of Laminar Proportional Amplifiers, Proc. HDL State-of-the-Art Symposium, Vol. 1, Adelphi, MD (Oct. 1974).

¹⁶T.M. Drzewiecki, A Fluidic Audio Intercom, 20th Anniversary of Fluidics Symposium, The American Society of Mechanical Engineers, (1981).

¹⁷T.M. Drzewiecki, A Fluidic Voice Communication System and Data Link, Ph.D. Thesis, Naval Post Graduate School, Monterey, Ca. (March 1980).

¹⁸T.M. Drzewiecki, A High-Order, Lumped-Parameter Jet-Dynamic Model for the Frequency Response of Laminar Proportional Amplifiers, 20th Anniversary of Fluidics Symposium, The American Society of Mechanical Engineers (1980).

The magnitude response may also exhibit a pronounced resonant peak at a frequency less than the frequency calculated by equation (122). This phenomenon is explained by Drzewiecki^{17,18} as a result of internal acoustic feedback. The mechanism of this feedback is described as follows. As the laminar jet oscillates within the LPA geometry, there is a spilling of flow to one side and then to the other. The flow spilled to the vents is radiated acoustically to the control region where it may combine with the control signal in the form of positive feedback. When the control input frequency equals the acoustic feedback frequency, one would expect that there would be an increase in the amplifier's gain. To determine the feedback frequency, one must first note that the jet deflection travels at one-half the average jet particle velocity. Therefore the signal is delayed by twice the jet transport time, T' , and the following equation can be written for the period, τ , of the acoustically caused oscillation. Note that travel time to the splitter is T' , but the feedback signal returns to the control region at the speed of sound. One complete cycle occurs in τ s, where a delay, T' , is experienced for a deflection in one direction and a delay, T' , is experienced for a deflection in the other direction.

$$\frac{1}{2}\tau = 2T' \quad , \quad (123)$$

where

$$T' = x_{sp}/U_A \quad , \quad (124)$$

$$U_A = C_d \sqrt{2P_s/\rho} \quad . \quad (125)$$

The frequency of oscillation due to internal feedback can be calculated from one over the period and is given by

¹⁷T.M. Drzewiecki, A Fluidic Voice Communication System and Data Link, Ph.D. Thesis, Naval Post Graduate School, Monterey, Ca. (March 1980).

¹⁸T.M. Drzewiecki, A High-Order, Lumped-Parameter Jet-Dynamic Model for the Frequency Response of Laminar Proportional Amplifiers, 20th Anniversary of Fluidics Symposium, The American Society of Mechanical Engineers (1980).

$$F_f = 1/T \quad (126)$$

Equation (126) can then be used to calculate the frequency at which resonant peaks from the acoustical feedback do occur. Equation (126) will be applied in Section 5 to calculate acoustically caused resonant peaks in the frequency response of the working prototype.

The fluidic modeling in this section has two main purposes. The flow force modeling is important because it will be used to show that increasing the bimorph supply pressure has a destabilizing effect on its dynamic response. The equivalent resistive fluid circuit analysis coupled with the LPA design equations allow the design of an LPA gain block with output characteristics that match the design intentions. Using the results of this section and Section 3, one can design and build an electropneumatic converter. The analysis, construction, and testing of a prototype design will be discussed in the next section.

5. DESIGN AND TESTING OF A VALVE SYSTEM

The equations developed in Sections 3 and 4 can now be used to design a valve system. A summary of the important physical properties of the prototype valve system is provided in Appendix A for reference. Once a valve system has been designed analytically, a working prototype is built. The working prototype is then tested to demonstrate the validity of the design equations. The experience gained through this process results in design changes that will give a better system response. These design changes are discussed in Section 6.

5.1 Analytical Design

The first step in designing a valve system is to identify what is important in the intended design. The static and dynamic response of the system is a function of the LPA gain block and the flapper-nozzle component. The required response of the system can be determined from a knowledge of the intended

system application. Once the valve's input and output requirements are identified, a system can be designed.

The most important aspect of building the first working prototype of a new design is to demonstrate that the idea works. It is also desirable to show that an organized method exists for improving that first design; in this case that means verifying the design equation of Sections 3 and 4. Once some confidence in the design equations has been established, these equations may be used for designing new prototypes for specific applications.

Since the LPA defines most of the output characteristics of the system, designing the LPA gain block is usually the initial analytical step in designing a valve system. Before the LPA gain block can be designed however, certain flapper-nozzle parameters must be assumed. This is because there are also certain design limitations placed on the bimorph. The diameter of the nozzles should be as small as possible to minimize the fluid flow forces. The diameter of the nozzles will then limit the minimum width of the bimorph. The generally accepted industry standard for the smallest diameter nozzle, to avoid clogging, is $D = 8.6 \times 10^{-4}$ m. Using highly filtered air this dimension could be reduced further. To insure a good overlap of the bimorph and the nozzle, the bimorph width is then chosen to be $W = 1.4 \times 10^{-3}$ m. Also the bimorph is commercially available in a single standard thickness. That thickness is given to be $T = 4.9 \times 10^{-4}$ m.

With the width and the thickness of the bimorph specified, the only remaining bimorph design parameter is its length, L . Equations (13) and (16) show that the first mode natural frequency of the bimorph is proportional to one over its length squared. Since speed of response is an important design criterion, it is desirable to reduce the length of the bimorph as much as possible. A shorter bimorph, though, will result in a reduced output displacement for a given applied voltage. The smaller displacement will result in a reduced pressure difference at the nozzles. This will require additional pneumatic amplification

to raise the pneumatic signal to the level obtained with the longer bimorph. The additional pneumatic amplification can be delivered with more LPA stages. The larger gain block will have a slower frequency response. This reduction in frequency response is caused by increased signal path length between elements and a lower bandwidth found in low supply pressure amplifiers which are necessary to amplify the reduced output of the nozzles. There is an optimum obtained by trading off bimorph size for number of amplifier stages.

The optimum length for a bimorph is therefore a function of the gain block used. The gain block describes the output characteristics of valve system and will therefore vary with the intended application. For the purpose of testing the design equations and building a working prototype of the system, it is not necessary to specify the gain block first. Therefore a bimorph with a practical length, resulting in a moderately high frequency response and a moderately high output displacement, is chosen. That length is chosen to be, $L = 1.5 \times 10^{-2}$ m. The natural frequency of a bimorph of this length is, $\omega_N = 1050$ Hz, and its maximum output displacement for a 15 V p-p input is -5.0×10^{-6} m. Once the validity of the design equations is shown, a designer could optimize the length of a bimorph for a specific LPA output requirement.

Once the bimorph is chosen, its specific and physical material properties are defined. These properties are given in Table 4. The equations developed in Section 3 are then applied to analytically predict the electromechanical system parameters. The results of these calculations are shown in Table 5.

Now that the bimorph has been chosen and its properties are identified, an LPA gain block can be designed for pneumatic amplification of the pressure signal generated downstream of the nozzles. A standard Corning made LPA gain block is chosen to verify the analysis. The resulting output of this gain block is used to verify the design equations and show their usefulness for developing an improved design for future application. The purposes of this prototype design and working

TABLE 4. PHYSICAL AND MATERIAL PROPERTIES OF LEAD ZIRCONATE TITANATE CERAMIC BIMORPH USED FOR WORKING PROTOTYPE

Property	Measured Value
Length, L	1.5×10^{-2} m
Width, W	1.4×10^{-3} m
Thickness, T	4.9×10^{-4} m
Nickel plate thickness, t_1	1.52×10^{-6} m
Lead zirconate titanate thickness, t_2	1.93×10^{-4} m
Brass shim thickness, t_3	1.03×10^{-4} m
Density, ρ	7.5×10^3 kg/m ³
Piezoelectric charge coefficient, d_{31}	-1.8×10^{-10} m/V
Piezoelectric voltage coefficient, g_{31}	-1.1×10^{-2} V-m/N
Nickel elastic modulus, E_1	1.26×10^{11} N/m ²
Lead zirconate titanate elastic modulus, E_2	1.09×10^{11} N/m ²
Brass elastic modulus, E_3	9.0×10^{10} N/m ²

TABLE 5. ANALYTICALLY PREDICTED SYSTEM PARAMETERS USED FOR WORKING PROTOTYPE

Parameter	Analytically Predicted Value
System spring constant, K_s	832 N/m
Effective mass, M	1.9×10^{-5} Kg
System damping, B	5×10^{-3} N-s/m (estimated)
Piezoelectric force constant, C_1	2.8×10^{-4} N/V
Piezoelectric back current constant, K_q	-2.3×10^{-4} A-s/m
Bimorph capacitance, C_T	1.1×10^{-9} F

model are to demonstrate that the device does work and that the design equations do predict its response.

Therefore an amplifier system with a three-stage preamplifier and a single-stage output amplifier is chosen for the design. A three-stage preamplifier is chosen because it would have sufficiently high bandwidth and sensitivity to detect and amplify the low pressure signal coming from the nozzles. The three stages of the preamplifier are self-staged. Each stage is a standard LPA design with its necessary geometric properties given in Table 6. The jet deflection angle of the amplifier is then designed to match the jet deflection of the output stage of the preamplifier as closely as possible.

TABLE 6. LPA PREAMPLIFIER GEOMETRIC PROPERTIES; STAGES 1, 2, AND 3

Parameter	Numerical Value
Supply nozzle width, b_s	2.5×10^{-4} m
Supply nozzle height, h_s	3.75×10^{-4} m
Aspect ratio, σ	1.5
Average control channel width normalized by b_s , \bar{B}_c	2.75
Control channel length normalized by b_s , X_c	10
Discharge coefficient, C_d	0.7
Momentum flux discharge coefficient, C_j	0.65
Blocked load gain, G_{PB}	9.0

Adopting the convention that stages 1, 2, and 3 are the identical pre-amplifier stages and stage 4 is the output amplifier stage makes for simpler reference when discussing static gain and frequency response. Equations (115) and (116) are combined so that the output amplifier stage, stage 4, can be matched

with stage 3, the last preamplifier stage. The modified Reynolds number, N_R' , is held constant, at its highest value which produces laminar flow, for all stages of the amplification. This corresponds to a modified Reynolds number of $N_R' = 120$. Therefore, solving for the fourth stage aspect ratio results in

$$\sigma(4) = \frac{b_s(3)}{b_s(4)} \sigma(3) \sqrt{\frac{1}{G_p(4)}} \quad (127)$$

The preamplifier parameters are $b_s(3) = 2.5 \times 10^{-4}$ m and $\sigma(3) = 1.5$ from Table 6. The output amplifier is block loaded for measurement purposes and therefore $G_p(4) = 10$. A standard LPA amplifier with $b_s(4) = 5.0 \times 10^{-4}$ m is employed in the output amplifier, and the aspect ratio of this stage is calculated to be $\sigma(4) = 0.24$. Viscous losses reduce gain for amplifiers with an aspect ratio below 0.3; therefore, some dynamic range is sacrificed to make $\sigma(4) > 0.3$. The standard thickness of the laminations require that the minimum aspect ratio of the fourth stage be $\sigma(4) = 0.5$. If the fourth stage is used to drive a load, $G_p(4)$ would decrease because of the reduced output resistance, and the optimum value of $\sigma(4)$ would have to increase. This situation results in a better match between the third and fourth stages.

Now that the gain block is defined, the overall static gain can be calculated. Equation (112) gives the gain of an amplifier stage as a function of its blocked load gain, the amplifier output resistance, and the attached load resistance. In a cascaded amplifier gain block the load resistance of the (N-1) stage equals the input resistance of the (N) stage. For the purpose of measurement the final amplifier stage will be blocked and its load resistance will be infinite. This will cause the gain of the final amplifier stage to equal its blocked load gain. The blocked load gain of each stage in the preamplifier is given in Table 6 as nine. The blocked load gain of the final amplifier stage is given to be ten. This increase is due to an improvement in the design of the final amplifier stage over the preamplifier stage. Therefore, writing the gain for an intermediate stage of amplification within the gain block results in

$$G_p(N-1) = \frac{G_{PB}(N-1)}{1 + \frac{R_o(N-1)}{R_i(N)}} \quad (128)$$

The ratio of the output resistance to the input resistance can be solved, using equations (109) and (110).

$$\frac{R_o(N-1)}{R_i(N)} = \frac{0.50 R_s(N-1)}{0.75 R_s(N)} \quad (129)$$

Applying equation (108) to equation (3) results in a more generalized expression,

$$\frac{R_o(N-1)}{R_i(N)} = 0.667 \left(\frac{\sigma(N)}{\sigma(N-1)} \right)^2 \left(\frac{b_s(N)}{b_s(N-1)} \right)^3 \quad (130)$$

For the first two stages of amplification within the preamplifier,

$$\frac{R_o(1)}{R_i(2)} = 0.677 \quad , \quad (131)$$

$$\frac{R_o(2)}{R_i(3)} = 0.677 \quad , \quad (132)$$

Stage three of the preamplifier is connected to the final stage amplifier and results in a resistance ratio of

$$\frac{R_o(3)}{R_i(4)} = 0.677 \left(\frac{\sigma(4)}{\sigma(3)} \right)^2 \left(\frac{b_s(4)}{b_s(3)} \right)^3 \quad ; \quad (133)$$

with $\sigma(4) = 0.5$ and $b_s(4) = 5.0 \times 10^{-4}$ m, equation (133) is solved.

$$\frac{R_o(3)}{R_i(4)} = 0.59 \quad . \quad (134)$$

The total system gain with the last stage blocked is given by

$$G_{Pt} = \frac{G_{PB}(1) G_{PB}(2) G_{PB}(3) G_{PB}(4)}{(1 + 0.677)^2 (1 + 0.659)} \quad , \quad (135)$$

$$G_{Pt} = 1650$$

(136)

To calculate the output pressure difference of the gain block, one must determine the input pressure difference. The static output pressure difference is therefore the static input pressure difference multiplied by the total LPA system gain given by equation (136). The input pressure difference to the LPA gain block, for a displacement of the end of the bimorph is given by equation (119). To calculate the final system output pressure difference several intermediate calculations will have to be made to develop values for the A_j coefficients which are used by equation (119).

The first stage amplifier is operated at a modified Reynolds number of $N_R' = 90$ to insure laminar flow. This results in a supply pressure and a supply flow given by equations (106) and (107) respectively, to that stage of amplification. This is given by

$$P_s(1) = 531 \text{ N/m}^2 \quad , \quad (137)$$

$$Q_s(1) = 1.95 \times 10^{-6} \frac{\text{m}^3}{\text{s}^2} \quad . \quad (138)$$

Equations (55) and (56) are then used to calculate the mass entrained flow.

$$W_e = 5.21 \times 10^{-8} \text{ kg/s} \quad . \quad (139)$$

The Reynolds number is found using equation (105). Then equation (59) is solved for the control channel resistance using the Reynolds number and the values listed in Table 5.

$$N_R = 500 \quad , \quad (140)$$

$$R_c = 6.05 \times 10^7 \frac{\text{kg}}{\text{sm}^3} \quad . \quad (141)$$

The vent resistance is calculated from equation (61) to be

$$R_v = 8.16 \times 10^8 \frac{\text{kg}}{\text{sm}^2} \quad . \quad (142)$$

With these values and with the density of air ρ , equal to 1.2 kg/m^3 , the nozzle radius, r , equal to $4.32 \times 10^{-4} \text{ m}$, the nozzle length, L_b , equal to $6.35 \times 10^{-3} \text{ m}$, the nozzle entrance coefficient, $C_e = 0.85^{13}$, and the nozzle underlap, $u = 3.81 \times 10^{-5} \text{ m}$, one can calculate the A_j coefficients. These coefficients are solved using equations (71) through (76) and are given by

$$A_1 = 1.92 \times 10^{-3} \sqrt{\frac{\text{kg}}{\text{m}}} \quad , \quad (143)$$

$$A_2 = 1.47 \times 10^{-9} \text{ m-s} \quad . \quad (144)$$

$$A_3 = 5.21 \times 10^{-8} \frac{\text{kg}}{\text{s}} \quad , \quad (145)$$

$$A_4 = 5.86 \times 10^{-7} \text{ m}^2 \quad , \quad (146)$$

$$A_5 = 1.13 \times 10^{-5} \sqrt{\text{kg-m}} \quad , \quad (147)$$

$$A_6 = 2.31 \times 10^{-3} \text{ m} \quad . \quad (148)$$

The supply pressure to the bimorph, P_{s1} , must now be calculated to deliver an input to the gain block which will maximize the system sensitivity but will not saturate the LPA gain block. To do this a bimorph supply pressure, P_{s1} , is assumed. Equation (81) is used to derive the first stage amplifier bias pressure for the assumed bimorph supply pressure. The intermediate value of P is then calculated with equation (91). The expression relating the pressure difference at the nozzles to the deflection of the end of the bimorph is then given by equation (119). The steady-state deflection of the end of the bimorph for an applied voltage is then given by solving equation (97) in the steady-state. This results in

$$x = \frac{-V_A C_5}{1 - C_0 C_4} \quad . \quad (149)$$

¹³B.W. Anderson, The Analysis and Design of Pneumatic Systems, John Wiley and Sons, Inc., New York, (1976).

The values of the C_j coefficients can be determined using equations (98) through (103). Substituting for V_A the maximum voltage to be delivered to the bimorph results in its maximum displacement. Using equation (119) one can determine the maximum pressure output of the nozzles. Multiplying this by the LPA system gain results in an expression for the maximum output pressure difference of the system for the maximum input voltage. This pressure difference is then checked against equation (120) in an optimally designed gain block to determine if the gain block has saturated. If the gain block is not optimally designed, the possibility exists that an intermediate stage could saturate prematurely. If the gain block has saturated or is significantly below saturation, the bimorph supply pressure is adjusted up or down to compensate for this. This iterative process is repeated until a satisfactory supply pressure to the bimorph is determined.

This technique is applied to the LPA gain block already developed. After several iterations, the supply pressure to the bimorph is calculated to be

$$P_{s1} = 36.0 \text{ N/m}^2 (2.7 \times 10^{-1} \text{ mm Hg}) . \quad (150)$$

This results in a first stage bias pressure, calculated with equation (81) of

$$P_o = 34.0 \text{ N/m}^2 (2.56 \times 10^{-1} \text{ mm Hg}) . \quad (151)$$

The intermediate value of P is then calculated using equation (91)

$$P = 1.41 \sqrt{\text{N/m}^2} \quad (152)$$

The expression relating the pressure difference output of the nozzles for an input motion of the end of the bimorph is given by equation (119) and is shown below.

$$\frac{P_1 - P_2}{X} = 2.0 \times 10^5 \frac{\text{kg}}{\text{s}^2 \text{ m}^2} \quad (153)$$

The maximum steady-state deflection of the end of the bimorph for a maximum steady-state applied voltage of 14 V is given by equation (149). To solve this equation the values of Table 5 are substituted into equations (95), (96) and (98) through (103) to solve for the C_j coefficients with $P = 0$

$$C_0 = 1.06 \times 10^{-1} \frac{\text{N}}{\text{m}}, \quad (154)$$

$$C_2 = 3.17 \times 10^{-5} \frac{\text{N-s}}{\text{m}}, \quad (155)$$

$$C_3 = 0.0 \frac{\text{s}^3}{\text{kg}}, \quad (156)$$

$$C_4 = 1.20 \times 10^{-3} \frac{\text{m}}{\text{N}}, \quad (157)$$

$$C_5 = -3.36 \times 10^{-7} \text{ m/v}, \quad (158)$$

$$C_6 = 0.0 \text{ s}^3, \quad (159)$$

$$C_7 = 2.28 \times 10^{-8} \text{ s}^2, \quad (160)$$

$$C_8 = 6.01 \times 10^{-6} \text{ s}, \quad (161)$$

Solving equation (149) results in

$$x \Big|_{\text{max}} = 5.0 \times 10^{-6} \text{ m} \quad (162)$$

Substituting equation (162) into equation (153) results in an expression for the maximum pressure difference output of the nozzles for the maximum input voltage of 15 V.

$$(P_1 - P_2) \Big|_{\text{max}} = 1.01 \text{ N/m}^2 \quad (7.6 \times 10^{-3} \text{ mm Hg})$$

With a total LPA system gain of $G_{pt} = 1650$, the output of the LPA gain block for the maximum output voltage is given by

$$(P_{10}(4) - P_{20}(4)) \Big|_{\text{max}} = 1.66 \times 10^3 \text{ N/m}^2 \quad (12.5 \text{ mm Hg}) \quad (163)$$

With the fourth-stage supply pressure at $P_s(4) = 2.13 \times 10^3 \text{ N/m}^2$ (16 mm Hg) calculated from equation (106), this much pressure recovery should cause the final-stage amplifier to operate in its nonlinear input-output region. However, the experimental results which follow show that this is not the case. For this particular LPA stage there is slightly better than 70% pressure recovery, but this should not be assumed in future designs.

Now that the system has been designed statically, it should be checked dynamically. Equation (122) is used to check the frequency response of the amplifiers. For the preamplifier, with $Z = 3$, the upper limit of the usable frequency range of the final stage amplifier, $Z = 1$, is found to be 2400 Hz. The natural frequency of the bimorph is given by equation (14) and is calculated to be 1050 Hz. To determine other frequencies that might give distortions in the magnitude response, equation (136) is used. Applying this equation to the final stage amplifier shows that a resonant peak might be expected at $F_f = 620$ Hz because of internal acoustic feedback. This resonant peak is later noted in the experimentally determined system frequency response. The magnitude of the peak is unknown, and this is an aspect of the LPA which is now under additional investigation^{17,18}.

The results of this dynamic check suggest that a reasonably flat magnitude response out to just below the resonant frequency of the bimorph can be expected from this system. The external series resistor, R_A , can be changed to vary the system's frequency response. This may help to further extend the usable frequency range of the valve system.

A final point to be considered in the analytical design is if the LPA gain block is necessary or if it is possible to increase the bimorph chamber supply pressure until the same pressure difference is available downstream of the nozzles, as was available at the output of the LPA. The gain block is necessary because the bimorph is very limited in its output force capability. Any significant bimorph chamber supply pressure will cause the electromechanical system to exhibit a poorer frequency response because of the destabilizing flow forces.

¹⁷T.M. Drzewiecki, A Fluidic Voice Communication System and Data Link, Ph.D. Thesis, Naval Post Graduate School, Monterey, Ca. (March 1980).

¹⁸T.M. Drzewiecki, A High-Order, Lumped-Parameter Jet-Dynamic Model for the Frequency Response of Laminar Proportional Amplifiers, 20th Anniversary of Fluidics Symposium, The American Society of Mechanical Engineers (1980).

This can be shown analytically if the characteristic equation of equation (97) is examined. This is given by

$$\left(\frac{C_6}{1 - C_0 C_4}\right)s^3 + \left(\frac{C_7 - C_2 C_3}{1 - C_0 C_4}\right)s^2 + \left(\frac{C_8 - C_0 C_3 - C_2 C_4}{1 - C_0 C_4}\right)s + 1 = 0. \quad (164)$$

Equation (164) is nonlinear with respect to the bimorph supply pressure, P_{s1} . A root locus can be plotted for equation (164) by varying P_{s1} , calculating all the intermediate steps and finding the roots of equation (164). This root locus is shown in Figure 17 for $R = 0.0$. Figure 16 shows that as P_{s1} is increased, there is a destabilizing effect on the system's response. For this reason, the bimorph supply pressure is chosen to be $P_{s1} = 36.0 \text{ N/m}^2$ ($2.7 \times 10^{-1} \text{ mm Hg}$), which results in an insignificant change in the dynamic behavior specified by equation (97).

5.2 Prototype

A prototype model of the valve system was then constructed using the dimensions outlined in the analytical design section. An assembly diagram for the design is shown in Figure 17. The prototype was built attempting to simplify its construction, minimize volumes to minimize fluid capacitance, and minimize passage lengths for reduced signal propagation time. This resulted in a device which was inexpensive to build and which delivered maximum bandwidth.

The assembly diagram of Figure 17 shows the construction of the housing containing the flapper-nozzle and the first stage of pneumatic amplification. Only the first LPA stage is shown to avoid confusion. The diagram also contains lines which are drawn for the purpose of flow visualization.

The two pneumatic inputs to the flapper-nozzle housing are the supply pressure to the bimorph and the supply pressure to the LPA gain block. The flow through nozzles is controlled by the position of the end of the bimorph. Figure 18 shows the bimorph deflected with more flow entering one nozzle than the other. The relative amount of flow is indicated by the thickness of the line used to re-

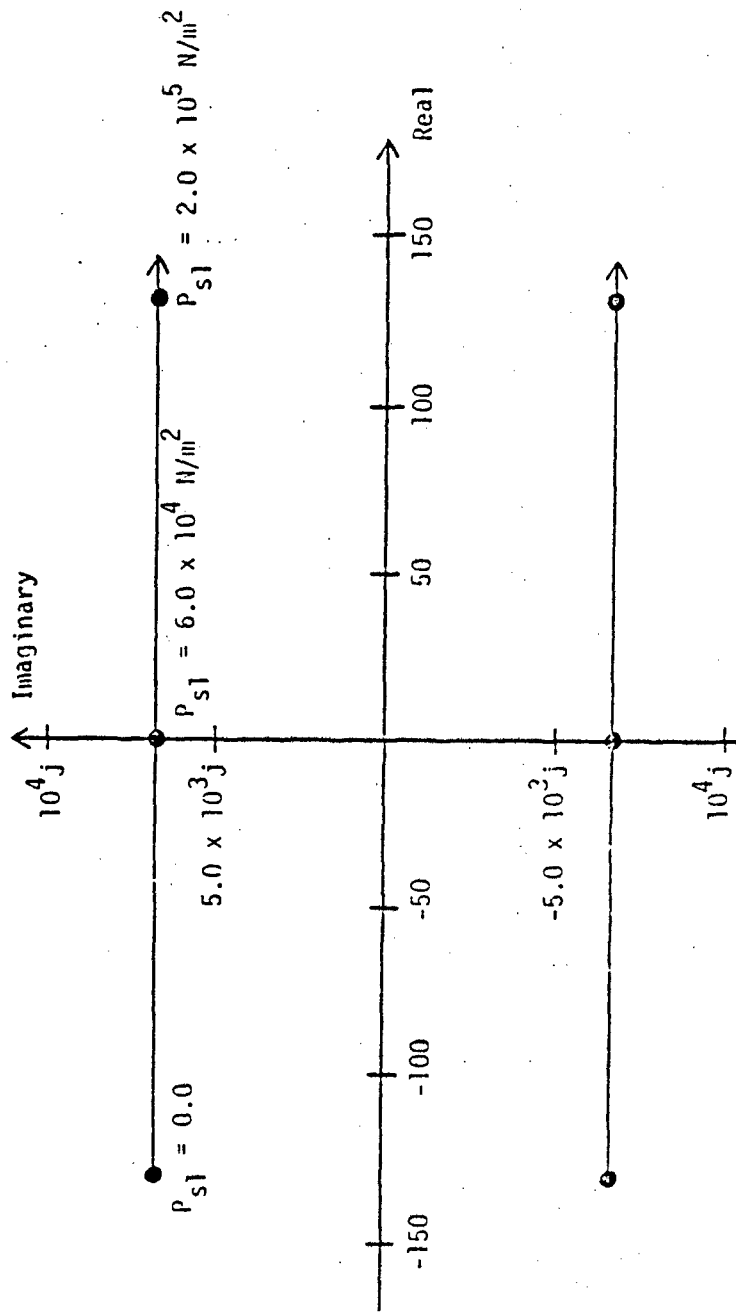


Figure 16. Locus of Equation 164
 $0.0 < P_{s1} < 2.0 \times 10^5 \text{ N/m}^2$
 $R = 0.0\Omega$

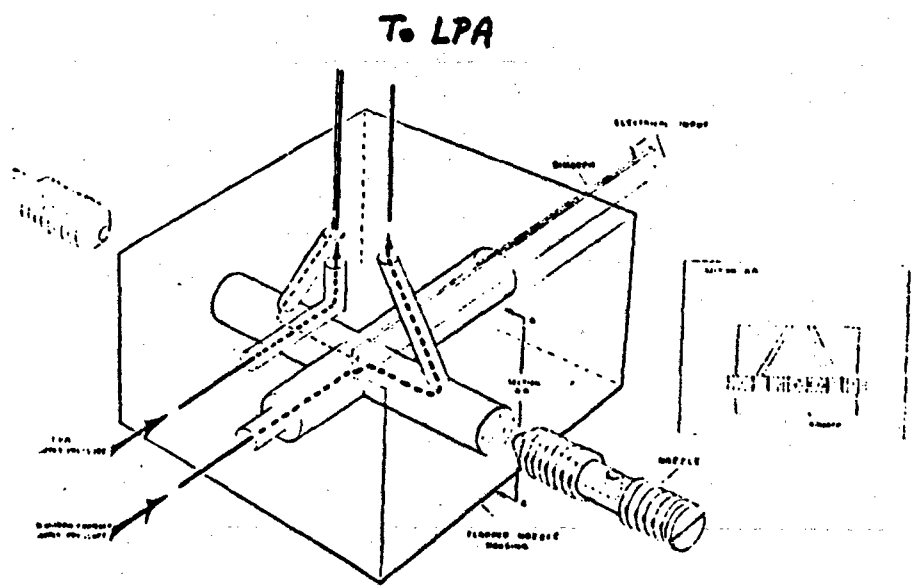


Figure 17. Assembly Drawing of Valve

present that flow. The outputs of the two nozzles are then channeled up through several laminations to the LPA lamination where these output pressures are used as the control input. The controls deflect the laminar supply jet, and a resulting output pressure difference is available at the LPA output ports. The output of this stage is then available to be channeled up to the input of a second LPA stage. This process is repeated for four stages of amplification in the working prototype.

5.3 Testing and Verification

The valve system is tested both statically and dynamically to determine the accuracy of the design equations used. The static input-output relationship for the system is shown in Figure 18. The system has a linear operating region of ± 7.0 volts about 0.0 volts with a system sensitivity of $1.2 \times 10^2 \text{ N/m}^2\text{-V}$, (0.9 mm Hg/V). This result compares favorably with the expected sensitivity of $1.1 \times 10^2 \text{ N/m}^2\text{-V}$, (0.8 mm Hg/V). The expected sensitivity is derived by dividing the maximum output pressure difference of the gain block given by equation (163) by the maximum input voltage of ± 7.0 volts.

Figure 18 also demonstrates that the system output exhibits hysteresis. The hysteresis is an inherent characteristic of the bimorph caused by the polarization of the crystal resulting from the applied supply voltage. The cause of this effect is explained earlier in Section 2.

The frequency response of the system was measured for a bender series resistance of $R_A = 0.0$ ohm. The results of that test along with the analytically predicted response of the system are shown in Figure 19. There are some inconsistencies between the measured and the predicted response on the magnitude plot. The most noticeable inconsistency is the difference in the size of the resonant peaks. The measured resonant peaks are smaller because the pneumatic input to the preamplifier is so large, for the electrical input magnitude chosen, that

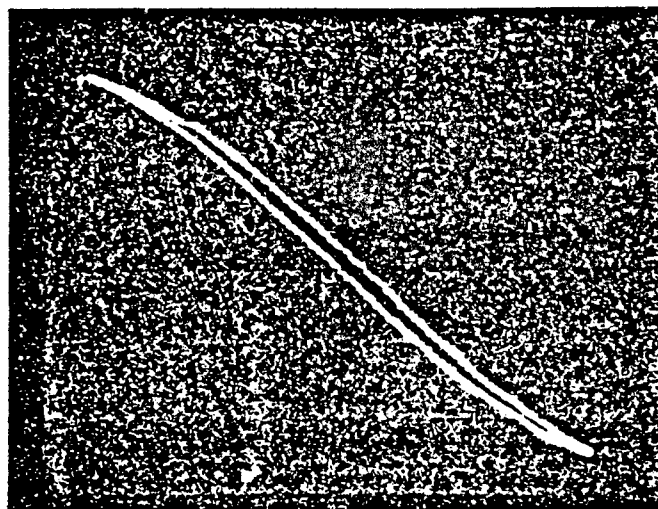


Figure 18. Static Input-Output Relationship of Valve System

1 Large Division Horizontal = 2.9V
1 Large Division Vertical = 410 N/m²

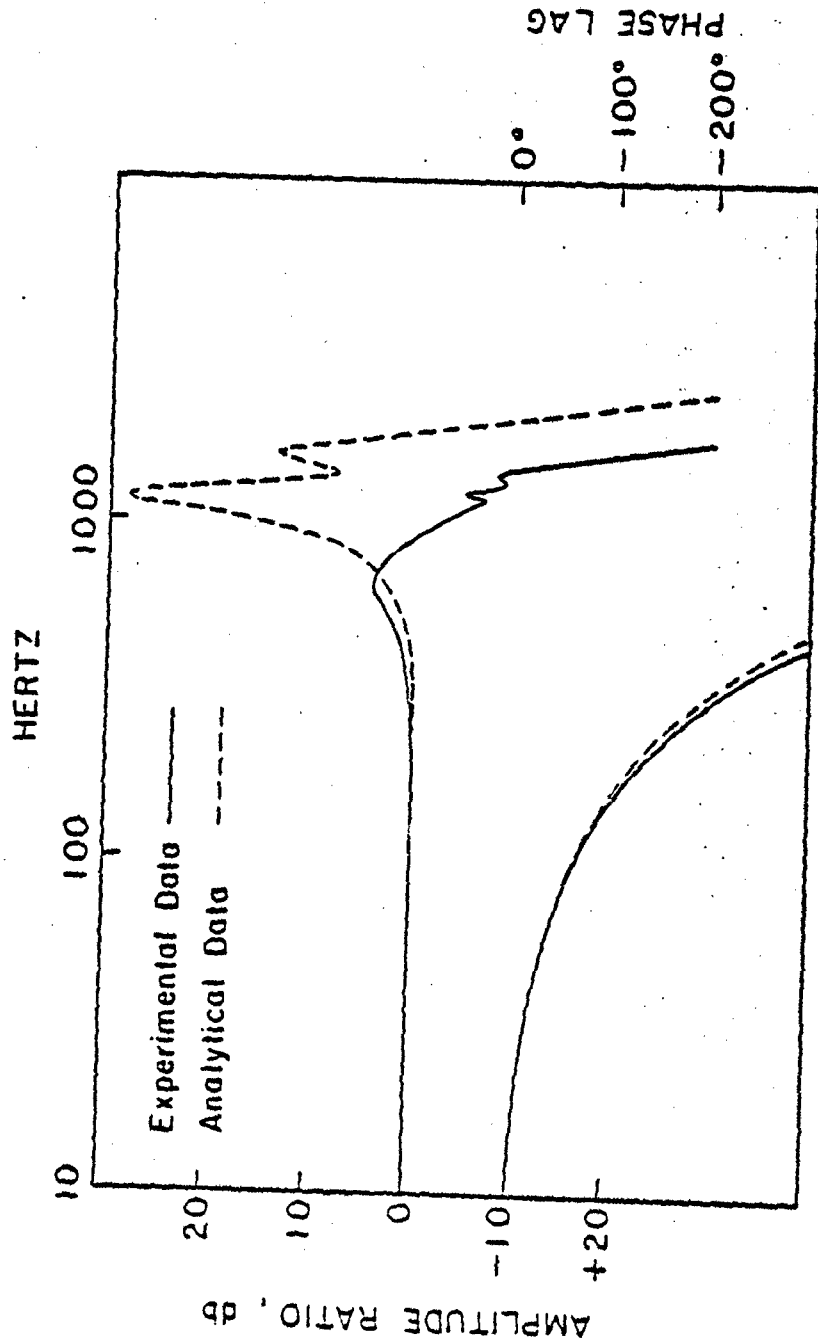


Figure 19. Measured and Predicted System Frequency Response
R = 0.0 MΩ

the preamplifier saturates. This saturation occurs, by design, for relatively small electrical inputs at the resonant frequency to obtain the maximum gain and bandwidth in the operating frequencies. A way to reduce this effect would be to place the bender resonance beyond the amplifier bandwidth limits. The LPA would then filter the resonant frequency of the bender and eliminate the saturation.

Figure 19 demonstrates that the system amplitude versus frequency response exhibits a resonance at 650 Hz. This resonance is a result of internal acoustic feedback in the fourth-stage amplifier. To analytically predict the frequency of maximum gain due to this phenomenon, equation (126) is utilized. With the amplifier nozzle to splitter distance, X_{sp} , equal to 4.0×10^{-3} m, the nozzle discharge coefficient, C_d , equal to 0.7, the amplifier supply pressure, P_s , equal to 4.8×10^3 P_A , and the density of air, ρ , equal to 1.2 kg/m^3 , the frequency of the jet oscillation, $1/T$, is calculated with equation (126) to be 620 Hz. This compares favorably with the 650 Hz resonance peak of Figure 19.

A comparison of the phase angle versus frequency plots of Figure 20 shows good agreement between the measured response and the calculated response. If 90° phase lag is the cutoff point for the usable frequency range of the system, this system has a usable frequency range from a DC level to 140 Hz.

If magnitude information is important in a system design, then sending a constant amplitude signal within the bandwidth of this device will result in minimum magnitude distortion of the input signal. This results because the system phase lag is due almost entirely to a transport delay due to the pneumatic signal path length. A series resistor may be added to the bender electrical supply to flatten the magnitude response over a greater frequency range. Figure 20 reveals the measured and predicted response for a series resistor, $R_A = 0.2 \text{ m}\Omega$. The plot shows that for a tolerance of ± 3 db of magnitude distortion, the system exhibits a nearly flat amplitude versus frequency response and a linear phase angle versus frequency relationship up to 1000 Hz.

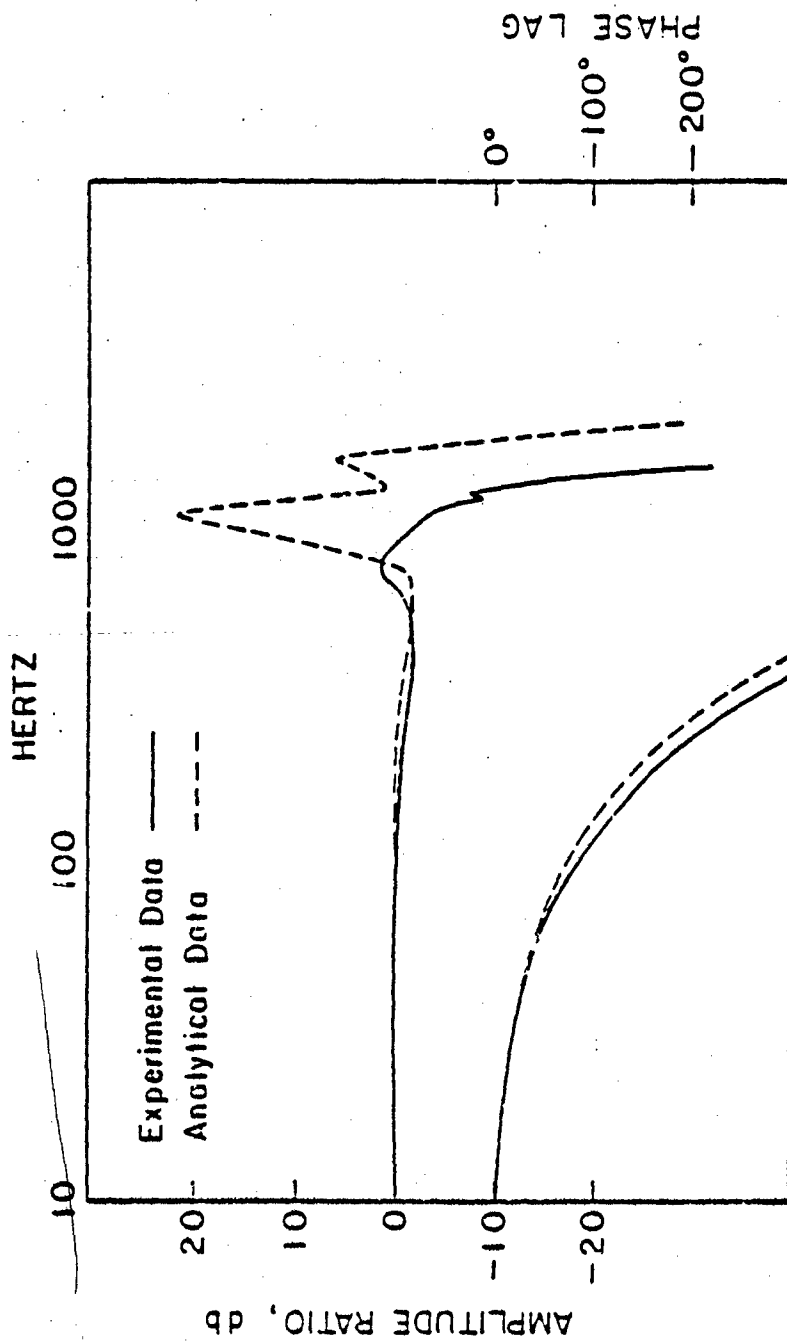


Figure 20. Measured and Predicted System Frequency Response

R = 0.2 MΩ

The test data indicate that the valve design does work. The data also indicate that the static and dynamic results are close to those predicted by the design equation. Now that a working prototype has been built, obvious improvements can be made. One improvement is to reduce the pneumatic signal path length. This should shorten the pneumatic time delay and improve the system's phase response. Another improvement would be to reduce the dimensions of the bimorph. This would improve the magnitude response of the system. A shorter bimorph would result in a reduced motion at the end of the bimorph for an applied voltage. This can be compensated for with an improved amplifier system. The amplifier system can be designed so that all stages operate at a high supply pressure. A high supply pressure results in a high supply velocity. Equation (122) shows that a gain block with a high supply velocity will exhibit improved magnitude versus frequency response. A high supply velocity also will reduce the time required for pneumatic signal propagation through the gain block. This should further improve the phase response of the system. The final section concerning future considerations, analytically develops a design that should exhibit an improved response.

6. FUTURE CONSIDERATIONS

Much can be learned about a design once an initial prototype has been built. Now that the original design has been shown to work and the design equations correctly predict its response, a new design can be developed using those equations. The new design should extend the usable frequency range of the device through a better choice of the piezoelectric bimorph and the attached LPA gain block. A summary of the important physical properties of the new prototype valve system is provided in Appendix B.

The new design objective is to improve the frequency response of the system. This is accomplished by reducing the dimensions of the bimorph and the LPA. Again, the width and thickness of the bimorph is fixed due to the specified

minimum nozzle diameter ($D = 8.6 \times 10^{-4}$ m) and the availability of standard bimorph sizes. Therefore the only remaining bimorph dimension that may be picked is its length. The length of the bimorph should be reduced as much as possible to maximize the frequency response. However, too short a bender will cause the nozzle output pressure signal to be so small that detecting it with the first stage amplifier will be difficult. To calculate a reduced length for the bimorph, a first-stage amplifier must be assumed. Then, with a knowledge of the gain and dynamic range of the first stage amplifier, one can calculate a suitable smaller bimorph length. This situation requires a certain feel for what might work best in the first-stage amplifier.

Because it is desired to improve the frequency response of the system, the first stage amplifier is chosen to have a supply nozzle width of $b_s(1) = 2.5 \times 10^{-4}$ m and an aspect ratio of $\sigma(1) = 1.0$. This results in a maximum supply pressure of $P_s(1) = 2.13 \times 10^3$ N/m², (16 mm Hg) from equation (106). The usable frequency range of this amplifier has been increased because of the choice of the aspect ratio and the supply nozzle width. This maximum usable frequency can be calculated with equation (122) and is given by $f = 4800$ Hz.

To determine the smallest length of a bimorph, which would produce a detectable input pressure signal to the first-stage amplifier, one notes from equation (22) that the deflection of the end of the bimorph varies with the square of its length. Using the same valve underlap in the design described here as was used in the first design found in Section 5 ($u = 3.8 \times 10^{-5}$ m), the pressure output of the valve varies proportionally with the deflection of the bimorph; therefore, the pressure output of the flapper-nozzle configuration must also vary with the square of the bimorph's length. With this knowledge of the first stage LPA geometry and the relationship between the bimorph's length and the output pressure difference available at the nozzles, a new bimorph length can be calculated.

Equation (119) states that the linear pressure recovery for an LPA stage is 70 percent of that stage's supply pressure. With $P_s(1) = 2.13 \times 10^3 \text{ N/m}^2$ (16 mm Hg), this corresponds to a maximum pressure recovery of $1.49 \times 10^3 \text{ N/m}^2$ (11.2 mm Hg). It will be assumed that the first stage operates with a gain of 10. This may be high, because the output is not blocked, but it will give a good approximation. This means that the maximum input pressure difference to this stage is $1.49 \times 10^2 \text{ N/m}^2$ (1.12 mm Hg). Drzewiecki has shown that a dynamic range of 100,000:1 can be expected for an LPA stage of this design¹⁷. Since the dynamic range is a ratio of the largest input to the smallest input which gives uniform gain, the smallest allowable input pressure difference to the first-stage amplifier can now be calculated. This is given by $1.5 \times 10^{-3} \text{ N/m}^2$ (1.1×10^{-5} mm Hg). Because some dynamic range in the electrical input signal is desired, the smallest allowable input pressure difference to the first stage is arbitrarily increased to $5.0 \times 10^{-1} \text{ N/m}^2$ (3.8×10^{-3} mm Hg).

Equation (163) gives an expression for the maximum output pressure difference available at the nozzles, for a maximum input voltage of 15 V. This expression is for the working prototype of Section 5 with a corresponding length, $L = 1.5 \times 10^{-2} \text{ m}$, and a corresponding output pressure difference of 1.01 N/m^2 (7.6×10^{-3} mm Hg). Since the square of the length of the proposed prototype should vary with the pressure output available downstream of the nozzles, the characteristics of the working prototype can be used to estimate a minimum length of the bimorph for the proposed prototype. This corresponds to $L = 1.05 \times 10^{-2} \text{ m}$. The new piezoelectric bimorph physical and material properties are summarized in Table 7.

The equations of Section 3 can then be used to calculate the electromechanical system parameters in the same manner that they were calculated in that section.

¹⁷T.M. Drzewiecki, A Fluidic Voice Communication System and Data Link, Ph.D. Thesis, Naval Post Graduate School, Monterey, Ca. (March 1980).

TABLE 7. PHYSICAL AND MATERIAL PROPERTIES OF LEAD ZIRCONATE TITANATE CERAMIC BIMORPH USED FOR PROPOSED PROTOTYPE

Property	Measured Value
Length, L	1.05×10^{-2} m
Width, W	1.4×10^{-3} m
Thickness, T	4.9×10^{-4} m
Nickel plate thickness, t_1	1.52×10^{-6} m
Lead zirconate titanate thickness, t_2	1.93×10^{-4} m
Brass shim thickness, t_3	1.03×10^{-4} m
Density, ρ	7.5×10^3 kg/m ³
Piezoelectric charge coefficient, d_{31}	-1.8×10^{-10} m/V
Piezoelectric voltage coefficient, g_{31}	-1.1×10^{-2} V-m/N
Nickel elastic modulus, E_1	1.26×10^{11} N/m ²
Lead zirconate titanate elastic modulus, E_2	1.09×10^{11} N/m ²
Brass elastic modulus, E_3	9.0×10^{10} N/m ²

Those results are summarized in Table 8. It can be noted from these parameters that the natural frequency of the bimorph has increased to 2300 Hz. These results are useful later in calculating an improved flapper-nozzle supply pressure.

Since the first stage of the gain block has already been designed and an approximate input sensitivity to that stage has been determined, it is logical to finish the design of the gain block. With that completed, the supply pressure to the flapper nozzle, which gives a maximum output pressure difference, can be calculated in the same manner it was done in Section 5.

The final three stages of amplification are chosen to be self-staged. Even though self-staging an amplifier three times results in a reduced usable frequency

TABLE 8. ANALYTICALLY PREDICTED SYSTEM PARAMETERS USED FOR
PROPOSED PROTOTYPE

Parameter	Analytically Predicted Value
System spring constant, K_s	2636 N/m
Effective mass, M	1.27×10^{-5} kg
System damping, B	5×10^{-3} N-s/m (estimated)
Piezoelectric force constant, C_1	-4.11×10^{-4} N/V
Piezoelectric back current constant, K_q	-3.43×10^{-4} A-s/m
Bimorph capacitance, C_T	5.0×10^{-10} F

range, the frequency range of each stage is so high that the reduced range is still very great. The aspect ratio of stages two, three, and four are given to be $\sigma(2) = \sigma(3) = \sigma(4) = 0.6$. The supply nozzle width for each stage is given to be $b_s(2) = b_s(3) = b_s(4) = 2.5 \times 10^{-4}$ m. Equation (106) defines the supply pressure to these stages as $P_s(2) = P_s(3) = P_s(4) = 5.8 \times 10^3$ N/m² (44 mm Hg). This amplifier design gives improved magnitude response, with $Z = 3$, as $f = 4000$ Hz.

The total gain of this LPA gain block can be calculated using the LPA design equations of Section 4 in the same manner as they were used to calculate the total gain of the gain block in Section 5. This results in a total system gain, with the last stage blocked, given by

$$G_{pt} = 2900 \quad (165)$$

Multiplying the total gain of the system, given in equation (165) by the available input pressure difference to the first stage given by 5.0×10^{-1} N/m² (3.8×10^{-3} mm Hg), results in a maximum output pressure difference of the LPA gain block given by 1.16×10^3 N/m² (8.7 mm Hg). This value is well within the linear pressure recovery of the last stage amplifier, and the design should work. To calculate a better value for the flapper-nozzle supply pressure, the

iterative process of Section 5 is used. After several iterations, the flapper-nozzle supply pressure, which gives a maximum of 70-percent pressure recovery to any intermediate stage within the gain block, is calculated to be

$$P_{s1} = 290 \text{ N/m}^2 \text{ (2.2 mm Hg)} \quad (166)$$

This results in a maximum steady-state output pressure difference of the LPA gain block for the maximum input voltage of 15 V given by

$$P_{01}(4) - P_{02}(4) \Big|_{\text{max}} = 4.0 \times 10^3 \text{ N/m}^2 \text{ (3.0} \times 10^1 \text{ mm Hg)} \quad (167)$$

The increased flapper-nozzle supply pressure will not affect the stability of the system. This can be determined by evaluating the roots of the system's characteristic equation given by equation (164) and noting that they are in the left half plane.

The design presented in this section should exhibit an improved frequency response and greater output sensitivity over the design presented and tested in Section 5. The improved frequency response is due to a shorter bimorph length and an LPA gain block engineered for fast response. The increased gain is a result of a better impedance match between individual LPA stages within the gain block. The final result is an improved system response.

A final consideration for a complete servovalve design is a last stage power amplifier. The power output of the LPA is somewhat limited by its small size and the requirement that it run with a relatively low supply pressure so that the jet remains laminar. Any type of power amplifier that might be added would have a tendency to reduce the bandwidth of this system. This will be true because a moving part power amplifier will have mechanical parts. This will require acceleration forces and some fluid to mechanical force amplification, which will introduce fluid capacitance. An example of this would be some sort of a diaphragm amplifier. A relatively large diaphragm may be necessary for sufficient pneumatic

amplification. The motion of the diaphragm will introduce a fluid capacitance to the system. The overall result will be a system which is capable of a far slower response but has a higher output power capabilities. An interesting field of study, for future research, would be the development of a fluidic power amplifier that would match an LPA stage. A power amplifier of this type would not only have application in this project but also in the other areas of LPA research where the sensing capabilities of the LPA are used in a computer control scheme. This includes such projects as temperature sensing and control¹⁹ or the use of the laminar jet angular rate sensor²⁰ in conjunction with the LPA in a complete computer controlled closed loop system.

¹⁹T.M. Drzewiecki and R.M. Phillippi, Fluidic Thermistors or Fluidic Temperature Sensing with Capillaries, Engineering for Power, Vol. 99, No. 3 (July 1977).

²⁰D.N. Wormley and D. Lee, Development of a Hydraulic, Fluidic Servovalve, Winter Annual Meeting, American Society of Mechanical Engineers (1980).

LITERATURE CITED

1. Application Note, Piezoelectric Bender Elements, Piezo Products Division, Gulton Industries, Inc. (1978).
2. F.M. Manion and T.M. Drzewiecki, Analytic Design of Laminar Proportional Amplifiers, Proc. HDL State-of-the-Art Symposium, Vol. I, Adelphi, MD (Oct. 1974).
3. C.K. Taft and B.M. Herrick, A Proportional Electro-Fluidic Pneumatic Valve Design, 20th Anniversary of Fluidics Symposium, The American Society of Mechanical Engineers, Chicago, Illinois (1980).
4. C.K. Taft and B.M. Herrick, A Proportional Piezoelectric Electro-Fluid Pneumatic Servo Valve Design, 1981 Joint Automatic Control Conference, The American Society of Mechanical Engineers, Charlottesville, Virginia (1981).
5. W.G. Cady, Piezoelectricity, McGraw-Hill Book Co., New York (1946).
6. S.Y. Lee, Piezoelectric Actuators for Fluid Control Applications, Eng. Proc., Fluid Control System, Pennsylvania State University (July 1965), p. 45.
7. E.O. Doebelin, Measurement Systems, McGraw-Hill Book Co., New York (1975).
8. W.P. Mason, Piezoelectric Crystals and Their Application to Ultrasonics, Van Nostrand, New York (1950).
9. E.O. Doebelin, System Dynamics: Modeling and Response, Charles E. Merrill Publishing Co., Columbus, OH (1972).
10. P.W. Anderson, Theory Ferroelectric Behavior of Barium Titanate, Ceramic Age, 57(4) (1951), pp. 29-30, 33, 53-55.
11. J.P. Den Hartog, Mechanical Vibrations, McGraw-Hill Book Company, Inc., New York (1956).
12. Piezoceramic Design Note, Gulton Industries, Metuchen, New Jersey (1978).
13. B.W. Anderson, The Analysis and Design of Pneumatic Systems, John Wiley and Sons, Inc., New York (1976).
14. D. McCloy and H.R. Martin, The Control of Fluid Power, John Wiley and Sons, Inc., New York (1973).
15. Harry Diamond Laboratories Staff, Technical Sheet FC-104, U.S. Army Harry Diamond Laboratories, Adelphi, MD (1977).
16. T.M. Drzewiecki, A Fluidic Audio Intercom, 20th Anniversary of Fluidics Symposium, The American Society of Mechanical Engineers, (1981).
17. T.M. Drzewiecki, A Fluidic Voice Communication System and Data Link, Ph.D. Thesis, Naval Postgraduate School, Monterey, California (March 1980).
18. T.M. Drzewiecki, A High-Order, Lumped-Parameter, Jet-Dynamic Model for the Frequency Response of Laminar Proportional Amplifiers, 20th Anniversary of Fluidics Symposium, The American Society of Mechanical Engineers (1980).

19. T.M. Drzewiecki and R.M. Phillippi, Fluidic Thermistors or Fluidic Temperature Sensing With Capillaries, Engineering for Power, Vol. 99, No. 3 (July 1977).
20. D.N. Wormley and D. Lee, Development of a Hydraulic, Fluidic Servovalve, Winter Annual Meeting, American Society of Mechanical Engineers (1980).

NOMENCLATURE

- A = Area, m^2
- A_j = Coefficients used to simplify notation defined as follows for $j = 1, 2, \dots, 6$

Equation	Physical Meaning (if any)	Units
$A_1 = C_e \rho \pi r (1 + \frac{R_c}{R_v}) \sqrt{2/\rho}$	-	$\sqrt{kg/m}$
$A_2 = \rho/R_v$	-	m-s
$A_3 = W_e$	Jet entrainment flow	kg/s
$A_3 = \pi r^2$	Nozzle Area	m^2
$A_5 = C_e \rho L_b \pi r \sqrt{2/\rho}$	-	$\sqrt{kg-m}$
$A_6 = 2C_e \pi r$	-	m

- B = System damping, N-s
- B_c = Normalized control channel width, dimensionless
- \bar{B}_c = Normalized average control channel width, dimensionless
- b_s = LPA supply nozzle width, m
- C_1 = Piezoelectric force constant, N/V
- C_j = Coefficients used to simplify notation defined as follows for $j = 1, 2, \dots, 8$

Equation	Physical Meaning (if any)	Units
$C_0 = \frac{4A_1 P^2 (A_4 - A_6 u)}{A_1 u + 2A_2 P} + 2A_6 P^2$	Fluid system spring constant	N/m
$C_2 = 2A_5 P$	Fluid system spring constant	N-s/m
$C_3 = \frac{C_T R}{K_s}$	-	s^3/kg
$C_4 = \frac{1}{K_s}$	-	m/N

$$C_5 = \frac{R_T C_1}{K_S (R_A + R_T)} \quad - \quad \text{m/V}$$

$$C_6 = \frac{C_T MR}{K_S} \quad - \quad \text{s}^3$$

$$C_7 = \frac{C_T BR + M}{K_S} \quad - \quad \text{s}^2$$

$$C_8 = \frac{(C_T K_S + C_1 K_q) R + B}{K_S} \quad - \quad \text{s}$$

- C_d = Discharge coefficient, dimensionless
 C_e = Entrance coefficient, dimensionless
 C_T = Piezoelectric capacitance, F
 C_0 = LPA supply nozzle momentum flux discharge, dimensionless
 D = Nozzle diameter, m
 d_{ik} = Piezoelectric d coefficient, m/V
 E = Equivalent modulus of elasticity, N/m^2
 E_1 = Nickel modulus of elasticity, N/m^2
 E_2 = Lead zirconate titanate modulus of elasticity, N/m^2
 E_3 = Brass modulus of elasticity, N/m^2
 F = Force on the control volume exerted by the bimorph, N
 f = Maximum usable LPA frequency, Hz
 F_f = Acoustic feedback frequency, s^{-1}
 F_X = Force on the bimorph exerted by the fluid, N
 F' = Force to deflect bimorph a distance Δ , N
 g_i = Piezoelectric g coefficient, V-m/N
 G_p = LPA gain, dimensionless
 G_{pB} = LPA blocked load gain, dimensionless
 G_{pt} = Total LPA system gain, dimensionless
 h_s = LPA supply nozzle height, m
 I = Moment of area, m^4

i	=	Electrical signal field direction, dimensionless
j	=	Integer, dimensionless
k	=	Stress direction, dimensionless
K	=	Coupling coefficient, dimensionless
K_q	=	Pizeoelectric back current constant, A-s/m
K_s	=	System spring constant, N/m
L	=	Bimorph length, m
L_b	=	Nozzle length, m
L_{b1}	=	Control volume length, side 1, m
L_{b2}	=	Control volume length, side 2, m
M	=	Effective mass of bimorph, K_g
m	=	Integer, dimensionless
M_A	=	Integer, dimensionless
N_R	=	Reynolds number, dimensionless
N'_R	=	Modified Reynolds number, dimensionless
\hat{n}	=	Unit normal vector, dimensionless
n	=	Integer, dimensionless
P	=	Coefficient used to simplify notation, $\sqrt{N/m^2}$
p	=	Bimorph polarity, dimensionless
P_0	=	LPA operating point bias pressure, N/m^2
P_1	=	Nozzle 1 pressure, N/m^2
P_2	=	Nozzle 2 pressure, N/m^2
P_{10}	=	LPA operating point bias pressure, side 1, N/m^2
P_{20}	=	LPA operating point bias pressure, side 2, N/m^2
P_A	=	Atmospheric pressure, N/m^2
P_{i1}	=	LPA input pressure, side 1, N/m^2
P_{i2}	=	LPA input pressure, side 2, N/m^2
P_{01}	=	LPA output pressure, side 1, N/m^2

P_{O2}	=	LPA output pressure, side 2, N/m^2
P_{C1}	=	LPA control channel pressure, side 1, N/m^2
P_{C2}	=	LPA control channel pressure, side 2, N/m^2
P_s	=	LPA supply pressure, N/m^2
P_{s1}	=	Flapper-nozzle supply pressure, N/m^2
P_v	=	Vent pressure, N/m^2
q	=	Charge produced, coulomb (C)
Q_e	=	Volumetric jet entrainment flow, ft^3/s
Q_s	=	Volumetric LPA supply flow, ft^3/s
R	=	Equivalent electrical resistance, ohm (Ω)
r	=	Nozzle radius, m
R_A	=	External electrical resistance, Ω
R_C	=	LPA control channel resistance, $kg\cdot m^4/s$
R_i	=	LPA input resistance, $kg\cdot m^4/s$
R_L	=	LPA load resistance, $kg\cdot m^4/s$
R_O	=	LPA output resistance, $kg\cdot m^4/s$
R_s	=	LPA supply nozzle resistance, $kg\cdot m^4/s$
R_T	=	Bimorph leakage resistance, Ω
R_v	=	LPA vent resistance, $kg\cdot m^4/s$
S	=	Laplace variable, s^{-1}
T	=	Bimorph thickness, m
t	=	Time, s
T'	=	Laminar jet transport time, s
t_1	=	Nickel plate thickness, m
t_2	=	Lead zirconate titanate thickness, m
t_3	=	Brass shim thickness, m
u	=	Nozzle underlap, m
U_1	=	LPA stage

U_2	=	LPA stage
U_3	=	LPA stage
U_4	=	Amplifier average jet particle velocity, m/s
U_S	=	Amplifier supply velocity, m/s
V	=	Node voltage, V
V_1	=	Control volume fluid velocity, side 1, m/s
V_2	=	Control volume fluid velocity, side 2, m/s
V_A	=	Supply voltage, V
\bar{V}	=	Velocity vector, m/s
ψ	=	Volume, m^3
W	=	Bimorph width, m
W_1	=	Control volume mass flow rate, side 1, kg/s
W_1'	=	Steady state continuity equation
W_2	=	Control volume mass flow rate, side 2, kg/s
W_2'	=	Steady state continuity equation
W_{1i}	=	Mass flow rate into control volume, side 1, kg/s
W_{2i}	=	Mass flow rate into control volume, side 2, kg/s
W_{10}	=	Mass flow rate out of control volume, side 1, kg/s
W_{20}	=	Mass flow rate out of control volume, side 2, kg/s
W_{A1}	=	Vent flow, side 1, kg/s
W_{A2}	=	Vent flow, side 2, kg/s
W_e	=	Mass jet entrainment flow, kg/s
W_{E1}	=	Nickel plate equivalent width, m
W_{E2}	=	Lead zirconate titanate equivalent width, m
W_{E3}	=	Brass shim equivalent width, m
X	=	Bimorph displacement, m
X_0	=	Bimorph operating point deflection, m
\dot{X}_0	=	Bimorph operating point velocity, m/s

X_2	=	LPA stage
X_3	=	LPA stage
X_{sp}	=	LPA stage
X_{sp}	=	LPA nozzle to splitter distance, m
Y_3	=	LPA stage
Z	=	Number of LPA self staged amplifier stages dimensionless
Z_3	=	LPA stage
α_{11}	=	Coefficient of elasticity, cm^2/dyne
α_{12}	=	Coefficient of elasticity, cm^2/dyne
α_{44}	=	Coefficient of elasticity, cm^2/dyne
Δ	=	Deflection of the free end of a cantilever mounted beam from an applied force, m
ϵ	=	Absolute dielectric coefficient, F/m
ζ	=	Bimorph damping ratio, dimensionless
θ	=	Angle, rad
ν	=	Kinematic viscosity, m^2/s
ρ	=	Fluid density, kg/m^3
σ	=	LPA aspect ratio, dimensionless
τ	=	Period of LPA laminar jet oscillation, s
ω_D	=	Bimorph natural frequency, rad/s
ω_N	=	Bimorph natural frequency, rad/s
Ω_1	=	Direction cosine, dimensionless
Ω_2	=	Direction cosine, dimensionless
Ω_3	=	Direction cosine, dimensionless

APPENDIX A -- SUMMARY OF THE PROPERTIES OF THE WORKING PROTOTYPE

A summary of the important physical properties of the working prototype developed in Section 5 is provided below for reference.

Flapper-Nozzle Housing

<u>Property</u>	<u>Measured Value</u>
Bimorph length, L	1.5×10^{-2} m
Bimorph width, W	1.4×10^{-3} m
Bimorph thickness, T	4.9×10^{-4} m
Nozzle underlap, u	3.8×10^{-5} m
Nozzle diameter, D	8.6×10^{-4} m
Nozzle length, L_b	6.35×10^{-3} m
Nozzle entrance coefficient, C_e	0.85
Bimorph chamber supply pressure, P_{s1}	3.6×10^1 N/m ²
Air density, ρ	1.2 kg/m ³

LPA Gain Block

Stages 1, 2, and 3:

<u>Property</u>	<u>Measured Value</u>
Supply nozzle width, b_s	2.5×10^{-4} m
Supply nozzle height, h_s	3.75×10^{-4} m
Aspect ratio, σ	1.5
Average control channel width normalized by b_s , B_c	2.75
Control channel length normalized by b_s , X_c	10
Discharge coefficient, C_d	0.7
Momentum flux discharge coefficient, C_0	0.65
Blocked load pressure gain, G_{pB}	9.0
Supply pressure, $P_{-}(1)$, $P_{-}(2)$, $P_{-}(3)$	5.31×10^2 N/m ²

Stage 4:

<u>Property</u>	<u>Measured Value</u>
Supply nozzle width, b_s	5.0×10^{-4} m
Supply nozzle height, h_s	2.5×10^{-4} m
Aspect ratio, σ	0.5
Average control channel Width normalized by b_s , \bar{B}_c	2.75
Control channel length normalized by b_s , X_c	10
Discharge coefficient, C_d	0.7
Momentum flux discharge coefficient, C_θ	0.65
Blocked load pressure gain, G_{PB}	9.0
Supply pressure, $P_s(4)$	2.13×10^3 N/m ²

Figure A-1 is a schematic drawing of the working prototype. This figure illustrates the flapper-nozzle housing along with four stages of pneumatic amplification. The maximum static output pressure difference of the nozzles is given for the maximum static displacement of the end of the bimorph. This pressure difference is then applied across the input port of an LPA gain block. The important geometric properties along with the cascaded gain and the resulting output pressure difference of each LPA stage are given.

Working Prototype

Bimorph: Length = $1.5 \times 10^{-2} \text{ m}$
 Width = $1.4 \times 10^{-3} \text{ m}$
 Thickness = $4.9 \times 10^{-4} \text{ m}$
 Nozzle Diameter: $D = 3.6 \times 10^{-4} \text{ m}$

Stage 1
 $G_p(1) = 5.4$

Stage 2
 $G_p(2) = 5.4$

Stage 3
 $G_p(3) = 5.7$

Stage 4
 $G_p(4) = 10.0$

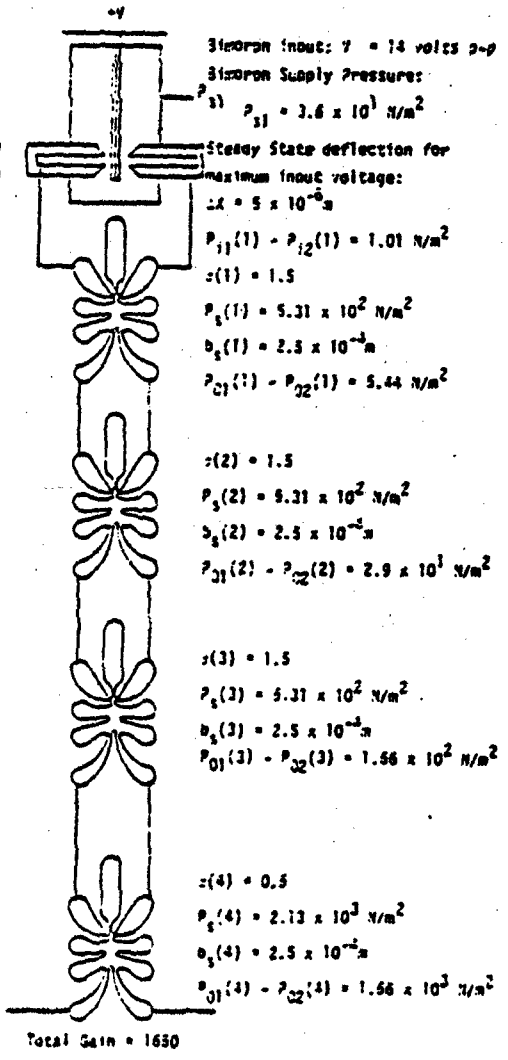


Figure A-1. Schematic Drawing of Working Prototype

APPENDIX B -- SUMMARY OF THE PROPERTIES OF THE PROPOSED PROTOTYPE

This appendix provides a summary of the important physical properties of the proposed prototype developed in Section 5.

Flapper-Nozzle Housing

<u>Property</u>	<u>Measured Value</u>
Bimorph length, L	1.05×10^{-2} m
Bimorph width, W	1.4×10^{-3} m
Bimorph thickness, T	4.9×10^{-4} m
Nozzle underlap, u	3.8×10^{-5} m
Nozzle diameter, D	8.6×10^{-4} m
Nozzle length, L_b	6.35×10^{-3} m
Nozzle entrance coefficient, C_e	0.85
Bimorph chamber supply pressure, P_{s1}	2.90×10^2 N/m ²
Air density, ρ	1.2 kg/m ³

LPA Gain Block

Stages 1:

<u>Property</u>	<u>Measured Value</u>
Supply nozzle width, b_s	2.5×10^{-4} m
Supply nozzle height, h_s	2.5×10^{-4} m
Aspect ratio, σ	1.0
Average control channel width normalized by b_s , \bar{B}_c	2.75
Discharge coefficient, C_d	0.7
Momentum flux discharge coefficient, C_0	0.65
Blocked load pressure gain, G_{pB}	10.0
Supply pressure, $P_s(1)$	2.13×10^2 N/m ²

Stages 2, 3, and 4:

<u>Property</u>	<u>Measured Value</u>
Supply nozzle width, b_s	2.5×10^{-4} m
Supply nozzle height, h_s	1.5×10^{-4} m
Aspect ratio, σ	0.6
Average control channel Width normalized by b_s , \bar{B}_c	2.75
Control channel length normalized by b_s , X_c	10
Discharge coefficient, C_d	0.7
Momentum flux discharge coefficient, C_θ	0.65
Blocked load pressure gain, G_{PB}	10.0
Supply pressure, $P_s(2)$, $P_s(3)$, $P_s(4)$	5.8×10^3 N/m ²

Figure B-1 is a schematic drawing of the proposed prototype. This figure illustrates the flapper-nozzle housing along with four stages of pneumatic amplification. The maximum static output pressure difference of the nozzles is given for the maximum static displacement of the end of the bimorph. This pressure difference is then applied across the input port of an LPA gain block. The important geometric properties along with the cascaded gain and the resulting output pressure difference of each LPA stage are given.

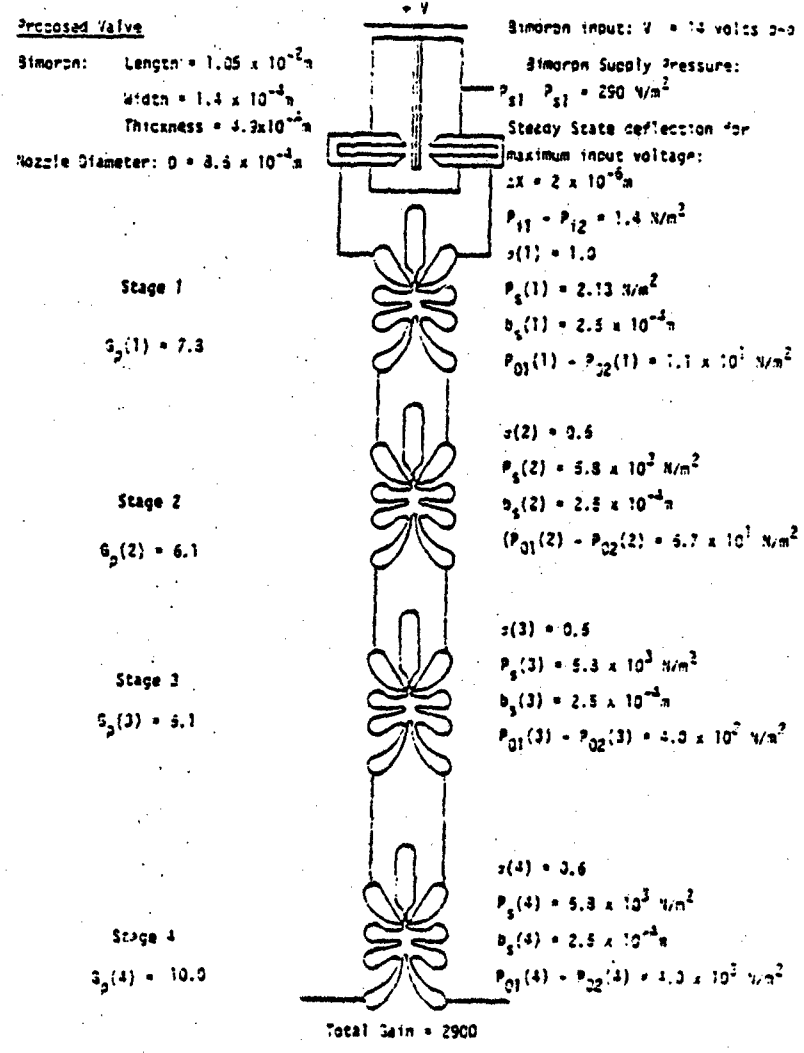


Figure B-1. Schematic Drawing of Proposed Prototype

DISTRIBUTION

ADMINISTRATOR
 DEFENSE TECHNICAL INFORMATION CENTER
 ATTN DTIC-DDA (12 COPIES)
 CAMERON STATION, BUILDING 5
 ALEXANDRIA, VA 22314

OFFICE OF THE DEPUTY CHIEF OF STAFF FOR
 RESEARCH, DEVELOPMENT & ACQUISITION
 DEPARTMENT OF THE ARMY
 ATTN DAMA-ARP-P
 ATTN DAMA-CSS-N
 WASHINGTON, DC 20310

COMMANDER IDDR&E
 PENTAGON, ROOM 3D 1089
 ATTN G. KOPCSAK
 WASHINGTON, DC 20310

DIRECTOR
 APPLIED TECHNOLOGY LABORATORY
 ATTN DAVDL-ATL-ASA
 FT EUSTIS, VA 23604

COMMANDER
 US ARMY ARMAMENT, MUNITIONS, &
 CHEMICAL COMMAND
 ATTN SARPA-TS-S #59
 ATTN DRDAR-LCN-C, A. E. SCHMIDLIN
 ATTN DRDAR-LCW-E, J. CONNORS
 ATTN DRDAR-SCF-IC, V. BAUMBARTH
 ATTN PBM-DPM (TAGLAIRINO)
 DOVER, NJ 07801

COMMANDER
 US ARMY ARMAMENT, MUNITIONS, &
 CHEMICAL COMMAND
 ATTN DRSAR-ASF, FUZE &
 MUNITIONS SUPPORT DIV
 ATTN DRSAR-RDF, SYS DEV DIV-FUZES
 ATTN DRSAR-RDG-T, R. SPENCER
 ATTN DRSAR-ASF
 ATTN DRSAR-LEP-L, TECH LIBRARY
 ROCK ISLAND, IL 61299

COMMANDER
 US ARMY ARMAMENT, MUNITIONS, &
 CHEMICAL COMMAND
 WATERVLIET ARSENAL
 ATTN SARWV-RDT-L
 ATTN DRDAR-LCB-RA, R. RACICOT
 WATERVLIET ARSENAL, NY 12189

BMD ADVANCED TECHNOLOGY CENTER
 PO BOX 1500
 ATTN J. PAPADOPOULOS
 HUNTSVILLE, AL 35807

DIRECTOR
 US ARMY BALLISTIC RESEARCH LABORATORY
 ATTN DRDAR-TSB-S (STINFO)
 ABERDEEN PROVING GROUP, MD 21005

US ARMY ELECTRONICS TECHNOLOGY
 & DEVICES LABORATORY
 ATTN DELET-DD
 FT MONMOUTH, NJ 07703

COMMANDER/DIRECTOR
 ATMOSPHERIC SCIENCES LABORATORY
 USA ERADCOM
 ATTN DELAS-AS (HOLT)
 ATTN DELAS-AS-T (R. RUBIO)
 WHITE SANDS MISSILE RANGE, NM 88002

COMMANDER
 US ARMY FOREIGN SCIENCE
 & TECHNOLOGY CENTER
 FEDERAL OFFICE BUILDING
 ATTN DRXST-SD1
 ATTN DRXST-IS3, C. R. MOORE
 220 7TH STREET, NE
 CHARLOTTESVILLE, VA 22901

COMMANDER
 US ARMY MATERIEL DEVELOPMENT &
 READINESS COMMAND
 ATTN DRCLD, JAMES BENDER
 5001 EISENHOWER AVENUE
 ALEXANDRIA, VA 22333

DIRECTOR
 US ARMY MATERIEL SYSTEMS
 ANALYSIS ACTIVITY
 ATTN DRXSY-MP
 ABERDEEN PROVING GROUND, MD 21005

COMMANDER
 US ARMY MATERIEL & MECHANICS
 RESEARCH CENTER
 ATTN R. KATZ
 WATERTOWN, MA 02172

COMMANDER
 US ARMY MISSILE COMMAND
 ATTN REDSTONE SCIENTIFIC INFORMATION
 CENTER, DRSMI-RBD
 ATTN DRSMI-RG, WILLIAM GRIFFITH
 ATTN DRSMI-TGC, J. C. DUNAWAY
 ATTN DRCPM-TOE, FRED J. CHEPLEN
 REDSTONE ARSENAL, AL 35898

COMMANDER
 US ARMY MISSILE & MUNITIONS
 CENTER & SCHOOL
 ATTN ATSK-CTD-F
 REDSTONE ARSENAL, AL 35809

DISTRIBUTION (Cont'd)

COMMANDER
US ARMY MOBILITY EQUIPMENT R&D CENTER
ATTN TECHNICAL LIBRARY (VAULT)
ATTN DRDME-EM, R. N. WARE
FT BELVOIR, VA 22060

US ARMY R&D GROUP (EUROPE)
BOX 15
ATTN CHIEF, AERONAUTICS BRANCH
ATTN CHIEF, ENGINEERING SCIENCES
FPO NEW YORK 09510

US ARMY RESEARCH OFFICE
PO BOX 12211
ATTN R. SINGLETON
RESEARCH TRIANGLE PARK, NC 27709

COMMANDER
US ARMY RSCH & STD GP (EUR)
ATTN CHIEF, PHYSICS & MATH BRANCH
FPO NEW YORK 09510

COMMANDER
US ARMY-TANK AUTOMOTIVE COMMAND
ARMOR & COMP DIV, DROTA-RKT
BLDG 215
ATTN M. WHITMORE
WARREN, MI 48090

COMMANDER
ATTN STEWS-AD-L, TECHNICAL LIBRARY
WHITE SANDS MISSILE RANGE, NM 88002

OFFICE OF NAVAL RESEARCH
DEPARTMENT OF THE NAVY
ATTN STANLEY W. DOROFF, CODE 438
ATTN D. S. SIEGEL, CODE 211
ARLINGTON, VA 22217

DEPARTMENT OF THE NAVY
R&D PLANS DIVISION
ROOM 5D760, PENTAGON
ATTN BENJ R. PETRIE, JR.
OP-987P4
WASHINGTON, DC 20350

COMMANDER
NAVAL AIR DEVELOPMENT CENTER
ATTN R. MCGIBONEY, 60134
ATTN CODE 8134, LOIS GUISE
ATTN D. KEYSER, 60134
WARMUNSTER, PA 19974

COMMANDING OFFICER
NAVAL AIR ENGINEERING CENTER
ATTN ESSD, CODE 9314, HAROLD OTT
LAKEHURST, NY 08733

NAVAL AIR SYSTEMS COMMAND
DEPARTMENT OF THE NAVY
ATTN CODE AIR-5162C1, J. BURNS
ATTN CODE AIR-5143, D. RETTA
WASHINGTON, DC 20361

COMMANDER
PACIFIC MISSILE TEST CENTER
ATTN CODE 3123, ABE J. GARRETT
ATTN CODE 1243, A. ANDERSON
POINT MUGU, CA 93042

COMMANDER
NAVAL ORDNANCE STATION
ATTN CODE 5123C, K. ENGLANDER
INDIAN HEAD, MD 20640

COMMANDANT
US NAVAL POSTGRADUATE SCHOOL DEPARTMENT
OF MECHANICAL ENGINEERING
ATTN CODE 69 Nm(NUNN)
MONTEREY, CA 93940

NAVAL RESEARCH LABORATORY
ATTN S. SEARLES, 117 BG A68
WASHINGTON, DC 20375

NAVAL SEA SYSTEMS COMMAND
SEA05R31
ATTN J. H. HARRISON
WASHINGTON, DC 20362

COMMANDER
NAVAL SHIP ENGINEERING CENTER
PHILADELPHIA DIVISION
ATTN CODE 6772
PHILADELPHIA, PA 19112

NAVAL SHIP RES & DEV CENTER
CODE 1619, K. READER
BETHESDA, MD 20084

COMMANDER
NAVAL SURFACE WEAPONS CENTER
ATTN CODE 413, CLAYTON MCKINDRA
WHITE OAK, MD 20910

COMMANDER
NAVAL WEAPONS CENTER
ATTN CODE 533, LIBRARY DIVISION
ATTN CODE 3636, C. BURMEISTER
CHINA LAKE, CA 93555

USHQ, AF SYSTEMS COMMAND
ATTN SGB, MAJ GEORGE JAMES
ANDREWS AFB, DC 20334

HQ, USAF/SAMI
WASHINGTON, DC 20330

DISTRIBUTION (Cont'd)

COMMANDER
AF AERO PROPULSION LABORATORY, AFSC
ATTN LESTER SMALL, AFWAL/POTC
WRIGHT-PATTERSON AFB, OH 45433

COMMANDER
ARMAMENT DEVELOPMENT & TEST CENTER
ATTN ADTC (DLOSL), TECH LIBRARY
ATTN DFLMA, DAVID T. WILLIAMS
EGLIN AIR FORCE BASE, FL 32542

COMMANDER
AIR FORCE AVIONICS LABORATORY
ATTN AARA-2, RICHARD JACOBS
WRIGHT-PATTERSON AFB, OH 45433

COMMANDER
AIR FORCE FLIGHT DYNAMICS LABORATORY
ATTN AFWAL/FIGL, H. SNOWBALL
ATTN AFWAL/PIER, R. J. DOBBEK
WRIGHT-PATTERSON AFB, OH 45433

AIR FORCE FLIGHT TEST CENTER
6510 ABG/SSD
ATTN TECHNICAL LIBRARY
EDWARDS AFB, CA 93523

AF INSTITUTE OF TECHNOLOGY, AU
ATTN LIBRARY AFIT (LD),
BLDG 640, AREA B
ATTN AFIT (ENM), MILTON E. FRANKE
WRIGHT-PATTERSON AFB, OH 45433

DIRECTOR
AF OFFICE OF SCIENTIFIC RESEARCH
ATTN NR
BOLLING AFB, DC 20332

COMMANDER
AF WEAPONS LABORATORY, AFSC
ATTN SUL, TECHNICAL LIBRARY
KIRTLAND AFB, NM 87117

DEPARTMENT OF ENERGY
FE-22
ATTN T. K. LAU
WASHINGTON, DC 20585

DEPARTMENT OF ENERGY
F-317, GTN (COAL GASIFICATION)
ATTN JIM CARR
WASHINGTON, DC 20585

FEDERAL BUREAU OF INVESTIGATION
J. EDGAR HOOVER BLDG
ATTN ROBERT WILLIS
WASHINGTON, DC 20585

JET PROPULSION LABORATORY
ATTN JOHN V. WALSH, MS 125-138
4800 OAK GROVE DRIVE
PASADENA, CA 91103

NASA AMES RESEARCH CENTER
ATTN MS 244-13, DEAN CHISEL
MOFFETT FIELD, CA 94035

NASA LANGLEY RESEARCH CENTER
ATTN MS 494, H. D. GARNER
ATTN MS 494, R. R. HELLBAUM
ATTN MS 185, TECHNICAL LIBRARY
HAMPTON, VA 23665

NASA SCIENTIFIC & TECH INFO FACILITY
PO BOX 8657
ATTN ACQUISITIONS BRANCH
BALTIMORE/WASHINGTON INTERNATIONAL
AIRPORT, MD 21240

SCIENTIFIC LIBRARY
US PATENT OFFICE
ATTN MRS. CURETON
WASHINGTON, DC 20231

UNIVERSITY OF ALABAMA
CIVIL & MINERAL ENGINEERING DEPT
PO BOX 1468
ATTN HAROLD R. HENRY
UNIVERSITY, AL 35486

UNIVERSITY OF ARKANSAS
TECHNOLOGY CAMPUS
PO BOX 3017
ATTN PAUL C. MCLEOD
LITTLE ROCK, AR 72203

UNIVERSITY OF ARKANSAS
MECHANICAL ENGINEERING
ATTN JACK H. COLE, ASSOC, PROF.
FAYETTEVILLE, AR 72701

CARNEGIE-MELLON UNIVERSITY
SCHENLEY PARK
ATTN PROF. W. T. ROULEAU,
MECH ENGR DEPT
PITTSBURGH, PA 15213

CASE WESTERN RESERVE UNIVERSITY
ATTN PROF. P. A. ORNER
ATTN PROF. B. HORTON
UNIVERSITY CIRCLE
CLEVELAND, OH 44106

THE CITY COLLEGE OF THE CITY
UNIVERSITY OF NY
DEPT OF MECH ENGR
ATTN PROF. L. JIJI

DISTRIBUTION (Cont'd)

THE CITY COLLEGE OF THE CITY
UNIVERSITY OF NY (Cont'd)
ATTN PROF. G. LOWEN
139TH ST. AT CONVENT AVE
NEW YORK, NY 10031

CLEVELAND STATE UNIVERSITY
FENN COLLEGE OF ENGINEERING
ATTN PROF. R. COMPARIN
CLEVELAND, OH 44115

DUKE UNIVERSITY
COLLEGE OF ENGINEERING
ATTN C. M. HARMAN
DURHAM, NC 27706

FRANKLIN INSTITUTE OF THE STATE
OF PENNSYLVANIA
ATTN KA-CHEUNG TSUI, ELEC ENGR DIV
ATTN C. A. BELSTERLING
20TH STREET & PARKWAY
PHILADELPHIA, PA 19103

IIT RESEARCH INSTITUTE
ATTN K. E. MCKEE
10 WEST 35TH STREET
CHICAGO, IL 60616

LEHIGH UNIVERSITY
DEPARTMENT OF MECHANICAL ENGINEERING
ATTN PROF. FORBES T. BROWN
BETHLEHEM, PA 19015

MASSACHUSETTS INSTITUTE OF TECHNOLOGY
ATTN ENGINEERING TECHNICAL REPORTS,
RM 10-408
ATTN DAVID WORMELY, MECH ENGR DEPT,
RM 3-146
77 MASSACHUSETTS AVENUE
CAMBRIDGE, MA 02139

MIAMI UNIVERSITY
DEPT OF ENG TECH
SCHOOL OF APPLIED SCIENCE
ATTN PROF. S. B. FRIEDMAN
OXFORD, OH 45056

MICHIGAN TECHNOLOGICAL UNIVERSITY
LIBRARY, DOCUMENTS DIVISION
ATTN J. HAWTHORNE
HOUGHTON, MI 49931

UNIVERSITY OF MISSISSIPPI
ATTN JOHN A. FOX
201 CARRIER HALL, DEPT OF MECH ENGR
UNIVERSITY, MS 38677

MISSISSIPPI STATE UNIVERSITY
DRAWER ME
ATTN C. J. BELL, MECH ENG DEPT
STATE COLLEGE, MS 39762

MISSISSIPPI STATE UNIVERSITY
DEPT OF AEROSPACE ENGINEERING
ATTN DAVID MURPHREE
MISSISSIPPI STATE, MS 39762

UNIVERSITY OF NEBRASKA LIBRARIES
ACQUISITIONS DEPT, SERIALS SECTIONS
ATTN ALAN GOULD
LINCOLN, NE 68508

UNIVERSITY OF NEW HAMPSHIRE
MECH ENGR DEPT, KINGSBURY HALL
ATTN PROF. CHARLES TAFT
ATTN PROF. DAVID LIMBERT
DURHAM, NH 03824

UNIVERSITY OF N. CAROLINA
INSTITUTE OF MARINE BIOMEDICAL RESEARCH
ATTN MICHAEL E. SHEEHAN
WILMINGTON, NC 28401

NEW JERSEY INSTITUTE OF TECHNOLOGY
DEPARTMENT OF MECHANICAL ENGINEERING
ATTN R. Y. CHEN
323 HIGH STREET
NEWARK, NJ 07102

OHIO STATE UNIVERSITY LIBRARIES
SERIAL DIVISION, MAIN LIBRARY
1958 NEIL AVENUE
COLUMBUS, OH 43210

OKLAHOMA STATE UNIVERSITY
SCHOOL OF MECH & AEROSPACE ENGR
ATTN PROF. KARL N. REID
STILLWATER, OK 74074

PENNSYLVANIA STATE UNIVERSITY
ATTN J. L. SHEARER
215 MECHANICAL ENGINEERING BUILDING
UNIVERSITY PARK, PA 16802

PENNSYLVANIA STATE UNIVERSITY
ENGINEERING LIBRARY
ATTN M. BENNETT, ENGINEERING LIBRARIAN
201 HAMMOND BLDG
UNIVERSITY PARK, PA 16802

PORTLAND STATE UNIVERSITY
DEPT OF ENGINEERING &
APPLIED SCIENCE
PO BOX 751
ATTN PROF. P. I. CHEN
PORTLAND, OR 97207

DISTRIBUTION (Cont'd)

PURDUE UNIVERSITY
SCHOOL OF MECHANICAL ENGINEERING
ATTN PROF. VICTOR W. GOLDSCHMIDT
ATTN PROF. ALAN T. MCDONALD
LAFAYETTE, IN 47907

ROCK VALLEY COLLEGE
ATTN KEN BARTON
3301 N. MULFORD ROAD
ROCKFORD, IL 61101

RUTGERS UNIVERSITY
LIBRARY OF SCIENCE & MEDICINE
ATTN GOVERNMENT DOCUMENTS DEPT
SANDRA R. LIVINGSTON
NEW BRUNSWICK, NJ 08903

SYRACUSE UNIVERSITY
DEPT OF MECH & AEROSPACE ENGINEERING
ATTN PROF. D. S. DOSANJH
139 E. A. LINK HALL
SYRACUSE, NY 13210

UNIVERSITY OF TENNESSEE
DEPT OF MECHANICAL ENGINEERING
ATTN PROF. G. V. SMITH
KNOXVILLE, TN 37916

UNIVERSITY OF TENNESSEE SPACE INST
ENERGY CONVERSION DIVISION
ATTN MARY ANN SCOTT
TULLAHOMA, TN 37388

UNIVERSITY OF TEXAS AT AUSTIN
DEPT OF MECHANICAL ENGINEERING
ATTN A. J. HEALEY
AUSTIN, TX 78712

THE UNIVERSITY OF TEXAS AT ARLINGTON
MECHANICAL ENGINEERING DEPARTMENT
ATTN ROBERT L. WOODS
ARLINGTON, TX 76019

TULANE UNIVERSITY
DEPT OF MECHANICAL ENGINEERING
ATTN H. F. HRUBECKY
NEW ORLEANS, LA 70118

UNION COLLEGE
MECHANICAL ENGINEERING
ATTN ASSOC. PROF. W. C. AUBREY
MECH ENGR DEPT, STEINMETZ HALL
SCHENECTADY, NY 12308

UNIVERSITY OF VIRGINIA
DEPT OF MECH & AEROSPACE ENGR
ATTN DAVID LEWIS
CHARLOTTESVILLE, VA 22090

VIRGINIA POLYTECHNIC INSTITUTE
OF STATE UNIV
MECHANICAL ENGINEERING DEPARTMENT
ATTN PROF. H. MOSES
BLACKSBURG, VA 24061

WASHINGTON UNIVERSITY
SCHOOL OF ENGINEERING
PO BOX 1185
ATTN W. M. SWANSON
ST LOUIS, MO 63130

WEST VIRGINIA UNIVERSITY
MECHANICAL ENGINEERING DEPARTMENT
ATTN RICHARD A. MAJURA
MORGANTOWN, WV 26505

WICHITA STATE UNIVERSITY
ATTN DEPT AERO ENGR, E. J. RODGERS
WICHITA, KS 67208

UNIVERSITY OF WISCONSIN
MECHANICAL ENGINEERING DEPARTMENT
ATTN FEDERAL REPORTS CENTER
ATTN NORMAN H. BEACHLEY, DIR
DESIGN ENGINEERING LABORATORIES
1513 UNIVERSITY AVENUE
MADISON, WI 53706

WORCESTER POLYTECHNIC INSTITUTE
ATTN GEORGE C. GORDON LIBRARY (TR)
ATTN TECHNICAL REPORTS
WORCESTER, MA 01609

BELL HELICOPTER COMPANY
PO BOX 482
ATTN R. D. YEARY
FT WORTH, TX 76101

BENDIX CORPORATION
ELECTRODYNAMICS DIVISION
ATTN D. COOPER
11600 SHERMAN WAY
N. HOLLYWOOD, CA 90605

BENDIX CORPORATION
RESEARCH LABORATORIES DIV
BENDIX CENTER
ATTN C. J. AHERN
ATTN LAEL TAPLIN
SOUTHFIELD, MI 48075

BOEING COMPANY, THE
PO BOX 3707
ATTN HENRIK STRAUB
SEATTLE, WA 98124

DISTRIBUTION (Cont'd)

BOWLES FLUIDICS CORPORATION
ATTN VICE PRES/ENGR
9347 FRASER AVENUE
SILVER SPRING, MD 20910

R. E. BOWLES
2105 SONDRRA COURT
SILVER SPRING, MD 20904

CONTROL SYSTEMS INNOVATION
ATTN N. F. MACIA
517 EAST ORION STREET
TEMPE, AZ 85283

CORNING GLASS WORKS
FLUIDIC PRODUCTS
ATTN R. H. BELLMAN
HOUGHTON PARK, B-2
CORNING, NY 14830

CHRYSLER CORPORATION
PO BOX 118
CIMS-418-33-22
ATTN L. GAU
DETROIT, MI 48231

JOHN DEERE PRODUCT ENGINEERING CENTER
ATTN V. S. KUMAR
WATERLOO, IA 50704

ENGINEERING SOCIETIES LIBRARY
ATTN ACQUISITIONS DEPARTMENT
ATTN HOWARD GORDON
345 EAST 47TH STREET
NEW YORK, NY 10017

FLUIDICS QUARTERLY
PO BOX 2989
ATTN D. H. TARUMOTO
STANFORD, CA 94305

FORD AEROSPACE & COMMUNICATIONS CORP
ATTN DR. JOSEPH M. ISEMAN
7235 STANDARD DRIVE
HANOVER, MD 21076

FOXBORO COMPANY
CORPORATE
RESEARCH DIV
ATTN JAMES VIGNOS
ATTN J. DECARLO
ATTN JOHN CHANG
ATTN TOM KEGEL
38 NEPONSET AVE
FOXBORO, MA 02035

GARRETT PNEUMATIC SYSTEMS DIVISION
PO BOX 5217
ATTN GARY FREDERICK
ATTN TREVOR SUTTON

GARRETT PNEUMATIC SYSTEMS DIVISION
(Cont'd)
ATTN TOM TIPPETTS
ATTN C. ABBOTT
111 SOUTH 34TH STREET
PHOENIX, AZ 85010

GRUMMAN AEROSPACE CORPORATION
TECHNICAL INFORMATION CENTER
ATTN C. W. TURNER, DOCUMENTS
LIBRARIAN
ATTN TED SORENSEN, MS B1535
ATTN JACK LEONARD, MS B1535
SOUTH OYSTER BAY ROAD
BETHPAGE, L. I., NY 11714

HAMILTON STANDARD
DIVISION OF UNITED AIRCRAFT CORPORATION
ATTN PHILIP BARNES
WINDSOR LOCKS, CT 06096

HONEYWELL, INC
ATTN J. HEDEEN
ATTN W. POSINGIES
1625 ZARTHAN AVE
MINNEAPOLIS, MN 55413

HONEYWELL, INC
ATTN RICHARD STEWART, MS 200
1100 VIRGINIA DRIVE
FT WASHINGTON, PA 19034

HUGHES HELICOPTERS
DIVISION OF SUMMA CORPORATION
CENTINELA & TEALE STREETS
ATTN LIBRARY 2/T2124
CULVER CITY, CA 90230

JOHNSON CONTROLS, INC
ATTN WARREN A. LEDERMAN
ATTN GEORGE JANU
507 E. MICHIGAN
MILWAUKEE, WI 53201

LEEDS & NORTHRUP CO
ATTN ERNEST VAN VALKENBURGH
DICKERSON ROAD
NORTH WALES, PA 19454

MOORE PRODUCTS COMPANY
ATTN R. ADAMS
SPRING HOUSE, PA 19477

MARTIN MARIETTA CORPORATION
AEROSPACE DIVISION
ATTN R. K. BRODERSON, MP 326
PO BOX 5837
ORLANDO, FL 32805

DISTRIBUTION (Cont'd)

MCDONNELL AIRCRAFT COMPANY
GUIDANCE & CONTROL MECHANICS DIVISION
ATTN ROYAL GUENTHER
ST LOUIS, MO 63166

MCDONNELL DOUGLAS ASTRONAUTICS CO
PROPULSION DEPARTMENT
ATTN V. E. HALOULAKOS (A3-226)
ATTN J. D. SCHWEIKLE (A3-226)
5301 BOLSA AVENUE
HUNTINGTON BEACH, CA 92647

NATIONAL FLUID POWER ASSOC.
ATTN JOHN R. LUEKE
DIR OF TECH SERVICES
3333 NORTH MAYFAIR ROAD
MILWAUKEE, WI 53222

NEOS, INC
3711 AIR PARK RD
ATTN A. J. OSTDIEK
LINCOLN, NE 68524

NORTHROP CORP, ELECTRONICS DIV
ATTN DESMOND NELSON,
SENIOR ENGINEER
ORGN C3133, W/C
2301 W. 120TH ST
HAWTHORNE, CA 90250

PLESSEY AEROSPACE LTD
ATTN A. ROSENBERG
1700 OLD MEADOW ROAD
MCLEAN, VA 22102

ROCKWELL INTERNATIONAL CORPORATION
COLUMBUS AIRCRAFT DIVISION, PO BOX 1259
ATTN MARVIN SCHWEIGER
ATTN LOUIS BIAFORE
4300 E. 5TH AVENUE
COLUMBUS, OH 43216

SCIENCE & TECHNOLOGY ASSOCIATES, INC
ATTN DR. T. DRZEWIECKI
1700 N. MOORE ST., SUITE 1920
ARLINGTON, VA 22209

SIKORSKY AIRCRAFT
ATTN J. R. SOEHNLEIN
NORTH MAIN STREET
STRATFORD, CT 06602

TELEDYNE BROWN ENGINEERING
CUMMINGS RESEARCH PARK
ATTN MELVIN L. PFICE, MS-44
HUNTSVILLE, AL 35807

TRITEC, INC
ATTN L. SIERACKI (2 COPIES)
PO BOX 56
COLUMBIA, MD 21045

UNITED TECHNOLOGIES RESEARCH CENTER
ATTN R. E. OLSON, MGR FLUID
DYNAMICS LABORATORY
400 MAIN STREET
E. HARTFORD, CT 06108

VOUGHT CORP
PO BOX 225907
ATTN KELLEY FLING
DALLAS, TX 75265

US ARMY ELECTRONICS RESEARCH
& DEVELOPMENT COMMAND
ATTN COMMANDER, DRDEL-CG
ATTN TECHNICAL DIRECTOR, DRDEL-CT
ATTN PUBLIC AFFAIRS OFFICE, DRDEL-IN

HARRY DIAMOND LABORATORIES
ATTN CO/TD/TSO/DIVISION DIRECTORS
ATTN RECORD COPY, 81200
ATTN HDL LIBRARY, 81100 (3 COPIES)
ATTN HDL LIBRARY (WOODBIDGE), 81100
ATTN TECHNICAL REPORTS BRANCH, 81300
ATTN LEGAL OFFICE, 97000
ATTN CHAIRMAN, EDITORIAL COMMITTEE
ATTN CORRIGAN, J., 20240
ATTN CHIEF, 13000
ATTN CHIEF, 13400 (20 COPIES)